

DOKUZ EYLÜL UNIVERSITY
GRADUATE SCHOOL OF NATURAL AND APPLIED SCIENCES

**RESIDUAL VIBRATION CONTROL OF
MANIPULATORS WITH TRAPEZOIDAL
VELOCITY PROFILE ACTUATIONS**

by
Şahin YAVUZ

February, 2016
İZMİR

**RESIDUAL VIBRATION CONTROL OF
MANIPULATORS WITH TRAPEZOIDAL
VELOCITY PROFILE ACTUATIONS**

**A Thesis Submitted to the
Graduate School of Natural and Applied Sciences of Dokuz Eylül University
In Partial Fulfillment of the Requirements for the Degree of Doctor of
Philosophy in Mechanical Engineering, Machine Theory and Dynamics
Program**

**by
Şahin YAVUZ**

**February, 2016
İZMİR**

Ph.D. THESIS EXAMINATION RESULT FORM

We have read the thesis entitled “RESIDUAL VIBRATION CONTROL OF MANIPULATORS WITH TRAPEZOIDAL VELOCITY PROFILE ACTUATIONS” completed by ŞAHİN YAVUZ under supervision of PROF. DR. HİRA KARAGÜLLE and we certify that in our opinion it is fully adequate, in scope and in quality, as a thesis for the degree of Doctor of Philosophy.



Prof. Dr. Hira KARAGÜLLE

Supervisor



Doç. Dr. Hasan ÖZTÜRK

Thesis Committee Member



Yrd.Doç. Dr. Yavuz ŞENOL

Thesis Committee Member



Prof. Dr. Hakan Başoğlu

Examining Committee Member

Doç. Dr. Zekeriya Gülçin



Examining Committee Member



Prof. Dr. Ayşe OKUR

Director

Graduate School of Natural and Applied Sciences

ACKNOWLEDGEMENTS

I would like to express my sincere indebtedness and gratitude to my thesis consultant Prof. Dr. Hira KARAGÜLLE, for all his time and effort. His guidance and input at every stage of my work truly helped me navigate this endeavor. I would also like to thank Assoc. Prof. Dr. Hasan ÖZTÜRK and Assist. Prof. Dr. Yavuz ŞENOL for the useful discussions on periodical meetings of this research.

I would also thank Assoc. Prof. Dr. Levent MALGACA, Assist. Prof. Dr. Murat AKDAG (Engineering Faculty of Dokuz Eylül University), my friend Dr. Serkan GÜLER and Murat HOCAOĞLU for their encouragement and intellectual input during the entire course of this thesis.

Finally, I would like to thank my parents and my sister who have supported me all the way since the beginning of my studies. Their love gave me forces to make this work.

Şahin YAVUZ

RESIDUAL VIBRATION CONTROL OF MANIPULATORS WITH TRAPEZOIDAL VELOCITY PROFILE ACTUATIONS

ABSTRACT

Nowadays, flexible systems are more desirable than the rigid systems in industrial. Flexible and light mechanical systems are more advantageous than rigid and heavy ones. The most current examples of flexible mechanical systems are robot manipulators. Flexible manipulators have smaller driving actuators and consume lower energy. However, residual vibrations occur due to the flexibility. Elimination or suppression of these vibrations by using different control strategies is a challenging problem for researchers.

This thesis deals with different aspects of modeling and control of flexible systems. Mechanical systems can be modeled by commercial programs such as ANSYS, by using finite element method theory or by using lumped mass-spring-damper systems. Obtaining mathematical model of the systems are important in order to observe the dynamic responses of the systems under different input profiles. In this study, different methods have been used to perform vibration analysis such as Runge-Kutta, Newmark, and ANSYS to reduce the residual vibrations of different systems.

Vibrations caused after finishing the motion are called as residual vibrations. Residual vibrations significantly affect positioning achievement of the end point in flexible systems. To control the residual vibrations of the mechanical system, different velocity profiles are applied with open loop control and both experimental and simulation results are compared to validate the accuracy of the proposed control strategies.

Keywords: Vibration control, mechanical systems, finite element analysis, residual vibrations.

TRAPEZ HIZ PROFİLİ İLE HAREKET ETTİRİLEN MANİPÜLATÖRLERDE ARTIK TİTREŞİMLERİN KONTROLÜ

ÖZ

Günümüzde, esnek sistemler rijit sistemlere göre endüstride daha çok tercih edilmektedir. Esnek ve hafif mekanik sistemler, rijit ve ağır olanlara göre daha avantajlıdır. Esnek mekanik sistemlerin en geçerli örneği robot manipülatörlerdir. Esnek manipülatörler düşük güçte aktüatörlere sahiptir ve daha az enerji harcarlar. Bununla birlikte, esneklikten dolayı artık titreşimler meydana gelir. Farklı kontrol stratejileri ile bu titreşimlerin yok edilmesi ya da azaltılması, araştırmacılar için ciddi bir problem olmaktadır.

Bu tez, esnek sistemlerin farklı modellenmesi ve kontrol yönleri ile ilgilenir. Mekanik sistemler ANSYS gibi ticari programlar ile, sonlu elemanlar teorisi ile ya da topaklanmış kütle-yay-sönüm elemanı sistemleri ile modellenebilir. Sistemlerin matematik modellerini elde etmek, farklı girdi profilleri altında dinamik cevaplarını gözlemlemek için oldukça önemlidir. Bu çalışmada, farklı mekanik sistemlerin artık titreşimlerini azaltmak için Runge-Kutta, Newmark ve ANSYS gibi farklı yöntemlerle titreşim analizi gerçekleştirilmiştir.

Hareket sonrası oluşan titreşimler artık titreşimler olarak adlandırılmaktadır. Artık titreşimler, esnek sistemlerde uç nokta konumlandırılmasında oldukça etkilidir. Mekanik sistemlerin artık titreşimlerini kontrol etmek için açık kontrol ile farklı hız profilleri uygulanmış ve önerilen kontrol stratejilerinin hassasiyetini doğrulamak için simülasyon ve deneysel sonuçlar karşılaştırılmıştır.

Anahtar kelimeler: Titreşim kontrolü, mekanik sistemler, sonlu elemanlar analizi, artık titreşimler.

CONTENTS

	Page
Ph.D. THESIS EXAMINATION RESULT FORM.....	ii
ACKNOWLEDGEMENTS	ii
ABSTRACT	iv
ÖZ	v
LIST OF FIGURES	ix
LIST OF TABLES.....	xii
CHAPTER ONE - INTRODUCTION	1
1.1 Introduction.....	1
1.2 Literature Survey.....	1
1.3 Scope of the Thesis.....	4
1.4 Organization of the Thesis.....	5
CHAPTER TWO - VIBRATION CONTROL OF A MULTI-DEGREE-OF-FREEDOM SYSTEM.....	7
2.1 Introduction.....	7
2.2 Mathematical Model of the System.....	8
2.2.1 Newton's Second Law of Motion.....	8
2.2.2 Lagrange's Equation	9
2.2.3 Eigenvalue Problem	13
2.3 Passive Vibration Control of 4-DOF Mechanical System.....	13
2.3.1 Runge-Kutta Method.....	16
2.3.2 Newmark Method	23
2.4 Active Vibration Control of 4-DOF Mechanical System.....	30
2.4.1 Newmark Solution for Closed Loop Control	30
2.4.2 Analytical Solution	31
2.4.3 Effect of Damping and Effectiveness of Controller Gains.....	34
2.4.4 Setting Control Parameters.....	36

2.5 Active Vibration Control of a Flexible Cantilever Beam by Newmark Method	41
2.5.1 Modelling of Flexible Beam	41
2.5.2 Active Vibration Control with Newmark Method	44
2.6 Active Vibration Control of a Single Link Flexible Manipulator by Newmark Method	47
2.6.1 Modeling of Single Link Manipulator Based on Finite Element Method	48
2.6.2 Damping	52
2.6.3 Motion	52
2.6.4 Forces	54
2.6.5 Vibration Signals	54
2.6.6 Modal Analysis	54
2.6.7 Numerical Values	55
2.6.8 Experimental System	56
2.6.9 Simulation and Experimental Results	57
2.6.10 Active Vibration Control of the Manipulator	58
2.7 Conclusion	62

CHAPTER THREE – VIBRATION CONTROL OF SINGLE-LINK FLEXIBLE COMPOSITE MANIPULATOR.....64

3.1 Introduction	64
3.2 Finite Element Vibration Analysis	67
3.3 Experimental System	70
3.4 Simulation and Experimental Results	72
3.5 Conclusion	83

CHAPTER FOUR – VIBRATION CONTROL OF SIX-AXIS SERIAL ROBOT WITH ANSYS APDL AND EXPERIMENTAL RESULTS85

4.1 Introduction	85
4.2 Analysis by ANSYS APDL Code based on Finite Element Theory	88
4.2.1 Finite Element Model	88

4.2.2 Damping	93
4.2.3 Motion	93
4.2.4 Vibration Signals	94
4.2.5 Modal Analysis	94
4.2.6 Numerical Values.....	95
4.3 Experimental Results of Vibration Control of Six-Axis Serial Robot	96
4.4 Conclusion	101
CHAPTER FIVE - CONCLUSION	103
REFERENCES	107

LIST OF FIGURES

	Page
Figure 2.1 4-DOF mass-damper-spring system ($m_1=m_2=m_3=m_4=1$ kg, $c_1=1.5$ Ns/m, $c_2=1.2$ Ns/m, $c_3=c_4=0.8$ Ns/m, $k_1=600$ N/m, $k_2=400$ N/m, $k_3=k_4=200$ N/m).....	8
Figure 2.2 Free-body diagram of the system.....	9
Figure 2.3 Trapezoidal velocity profile.....	13
Figure 2.4 Triangular velocity profile $t_i=[1.5202,0,0.4798,2]$	16
Figure 2.5 Time response of the end point for the triangular velocity profile a) Displacement and b) Acceleration.....	19
Figure 2.6 Residual vibrations of the end point for triangular velocity profile a) Displacement and b) Acceleration.....	20
Figure 2.7 Residual vibrations of the end point for the triangular velocity profile a) Displacement, b) Acceleration and c) Input profile	21
Figure 2.8 Newmark and Runge-Kutta superposed for $[*,0,t_{1h},2]$ a) Displacement and b) Acceleration	24
Figure 2.9 Residual vibrations of Newmark and Runge-Kutta superposed for $[*,0,t_{1h},2]$ a) Displacement and b) Acceleration.....	25
Figure 2.10 Trapezoidal velocity profile $t_i=[3.0403,0.4798,0.4798,4]$	26
Figure 2.11 Residual vibrations of the end point for the trapezoidal velocity profile a) Displacement, b) Acceleration and c) Input profile	28
Figure 2.12 Change of the RMS values of the residual vibration signals versus the deceleration time for Case-3 and Case-4	29
Figure 2.13 Block diagram for integration of closed loop control action into Newmark solution.....	30
Figure 2.14 Approximate model of the step input, (a) displacement, (b) velocity and (c) acceleration.	30
Figure 2.15 Solution by the Newmark method for undamped system, ($K_p=10$, $K_i=5$, $K_d=0.5$).....	31
Figure 2.16 Block diagram of the system	32
Figure 2.17 Analytic solution for the undamped system, ($K_p=10$, $K_i=5$, $K_d=0.5$)	33
Figure 2.18 Comparison of the Control-ON results ($K_p=10$, $K_i=5$, $K_d=0.5$)	34

Figure 2.19 Comparison of controlled results for damped system. ($K_p=10$, $K_i=5$, $K_d=0.5$).....	35
Figure 2.20 Comparison of open loop and closed loop results for the damped system, a) $K_p=0.5$, $K_i=0$, $K_d=0$, b) $K_p=0.5$, $K_i=0$, $K_d=0.2$, c) $K_p=0.5$, $K_i=3$, $K_d=0.2$	37
Figure 2.21 Comparison of closed loop results for undamped system, a) $K_p=0.05$, $K_i=0$, $K_d=0.01$, b) $K_p=0.5$, $K_i=0$, $K_d=0.2$, c) $K_p=0.5$, $K_i=3$, $K_d=0.2$	38
Figure 2.22 The model of cantilever beam	42
Figure 2.23 The finite element model of flexible beam.....	43
Figure 2.24 Closed loop block diagram.....	44
Figure 2.25 Control-OFF and Control-ON responses ($L_c=168\text{mm}$, $K_p=8$, $K_i=0.5$, $K_d=0.5$,).....	46
Figure 2.26 (a) Model, (b) FE model, (c) starting and stopping locations of the manipulator.....	48
Figure 2.27 The angular trapezoidal velocity profile of the motor.....	53
Figure 2.28 Experimental system, (a) planar manipulator, (b) pc-based motion and measurement system.....	56
Figure 2.29 Closed loop block diagram.....	58
Figure 2.30 Vibration responses for $\theta_m=90^\circ$ and $\mathbf{q}_m = [* , 0, 0.1, 1]$	59
Figure 2.31 Vibration responses for $\theta_m=90^\circ$ and $\mathbf{q}_m = [* , 0.1, 0.1, 1]$	60
Figure 2.32 Change of the RMS values of the residual vibration signals versus the proportional gain for $\mathbf{q}_m=[* , 0, 0.1, 1]$	61
Figure 2.33 Change of the RMS values of the residual vibration signals versus the proportional gain for $\mathbf{q}_m=[* , 0.1, 0.1, 1]$	62
Figure 3.1 The FE model of the composite manipulator.	68
Figure 3.2 Trapezoidal velocity profile.....	69
Figure 3.3 Experimental system.....	70
Figure 3.3 Experimental system (cont.).....	71
Figure 3.4 Vibration responses for Case-1 for $[0/90]$ lay-up (a) $\mathbf{q}_m = [* , 0, t_{1h}, t_m]$, (b) $\mathbf{q}_m = [* , 2t_{1h}, t_{1h}, t_m]$ and $[45/-45]$ lay-up (c) $\mathbf{q}_m = [* , 0, t_{1h}, t_m]$, (d) $\mathbf{q}_m = [* , 2t_{1h}, t_{1h}, t_m]$	75

Figure 3.5	Vibration responses for Case-1 for [0/90] lay-up (a) $\mathbf{q}_m = [*,0,2t_{1h},t_m]$, (b) $\mathbf{q}_m = [*,2t_{1h}, 2t_{1h},t_m]$ and [45/-45] lay-up (c) $\mathbf{q}_m = [*,0, 2t_{1h},t_m]$, (d) $\mathbf{q}_m = [*,2t_{1h}, 2t_{1h},t_m]$	77
Figure 3.6	Change of the RMS values of the residual vibration signals versus the deceleration time for Case-1 (a) [0/90] and (b) [45/-45].	82
Figure 4.1	(a) Solid model and (b) line model of the robot.	89
Figure 4.2	Beam model of the robot in ANSYS	90
Figure 4.3	The flow chart for the analysis in ANSYS.....	93
Figure 4.4	The angular velocity profile of motors.....	94
Figure 4.5	Experimental system of the robot.	96
Figure 4.6	Measurement system	97
Figure 4.7	Motion parameters.	97
Figure 4.8	(a) The starting position and (b) the stopping position.	98
Figure 4.9	Example signals for [$t_{acc}, t_{con}, t_{dec}, t_m$]=[*,0, T_{1h} ,1] (a) Simulation, (b) Experiment	99
Figure 4.10	Example signals for [$t_{acc}, t_{con}, t_{dec}, t_m$]=[*,0,2 T_{1h} ,1] (a) Simulation, (b) Experiment	100
Figure 4.11	Change of rms values of residual vibration signals versus the deceleration time for M1.....	100

LIST OF TABLES

	Page
Table 2.1 Motion input.....	22
Table 2.2 Motion input for Case-5	28
Table 2.3 Motion input for Case-6	29
Table 2.4 Closed loop results for damped system	36
Table 2.5 Closed loop results for undamped system	36
Table 2.6 Properties of the beam.....	42
Table 2.7 Closed loop results for different control gains.....	46
Table 2.8 The effect of the number of element on dynamic behavior.....	47
Table 2.9 Beam FE's on the system	49
Table 2.10 Properties of the manipulator.....	55
Table 2.11 Natural frequencies of the manipulator	57
Table 2.12 Case results for the manipulator.....	60
Table 3.1 Properties of the composite manipulator	69
Table 3.2 Natural frequencies of the composite manipulator	72
Table 3.3 Motion cases	74
Table 3.4 RMS and reduction ratios for Case-1	79
Table 3.5 RMS and reduction ratios for Case-2	80
Table 3.6 RMS and reduction ratios for Case-3	80
Table 3.7 RMS and reduction ratios for Case-4	80
Table 3.8 RMS and reduction ratios for Case-5	81
Table 4.1 Cross-sections of the members	91
Table 4.2 Properties of MPC184 element.....	92
Table 4.3 Properties of experimental system	95
Table 4.4 RMS and reduction ratios for Case-1.....	99

CHAPTER ONE

INTRODUCTION

1.1 Introduction

Flexible and light mechanical systems are more advantageous than rigid and heavy ones. The most current examples of flexible mechanical systems are robot manipulators. Flexible manipulators have smaller driving actuators and consume lower energy. However, residual vibrations occur due to the flexibility. This affects the settling time and accuracy at the end point while operating with high speeds. Elimination or suppression of these vibrations by using different control strategies is a challenging problem for researchers.

1.2 Literature Survey

The mathematical model of manipulators can be constructed by the finite element method or analytical methods (Benosman & LeVey, 2004). The governing differential equations of dynamic systems can be solved by using numerical methods (Fung, 1997; Owren & Simonsen, 1995; Zhang et al., 1999) or commercial engineering programs (Karagülle & Malgaca, 2004).

One link flexible robot arm can be modeled with linear models, and multi-link manipulators can be modeled with nonlinear models. Basic spring-mass discrete models, linear Euler-Bernoulli partial differential equations, generalized Newton-Euler algorithms, Lagrangian equations, associated to a Rayleigh-Ritz elastic field decomposition method and finite element decomposition or modal decomposition have been used to analyze multi-body flexible manipulators (Benosman & LeVey, 2004). Fung (1997) presented a sub-stepping procedure to construct unconditionally stable higher-order accurate algorithms based on the Newmark method. Owren and Simonsen (1995) used Runge-Kutta Method for the time integration of the equations of motion in structural dynamics. Zang et al. (1999) developed a stochastic Newmark algorithm which is appropriate for earthquakes and sea waves. Karagulle and

Malgaca (2004) studied on the effect of the flexibility on the trajectory of a planar two-link manipulator using integrated computer-aided design/analysis (CAD/CAE) procedures. They also presented a work to analyze active vibration control in smart structures by ANSYS (Karagülle et al., 2004).

Residual vibration amplitudes of flexible robot manipulators can be suppressed by using passive or active control. Passive control, which deals with the open loop system, can be achieved by motion commands (Meckl & Seering, 1985; Jayasuriya & Choura, 1991; Shan et al., 2005; Shin & Brennan, 2008; Singhose et al., 1994). Active control requires the closed loop model and an external actuator. Piezoelectric elements are widely used for the vibration control of flexible structures (Gaudenzi et al., 2000; Hassan et al., 2007; Xianmin et al., 2002).

A brief summary of the vibration control strategies of flexible systems are given here. Meckl and Seering (1985) investigated open loop control of such systems by using “bang bang” control function and another control function to avoid resonance. They also examined the performance of a control function for a ramp input. This study was expanded by Singhose and et al. (1994), who used input shaping with impulse series. They showed that negative input shapers yield much faster rise time than positive input shapers. Jayasuriya and Choura (1991) developed an open loop force function which demolishes the residual vibrations due to minimum energy law while reducing the system response time. Shan et al. (2005) developed the modified input shaping method for multimode vibration suppression. The method is applied on a single link flexible manipulator and the researchers proposed the modified input shaping to get much better performance than the traditional input shaping method. On the other hand, Shin and Brennan (2008) considered a cantilever beam and suggested two methods for suppressing the residual vibration of a single degree of freedom system without any control. They proved that the second method which is similar to the input shaping method can control both position and time simultaneously.

Numerical simulations were carried out for active control of a 4-bar linkage mechanism with piezoelectric actuators and sensors using the reduced modal controller, the classical and the robust H_∞ controller (Xianmin et al., 2002). Simulation and experimental studies were conducted for vibration suppression of a flexible one-link manipulator using piezoceramic actuators with of model-based predictive controller (Hassan et al., 2007). Gaudenzi et al. (2000) studied on the vibration reduction for an active cantilever beam by using piezo-patches. They used a single-input single-output feedback closed loop control system for control strategy.

A literature review of vibration control techniques of composite beams are given in references (Bandopadhyaya et al., 2008; Gandhi & Mevada, 2013; Ji et al., 2009; Kang et al., 2002; Raja et al., 2002; Zoric et al., 2013). Gandhi and Mevada (2013) presented a finite element model based on the third order theory for the active vibration control of composite beams. They used piezoelectric sensor to provide a damping effect on the composite beam with a negative velocity feedback in a closed loop control. Raja et al. (2002) used two different type of piezoelectric actuators for active vibration control of composite sandwich beams: extension-bending and shear actuators. They developed a control scheme based on the linear quadratic regulator/independent modal space control method and provided the shear actuator is more efficient that the extension-bending actuator for the same control strategy. Zoric et al. (2013) presented the optimized fuzzy logic controller for vibration control of thin-walled composite beams. They modeled the composite beam by using finite element method and suggested the applied fuzzy logic control with adjusting the input scaling factor. They compared the results with the fuzzy logic control method with constant input scaling to provide the efficiency of their method. Bandopadhyaya et al. (2008) used ionic polymer metal composite (IPMC) as an active damper to control a single-link flexible manipulator. They proposed the suitable positions to fix two IPMC actuators based on modal approach to suppress vibrations efficiently. Ji et al. (2009) improved synchronized switch damping on voltage (SSDV) approach to control the vibrations of a composite beam. The proposed approach adjusted the voltage coefficient which controls the damping efficiency adaptively and they showed that the improved SSDV approach is the most stable

compared with previous SSDV techniques. In control techniques, passive control is used as changing the damping ratio by using different orientation angles. Kang et al. (2002) investigated the interaction between active and passive vibration control characteristics on laminated composite beams. They used velocity feedback control as an active vibration and different orientation angles with different layers as a passive control to use modal damping.

The dynamic model of robot manipulators can be considered as a lumped multi degree of freedom system (Connor & Lang, 1998; Vincent et al., 1989). A position control algorithm using mechanical waves for the lumped parameter system was developed (Connor & Lang, 1998). Vincent et al. (1989) designed a two-stage control algorithm for concentric parameter systems. The first stage of this algorithm is open loop high speed positioning and the second stage is closed loop damping. The lumped-parameter methods are also used for rigid footings models (Andersen, 2010).

The problem of vibration control in lumped parameter systems also has a popular research area for different engineering areas, such as automotive (Priyondoko et al., 2009; Sun et al., 2011; Yang et al., 2014) and construction (Muresan et al., 2014; Wang & Lin, 2007). In civil engineering, active and passive vibration control with tuned mass damper, active tuned mass damper, viscoelastic damper are proposed for seismic mitigation and earthquake excitation.

1.3 Scope of the Thesis

In industrial, flexible systems have begun to take place of rigid systems. Rigid systems become unwieldy compared to flexible systems. Therefore, flexible and light mechanical systems are more advantageous than rigid and heavy ones. The most commonly examples of flexible mechanical systems are robot manipulators. Flexible manipulators have smaller driving actuators, can reach high speeds due to being light and thus consume lower energy. Since flexible systems are more desirable, residual vibrations occur due to the flexibility. Elimination or suppression of these vibrations by using different control strategies is a challenging problem for researchers.

The main idea of this thesis is to develop modeling and control of flexible systems with different approaches. Some mechanical systems can be idealized as one-degree-of-freedom mass-spring-damper systems. But the system becomes more complex, it is difficult to establish mathematical model. Therefore, it is required to construct the finite element models based on finite element theory or use the commercial programs such as ANSYS to define the mathematical models of the mechanical systems. In this thesis, different methods have been used to perform vibration analysis and different passive control techniques have been applied to different systems to reduce the residual vibrations of different systems.

Different systems are investigated in this thesis such as four-degree-of freedom mass-spring damper system, single-link composite manipulator with different orientations and six axis serial robot. The mathematical model of these systems are obtained with different methods and passive vibration control strategies are applied. Both experimental and simulation results are compared to validate the accuracy of the proposed control strategies.

1.4 Organization of the Thesis

This thesis consists of seven chapters (including the introducing and the conclusions) and the appendices.

Chapter 1 presents the literature survey, scope, and organization of the thesis.

Chapter 2 presents two different method for modeling four-degree-of-freedom system: Newton's Second Law and Lagrange. Dynamic analysis of the multi-degree-of-freedom system are performed with Runge-Kutta and Newmark method and compared the results. A Passive vibration control based on the fundamental frequency of the system is presented and compared the results with Runge-Kutta and Newmark solutions. An active vibration is integrated into Newmark solution for four degree-of-freedom system, cantilever flexible beam and rotating flexible manipulator. The results of Newmark solution is compared with analytical solutions.

The systems whose mathematical models cannot be established analytically such as cantilever flexible beam and rotating flexible manipulator can be analyzed with the numerical methods. The active vibration control of cantilever flexible beam and rotating flexible manipulator is also presented with Newmark solution.

Chapter 3 presents the vibration control of a single-link flexible composite manipulator with [0/90] and [45/-45] lay-ups using the trapezoidal and triangular motion profiles. Theoretical vibration results are obtained using the finite element method and experiments are conducted to verify the finite element vibration results. Satisfactory reduction ratios are achieved theoretically and experimentally in the residual vibration amplitudes of the composite manipulator with a passive control approach.

Chapter 4 presents a vibration control of a six-axis serial robot. For the study of the robot, the members are modeled in ANSYS with ANSYS Parametric Design Language (APDL) based on the finite element theory. The simulation results obtained in ANSYS are compared with the experimental results.

Finally, in Chapter 5, the conclusions and the suggestions for the future works for mechanical systems are presented.

CHAPTER TWO

VIBRATION CONTROL OF A MULTI-DEGREE-OF-FREEDOM SYSTEM

2.1 Introduction

Many engineering systems undergo undesirable vibrations. Vibration control in mechanical systems is an important problem, by means of which vibrations are suppressed or at least attenuated. In this direction it has been common the use of passive and active vibration control such as improving various control algorithms, using active and passive dampers, active, semi-active actuators.

Hoshichima and Ikeda (1998) considered a vibration suppression problem for a mechanical transfer system, where the work is connected with the hand of a transfer machine by a spring and a damper. They introduced state equation including the jerk and acceleration of the hand to compute a state feedback gain using the Linear Quadratic Control theory. Karagülle and Malgaca (2003) examined a closed loop control on three degrees of freedom mechanical system by using Runge-Kutta Method.

Benosman & LeVey (2004) presented a survey on control of residual vibrations at robots and flexible structures. Dynamic analysis of flexible robots investigated with classification of one axis, two axis and multi axis (Dwivedy & Eberhard, 2006). Active and passive control can apply for controlling of the residual vibrations (Preumont, 2002). Residual vibrations of flexible structures can decrease by changing motion commands with open loop control (Pereira et al., 2012; Mimmi and Pennacchi, 2001; Shan et al., 2005). Diken and Alghamdi (2003) applied the control for controlling the residual vibrations on rotating an aluminum beam by using motion profile.

2.2 Mathematical Model of the System

The system in Figure 2.1 is considered as an example to obtain the mathematical model.

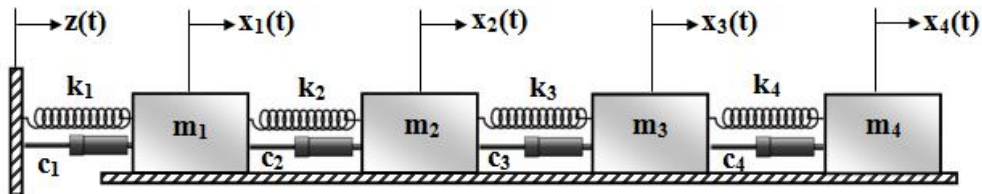


Figure 2.1 4-DOF mass-damper-spring system ($m_1=m_2=m_3=m_4=1$ kg, $c_1=1.5$ Ns/m, $c_2=1.2$ Ns/m, $c_3=c_4=0.8$ Ns/m, $k_1=600$ N/m, $k_2=400$ N/m, $k_3=k_4=200$ N/m).

The parameters in the figure m_1 , m_2 , m_3 , m_4 and c_1 , c_2 , c_3 , c_4 and k_1 , k_2 , k_3 , k_4 are the masses, the dampers and the spring constants, respectively. The parameters $x_1(t)$, $x_2(t)$, $x_3(t)$ and $x_4(t)$ are the displacement of each mass. $z(t)$ is the base excitation as the input of the open loop system. t is the time. The displacement $x_4(t)$ of the end mass is evaluated as the open loop system response.

In this chapter, two different methods will be used to derive the equation of motion of the system: Newton's Second Law and Lagrange's Equation. Newton method needs to draw free-body diagram of the masses or rigid body diagram and indicate all the active and reactive forces acting on the masses or rigid body. Lagrange's equation uses kinetic energy, potential energy and virtual work of the system to obtain equation of motion.

2.2.1 Newton's Second Law of Motion

Newton's second law of motion can be stated as follows: *The rate of change of momentum of a mass is equal to the force acting on it* (Rao, 2011).

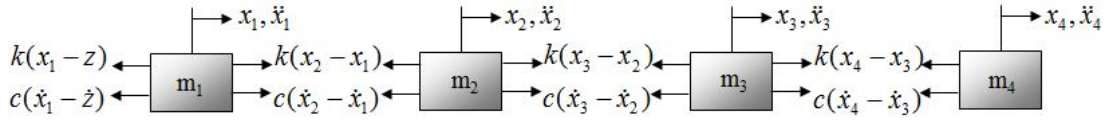


Figure 2.2 Free-body diagram of the system

If mass m is displaced a distance $\vec{x}(t)$ when acted upon by a resultant force $\vec{F}(t)$ in the same direction, Newton's second law of motion gives

$$\vec{F}(t) = m\ddot{\vec{x}}(t) \quad (2.1)$$

Applying Equation 2.1 to each mass for the static equilibrium

$$-k_1(x_1 - z) - c_1(\dot{x}_1 - \dot{z}) + k_2(x_2 - x_1) + c_2(\dot{x}_2 - \dot{x}_1) = m_1\ddot{x}_1 \quad (2.2)$$

$$-k_2(x_2 - x_1) - c_2(\dot{x}_2 - \dot{x}_1) + k_3(x_3 - x_2) + c_3(\dot{x}_3 - \dot{x}_2) = m_2\ddot{x}_2 \quad (2.3)$$

$$-k_3(x_3 - x_2) - c_3(\dot{x}_3 - \dot{x}_2) + k_4(x_4 - x_3) + c_4(\dot{x}_4 - \dot{x}_3) = m_3\ddot{x}_3 \quad (2.4)$$

$$-k_4(x_4 - x_3) - c_4(\dot{x}_4 - \dot{x}_3) = m_4\ddot{x}_4 \quad (2.5)$$

Equations 2.2-2.5 can be arranged as

$$m_1\ddot{x}_1 + (c_1 + c_2)\dot{x}_1 - c_2\dot{x}_2 + (k_1 + k_2)x_1 - k_2x_2 = k_1z + c_1\dot{z} \quad (2.6)$$

$$m_2\ddot{x}_2 + c_2\dot{x}_1 + (c_2 + c_3)\dot{x}_2 + c_3\dot{x}_3 + k_2x_1 + (k_2 + k_3)x_2 - k_3x_3 = 0 \quad (2.7)$$

$$m_3\ddot{x}_3 + c_3\dot{x}_2 + (c_3 + c_4)\dot{x}_3 + c_4\dot{x}_4 + k_3x_2 + (k_3 + k_4)x_3 - k_4x_4 = 0 \quad (2.8)$$

$$m_4\ddot{x}_4 - c_4\dot{x}_3 + c_4\dot{x}_4 - k_4x_3 + k_4x_4 = 0 \quad (2.9)$$

2.2.2 Lagrange's Equation

The equations of motion of a vibrating system can often be derived in terms of generalized coordinates by using Lagrange's equations. Lagrange's equations can be stated, for a n -degree-of-freedom, as

$$\frac{d}{dt} \left(\frac{\partial L}{\partial \dot{q}_j} \right) - \frac{\partial L}{\partial q_j} = Q_j, \quad j = 1, 2, \dots, n \quad (2.10)$$

where, q is generalized coordinate for j , $\dot{q}_j = \partial q_j / \partial t$ is the generalized velocity, Q_j is the generalized force corresponding to the generalized coordinate q_j . The forces represented by generalized force Q_j may be damping forces or external forces acting on the system. L is the Lagrangian which is given by

$$L = T - V \quad (2.11)$$

Here, T is kinetic energy and V is potential energy of the system. The terms of kinetic energy, potential energy and virtual work are derived to obtain the equations of motion of the system.

For the system in Figure 2.1, $q_1 = x_1$, $q_2 = x_2$, $q_3 = x_3$ and $q_4 = x_4$. The kinetic energy of the system is given by

$$T = \frac{1}{2} m_1 \dot{x}_1^2 + \frac{1}{2} m_2 \dot{x}_2^2 + \frac{1}{2} m_3 \dot{x}_3^2 + \frac{1}{2} m_4 \dot{x}_4^2 \quad (2.12)$$

The potential energy of the system can be written as

$$V = \frac{1}{2} k_1 (x_1 - z)^2 + \frac{1}{2} k_2 (x_2 - x_1)^2 + \frac{1}{2} k_3 (x_3 - x_2)^2 + \frac{1}{2} k_4 (x_4 - x_3)^2 \quad (2.13)$$

And the final term, virtual work of the system is given by

$$\begin{aligned} \delta W = & -c_1 (\dot{x}_1 - \dot{z}) \delta (x_1 - z) - c_2 (\dot{x}_2 - \dot{x}_1) \delta (x_2 - x_1) \\ & - c_3 (\dot{x}_3 - \dot{x}_2) \delta (x_3 - x_2) - c_4 (\dot{x}_4 - \dot{x}_3) \delta (x_4 - x_3) \end{aligned} \quad (2.14)$$

Since $z(t)$ is the base excitation as the input, this term cannot be taken as generalized coordinate. So, Equation 2.14 can be arranged as follows

$$\begin{aligned} \delta W = & (c_1 \dot{z} - (c_1 + c_2) \dot{x}_1 + c_2 \dot{x}_2) \delta x_1 + (c_2 \dot{x}_1 - (c_2 + c_3) \dot{x}_2 + c_3 \dot{x}_2) \delta x_2 \\ & (c_3 \dot{x}_2 - (c_3 + c_4) \dot{x}_3 + c_4 \dot{x}_4) \delta x_3 + (c_4 \dot{x}_3 - c_4 \dot{x}_4) \delta x_4 \end{aligned} \quad (2.15)$$

Since there is no term of \dot{x} in the potential energy and x in the kinetic energy, these terms tend to zero. Equation 2.10 can be arranged for this system as

$$\frac{d}{dt} \left(\frac{\partial E_1}{\partial \dot{q}_j} \right) + \frac{\partial E_2}{\partial q_j} = Q_j, \quad j = 1, 2, \dots, n \quad (2.16)$$

By differentiating the expressions of kinetic energy and potential energy required by Equation 2.16 and substituting Equation 2.15 into resulting generalized force for each generalized coordinates, the equation of motion of the system can be obtained. The equation of motion of the system for the generalized coordinate x_1 can be written as

$$\begin{aligned} & \frac{d}{dt} \left(\frac{\partial \left(\frac{1}{2} m_1 \dot{x}_1^2 + \frac{1}{2} m_2 \dot{x}_2^2 + \frac{1}{2} m_3 \dot{x}_3^2 + \frac{1}{2} m_4 \dot{x}_4^2 \right)}{\partial \dot{x}_1} \right) \\ & + \frac{\partial \left(\frac{1}{2} k_1 (x_1 - z)^2 + \frac{1}{2} k_2 (x_2 - x_1)^2 + \frac{1}{2} k_3 (x_3 - x_2)^2 + \frac{1}{2} k_4 (x_4 - x_3)^2 \right)}{\partial x_1} \\ & = c_1 \dot{z} - (c_1 + c_2) \dot{x}_1 + c_2 \dot{x}_2 \end{aligned} \quad (2.17)$$

Derivating the first terms in the bracket with respect to \dot{x}_1 and the second term with respect to x_1

$$\frac{d}{dt} (m_1 \dot{x}_1) + k_1 (x_1 - z) - k_2 (x_2 - x_1) = c_1 \dot{z} - (c_1 + c_2) \dot{x}_1 + c_2 \dot{x}_2 \quad (2.18)$$

Derivating the terms in the first bracket with respect to t

$$m_1\ddot{x}_1 + k_1(x_1 - z) - k_2(x_2 - x_1) = c_1\dot{z} - (c_1 + c_2)\dot{x}_1 + c_2\dot{x} \quad (2.19)$$

So, the mathematical model of the system for the generalized coordinate x_1 can be represented as

$$m_1\ddot{x}_1 + (c_1 + c_2)\dot{x}_1 - c_2\dot{x}_2 + (k_1 + k_2)x_1 - k_2x_2 = k_1z + c_1\dot{z} \quad (2.20)$$

The same processes are applied to the other generalized coordinates x_2 , x_3 and x_4 along Equation 2.17-2.19, the equations of motion of the system are found as follows

$$m_2\ddot{x}_2 - c_2\dot{x}_1 + (c_2 + c_3)\dot{x}_2 - c_3\dot{x}_3 - k_2x_1 + (k_2 + k_3)x_2 - k_3x_3 = 0 \quad (2.21)$$

$$m_3\ddot{x}_3 - c_3\dot{x}_2 + (c_3 + c_4)\dot{x}_3 - c_4\dot{x}_4 - k_3x_2 + (k_3 + k_4)x_3 - k_4x_4 = 0 \quad (2.22)$$

$$m_4\ddot{x}_4 - c_4\dot{x}_3 + c_4\dot{x}_4 - k_4x_3 + k_4x_4 = 0 \quad (2.23)$$

The equation of motion for the multi-degrees of freedom vibrating system is given as

$$\mathbf{M}\ddot{\mathbf{q}} + \mathbf{C}\dot{\mathbf{q}} + \mathbf{K}\mathbf{q} = \mathbf{u} \quad (2.24)$$

where \mathbf{M} , \mathbf{C} , and \mathbf{K} are the mass, damping, and rigidity square matrices, respectively. $\mathbf{q}=[x_1, x_2, x_3, x_4]^T$ where T stands for the transpose. \mathbf{u} is the input column vector. The following matrices are found:

$$\mathbf{M} = \begin{bmatrix} m_1 & 0 & 0 & 0 \\ 0 & m_2 & 0 & 0 \\ 0 & 0 & m_3 & 0 \\ 0 & 0 & 0 & m_4 \end{bmatrix}$$

$$\mathbf{C} = \begin{bmatrix} c_1 + c_2 & -c_2 & 0 & 0 \\ -c_2 & c_2 + c_3 & -c_3 & 0 \\ 0 & -c_3 & c_3 + c_4 & -c_4 \\ 0 & 0 & -c_4 & c_4 \end{bmatrix}$$

$$\mathbf{K} = \begin{bmatrix} k_1 + k_2 & -k_2 & 0 & 0 \\ -k_2 & k_2 + k_3 & -k_3 & 0 \\ 0 & -k_3 & k_3 + k_4 & -k_4 \\ 0 & 0 & -k_4 & k_4 \end{bmatrix}$$

and

$$\mathbf{u} = [k_1 z(t) + c_1 \dot{z}(t), 0, 0, 0]^T. \quad (2.25)$$

2.2.3 Eigenvalue Problem

The following eigenvalue equation is solved to find undamped natural frequencies, ω , (Kuo & Golnaraghi, 2003).

$$|-\omega^2 \mathbf{M} + \mathbf{K}| = 0 \quad (2.26)$$

The undamped natural frequencies are found as 1.042, 2.738, 3.899 and 5.652 Hz.

2.3 Passive Vibration Control of 4-DOF Mechanical System

In this section, passive control of residual vibrations will be evaluated on four degrees of freedom flexible mechanical system with base excitation which has existing analytical solution. The system is indicated in Figure 2.1.

To model of the input, the trapezoidal profile which is taken into account for the instantaneous values of z is shown in Figure 2.3.

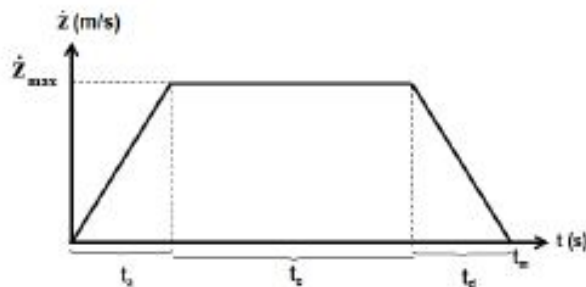


Figure 2.3 Trapezoidal velocity profile

Here, t_a is rising acceleration time, t_c is passing time with constant speed, t_d is deceleration time, \dot{z}_{\max} is maximum velocity and t_m is the motion time. In trapezoidal velocity profile, \dot{z}_{\max} and t_m are determined

$$\dot{z}_{\max} = \frac{d_0}{t_m - 0.5t_a - 0.5t_d} \quad (2.27)$$

$$t_m = t_a + t_c + t_d \quad (2.28)$$

At the calculation of the maximum velocity, d_0 is replaced which belongs to ground input. Two different velocity profile is considered for residual vibrations control:

1. Triangular velocity profile
2. Trapezoidal velocity profile

Equations (2.27) and (2.28) are the equations for calculating trapezoidal velocity profiles. In Equation (2.28), in the case of $t_c=0$ the velocity profile shown in Figure 2.3 becomes the triangular velocity profile. In triangular velocity profile, \dot{z}_{\max} and t_m are determined

$$\dot{z}_{\max} = \frac{d_0}{0.5t_a + 0.5t_d} \quad (2.29)$$

$$t_m = t_a + t_d \quad (2.30)$$

In the literature, residual vibrations are reduced with the motion control of mostly one link robot manipulators. In the studies, it is emphasized that the vibration control is established when t_a is chosen equal to the multiples of the period of the first natural frequency of the system for triangular and cycloid velocity profiles.

Controlling residual vibrations of the vibration system can be reduced by arranging the calculation of time parameters of these velocity profiles based on the knowledge of the system dynamics.

In this instance, one of the time parameters can be determined with the equations as shown below according to Equation (2.28) in trapezoidal velocity profile or Equation (2.30) in triangular velocity profile.

$$t_{jh} = \frac{1}{2f_{jd}} \quad (2.31)$$

Here f_{jd} is damped natural frequency corresponding to the j th natural frequency in Hz of the vibration system shown in Figure 2.1. t_{jh} is the calculated time by considering the j th natural frequency of the system. In velocity profiles, the values of time parameters can be obtained as the multiples of t_{1h} , t_{2h} , t_{3h} or t_{4h} .

Let the time parameters belongs to velocity profile be $t_i = [t_a, t_c, t_d, t_m]$. Assume that the displacement (d_0) and motion time (t_m) are known. $t_c = 0$ for triangular velocity profile and for example the deceleration time is determined as $t_d = t_{1h}$. In this case, t_a can be calculated from the Equation (2.30). Accordingly, velocity profile parameters are arranged as $t_i = [*, 0, t_{1h}, t_m]$. Maximum velocity is calculated from the Equation (2.29). If trapezoidal velocity profile is applied, velocity profile can be arranged as $t_i = [*, t_{1h}, t_{1h}, t_m]$. Here $t_c = t_{1h}$, $t_d = t_{1h}$, t_a can be calculated from the Equation (2.28) and maximum velocity can be calculated from the Equation (2.27).

Natural frequencies of the system are determined by taking the motion inputs $z=0$ and $\dot{z} = 0$ in Equation (2.26). Undamped natural frequencies of the system are determined as $f_{n1}=1.042$ Hz, $f_{n2}=2.738$ Hz, $f_{n3}=3.899$ Hz and $f_{n4}=5.652$ Hz. The damping ratio corresponding to the first natural frequency is 0.011, the damping ratio corresponding to the second natural frequency is 0.029, the damping ratio corresponding to the third natural frequency is 0.041 and the damping ratio corresponding to the fourth natural frequency is 0.052. Accordingly, damped natural frequencies of the system are calculated as $f_{d1}=1.042$ Hz, $f_{d2}=2.737$ Hz, $f_{d3}=3.894$ Hz and $f_{d4}=5.644$ Hz, respectively.

Let the numerical values belong to motion inputs of the system be $d_0=0.05$ m and $t_m=2$ s. In the case of the system input is triangular profile, velocity and displacement graphics are shown in Figure 2.4.

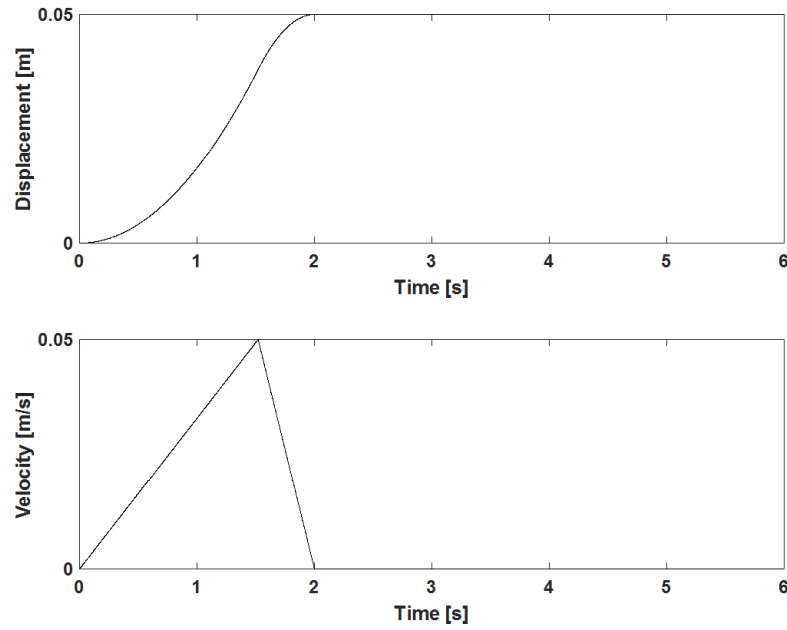


Figure 2.4 Triangular velocity profile $t_i=[1.5202,0,0.4798,2]$

The residual vibrations of the vibration system can be solved numerically such as Runge-Kutta and Newmark method. Thus, desired displacement and acceleration responses of the end point can be obtained based on time. In Runge-Kutta method, the equations of motion of the system are arranged as state variable. In Newmark method, the equations of motion of the system are written as matrix form.

2.3.1 Runge-Kutta Method

Until about 1970, the most Runge-Kutta method has probably been the original classical formula that is a generalization of Simpson's rule (Atkinson, 1989). The method is

$$y_{n+1} = y_n + \frac{h}{6}[V_1 + 2V_2 + 2V_3 + V_4] \quad (2.32)$$

$$\begin{aligned} V_1 &= f(t_n, y_n) & V_2 &= f\left(t_n + \frac{1}{2}h, y_n + \frac{1}{2}hV_1\right) \\ V_3 &= f\left(t_n + \frac{1}{2}h, y_n + \frac{1}{2}hV_2\right) & V_4 &= f(t_n + h, y_n + hV_3) \end{aligned} \quad (2.33)$$

Here y_{n+1} is the Runge-Kutta approximation of $y(t_{n+1})$, and the next value (y_{n+1}) is determined by the present value y_n plus the weighted average of four increments, where each increment is the product of the size of the interval, h , and an estimated slope specified by function f on the right-hand side of the differential equation.

The mathematical model of the system given in Equations (2.6-2.9) can be written as state-space form.

$$\begin{aligned}
\dot{x}_1 &= v_1 \\
\dot{x}_2 &= v_2 \\
\dot{x}_3 &= v_3 \\
\dot{x}_4 &= v_4 \\
\dot{v}_1 &= -\frac{(c_1 + c_2)}{m_1} v_1 + \frac{c_2}{m_1} v_2 - \frac{(k_1 + k_2)}{m_1} x_1 + \frac{k_2}{m_1} x_2 + \frac{c_1}{m_1} \dot{z} + \frac{k_1}{m_1} z \\
\dot{v}_2 &= \frac{c_2}{m_2} v_1 - \frac{c_2 + c_3}{m_2} v_2 + \frac{c_3}{m_2} v_3 + \frac{k_2}{m_2} x_1 - \frac{k_2 + k_3}{m_2} x_2 + \frac{k_3}{m_2} x_3 \\
\dot{v}_3 &= \frac{c_3}{m_3} v_2 - \frac{c_3 + c_4}{m_3} v_3 + \frac{c_4}{m_3} v_4 + \frac{k_3}{m_3} x_2 - \frac{k_3 + k_4}{m_3} x_3 + \frac{k_4}{m_3} x_4 \\
\dot{v}_4 &= \frac{c_4}{m_4} v_3 - \frac{c_4}{m_4} v_4 + \frac{k_4}{m_4} x_3 - \frac{k_4}{m_4} x_4
\end{aligned} \tag{2.34}$$

The state-space form can be arranged as matrix form.

$$\begin{Bmatrix} \dot{x}_1 \\ \dot{x}_2 \\ \dot{x}_3 \\ \dot{x}_4 \\ \dot{v}_1 \\ \dot{v}_2 \\ \dot{v}_3 \\ \dot{v}_4 \end{Bmatrix} = \begin{bmatrix} 0 & 0 & 0 & 0 & 1 & 0 & 0 & 0 \\ 0 & 0 & 0 & 0 & 0 & 1 & 0 & 0 \\ 0 & 0 & 0 & 0 & 0 & 0 & 1 & 0 \\ 0 & 0 & 0 & 0 & 0 & 0 & 0 & 1 \\ -\frac{k_1 + k_2}{m_1} & \frac{k_2}{m_1} & 0 & 0 & -\frac{c_1 + c_2}{m_1} & \frac{c_2}{m_1} & 0 & 0 \\ \frac{k_2}{m_2} & -\frac{k_2 + k_3}{m_2} & \frac{k_3}{m_2} & 0 & \frac{c_2}{m_2} & -\frac{c_2 + c_3}{m_2} & \frac{c_3}{m_2} & 0 \\ \frac{k_3}{m_3} & -\frac{k_3 + k_4}{m_3} & \frac{k_4}{m_3} & 0 & 0 & \frac{c_3}{m_3} & -\frac{c_3 + c_4}{m_3} & \frac{c_4}{m_3} \\ 0 & \frac{k_4}{m_4} & -\frac{k_4}{m_4} & 0 & 0 & \frac{c_4}{m_4} & -\frac{c_4}{m_4} & 0 \\ 0 & 0 & \frac{k_4}{m_4} & -\frac{k_4}{m_4} & 0 & 0 & \frac{c_4}{m_4} & -\frac{c_4}{m_4} \end{bmatrix} \begin{Bmatrix} x_1 \\ x_2 \\ x_3 \\ x_4 \\ v_1 \\ v_2 \\ v_3 \\ v_4 \end{Bmatrix} + \begin{bmatrix} 0 & 0 \\ 0 & 0 \\ 0 & 0 \\ 0 & 0 \\ \frac{c_1}{m_1} & \frac{k_1}{m_1} \\ 0 & 0 \\ 0 & 0 \\ 0 & 0 \end{bmatrix} \begin{Bmatrix} \dot{z} \\ z \end{Bmatrix} \tag{2.35}$$

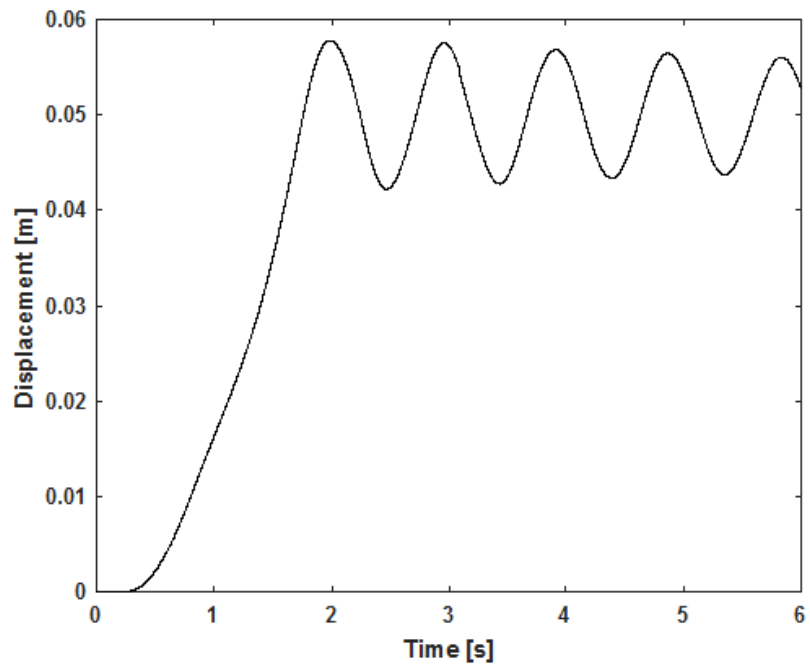
Here, $x_1(t)$, $x_2(t)$, $x_3(t)$ and $x_4(t)$ denote the displacements of the masses, $v_1(t)$, $v_2(t)$, $v_3(t)$ and $v_4(t)$ denote the velocity of the masses. These equations can be solved by Runge-Kutta method. Instantaneous values of $x_1(t)$, $x_2(t)$, $x_3(t)$, $x_4(t)$, $v_1(t)$, $v_2(t)$, $v_3(t)$ and $v_4(t)$ are determined with Δt interval starting from $t=0$. Instantaneous values of z and \dot{z} at the right hand side of the equation is necessary. In base excitation system, \dot{z} is the velocity of the input and z is displacement input which is the integral of the velocity input.

In the solution of Runge-Kutta method, displacements and velocity inputs are prepared to evaluate residual vibrations as shown in Figure 2.4. The time signal is arranged as $t=t_m+4$, so residual vibrations are determined for 4 s. Vibration response of $x_4(t)$ of the end point of the system obtaining by Runge-Kutta method are shown in Figure 2.5.

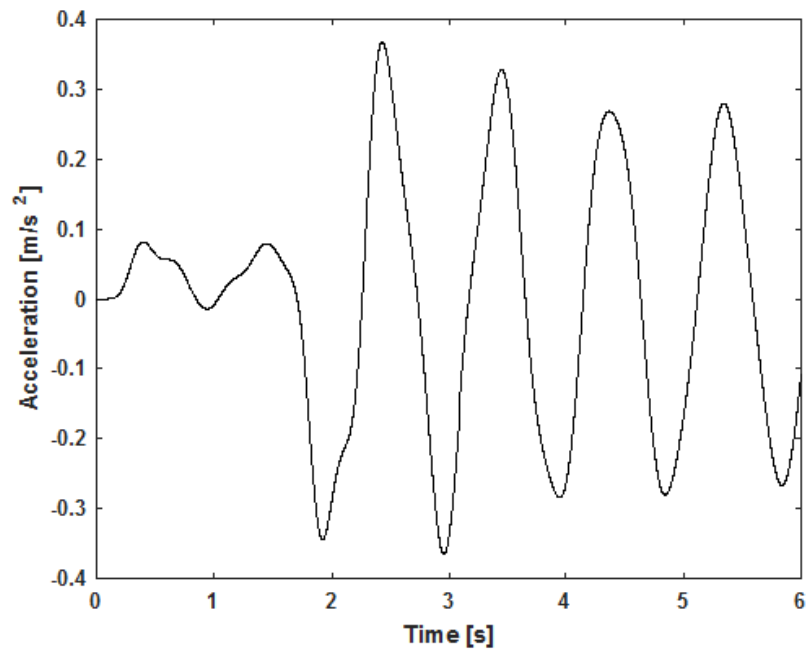
As seen in Figure 2.5, the end point of the system reaches 0.05 m in 2 s. In order to observe the residual vibrations better, displacement value (d_0) is subtracted from the response and the response between 2-6 s obtained after motion is shown in Figure 2.6.

Applying the motion input as triangular velocity profile, it is observed that the residual vibration levels are high for $t_d=t_{1h}$, and residual vibration levels are significantly decreased for $t_d=2t_{1h}$. The reduction in vibration levels can be given numerically by calculating RMS values of residual vibration signals. RMS values of residual vibration signals reduced from 0.0078 m for $t_d=t_{1h}$ to $2.6462e-4$ m for $t_d=2t_{1h}$ and 99.66% reduction in vibration level has been achieved.

The results are given in Table 2.1 for the different time parameters.

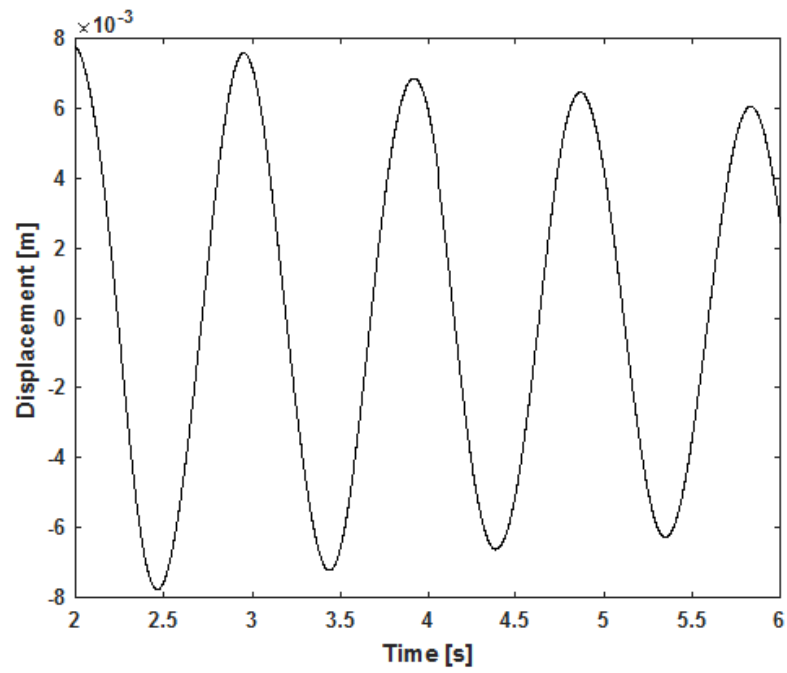


a)

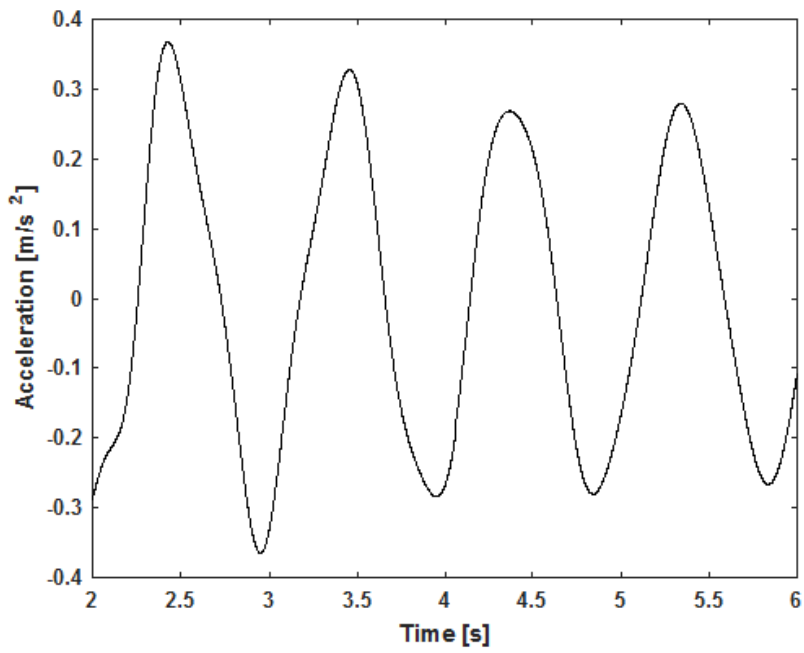


b)

Figure 2.5 Time response of the end point for the triangular velocity profile a) Displacement and b) Acceleration



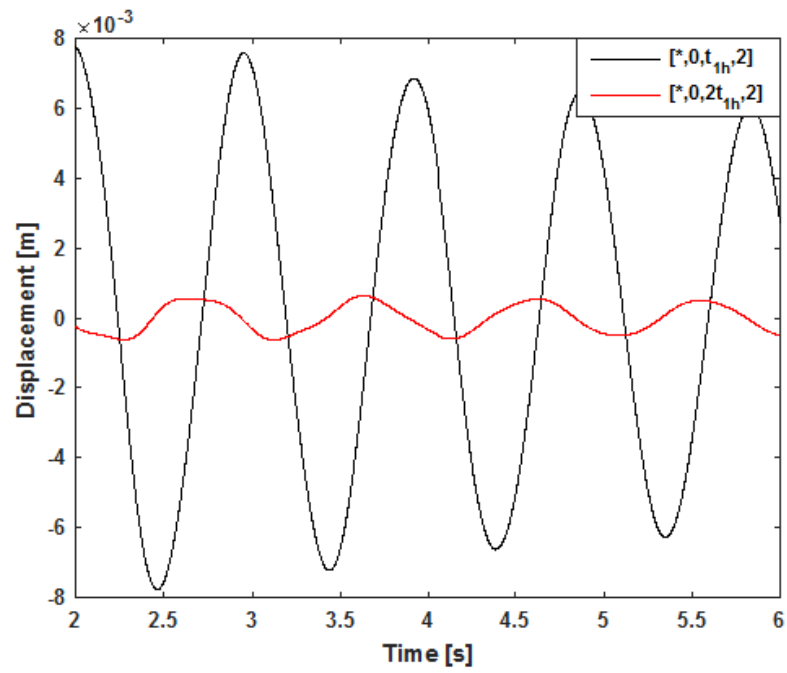
a)



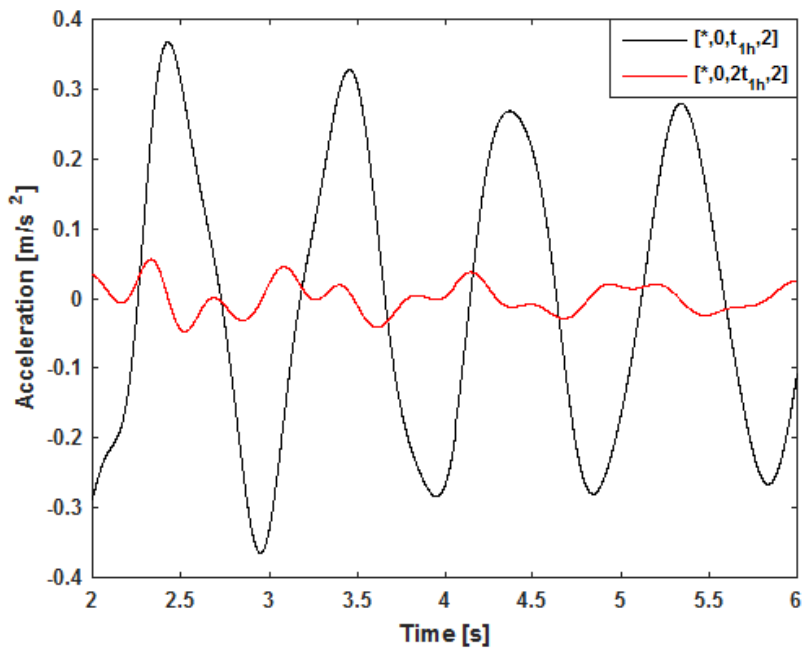
b)

Figure 2.6 Residual vibrations of the end point for triangular velocity profile a) Displacement and b) Acceleration

Arranging motion inputs as $\mathbf{t}_i = [*, 0, 2t_{1h}, t_m]$ to reduce the residual vibrations, the response is shown in Figure 2.7. The calculated value is indicated with “*” in \mathbf{t}_i .

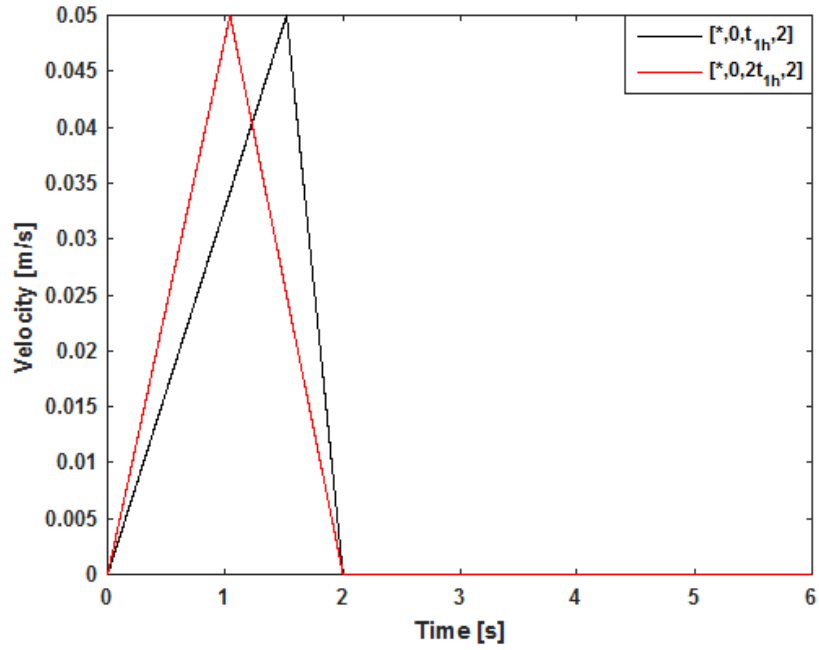


(a)



b)

Figure 2.7 Residual vibrations of the end point for the triangular velocity profile a) Displacement, b) Acceleration and c) Input profile



c)

Figure 2.7 Residual vibrations of the end point for the triangular velocity profile a) Displacement, b) Acceleration and c) Input profile (cont.)

Table 2.1 Motion input

Motion	$t_i=[*,0,t_{1h},t_m]$	\dot{z}_{max} (m/s)	RMS (m)	Reduction %	RMS (m/s²)
Case1_a	[*,0, t _{1h} ,t _m]	0.05	0.0078	-	0.2856
Case1_b	[*,0, 2t _{1h} ,t _m]	0.05	2.6462e-04	99.66	0.0336
Case1_c	[*,0, 3t _{1h} ,t _m]	0.05	0.0066	15.82	0.2081
Case1_d	[*,0, 4t _{1h} ,t _m]	0.05	0.0019	97.56	0.06
Case2_a	[*,0, t _{2h} ,t _m]	0.05	0.0049	-	0.0575
Case2_b	[*,0, 2t _{2h} ,t _m]	0.05	0.0085	-	0.4052
Case2_c	[*,0, 3t _{2h} ,t _m]	0.05	0.0066	-	0.2237
Case2_d	[*,0, 4t _{2h} ,t _m]	0.05	0.0028	-	0.1298
Case3_a	[*,0, t _{3h} ,t _m]	0.05	0.0033	-	0.0123
Case3_b	[*,0, 2t _{3h} ,t _m]	0.05	0.0069	-	0.2160
Case3_c	[*,0, 3t _{3h} ,t _m]	0.05	0.0086	-	0.4015
Case3_d	[*,0, 4t _{3h} ,t _m]	0.05	0.0072	-	0.2481
Case4_a	[*,0, t _{4h} ,t _m]	0.05	0.0022	-	0.0045
Case4_b	[*,0, 2t _{4h} ,t _m]	0.05	0.0047	-	0.05
Case4_c	[*,0, 3t _{4h} ,t _m]	0.05	0.0071	-	0.2396
Case4_d	[*,0, 4t _{4h} ,t _m]	0.05	0.0085	-	0.4016

Analyzing the results of motion inputs, it is observed that the even multiples of t_{1h} has more effective reduction compared to odd multiples of t_{1h} .

Arranging the motion input as choosing f_{1d} , the reduction of vibration levels is %99.66, arranging the motion input as choosing f_{2d} , f_{3d} or f_{4d} , there is no reduction of vibration level between cases. Evaluating RMS values of residual vibrations, it is observed that the first natural frequency f_{1d} is more effective for vibration control.

2.3.2 Newmark Method

The Newmark solution (Newmark, 1959) is given below. A time step, Δt , is chosen for the solution as $\Delta t < 1/(20f_{\max})$, where f_{\max} is the highest natural frequency considered. Δt is taken as 0.0088 s. Knowing the solution at a time step, the solution at the subsequent time step is found by the numerical integration. t_n and t_{n+1} are the successive values for the time, and $\Delta t = t_{n+1} - t_n$. The solution is given as

$$(\mathbf{a}_0 \mathbf{M} + \mathbf{a}_1 \mathbf{C} + \mathbf{K}) \mathbf{q}_{n+1} = \mathbf{u} + \mathbf{M}(\mathbf{a}_0 \mathbf{q}_n + \mathbf{a}_2 \dot{\mathbf{q}}_n + \mathbf{a}_3 \ddot{\mathbf{q}}_n) + \mathbf{C}(\mathbf{a}_1 \mathbf{q}_n + \mathbf{a}_4 \dot{\mathbf{q}}_n + \mathbf{a}_5 \ddot{\mathbf{q}}_n) \quad (2.36)$$

$$\ddot{\mathbf{q}}_{n+1} = \mathbf{a}_0 (\mathbf{q}_{n+1} - \mathbf{q}_n) - \mathbf{a}_2 \dot{\mathbf{q}}_n - \mathbf{a}_3 \ddot{\mathbf{q}}_n, \quad \dot{\mathbf{q}}_{n+1} = \mathbf{q}_n + \mathbf{a}_6 \ddot{\mathbf{q}}_n + \mathbf{a}_7 \ddot{\mathbf{q}}_{n+1} \quad (2.37)$$

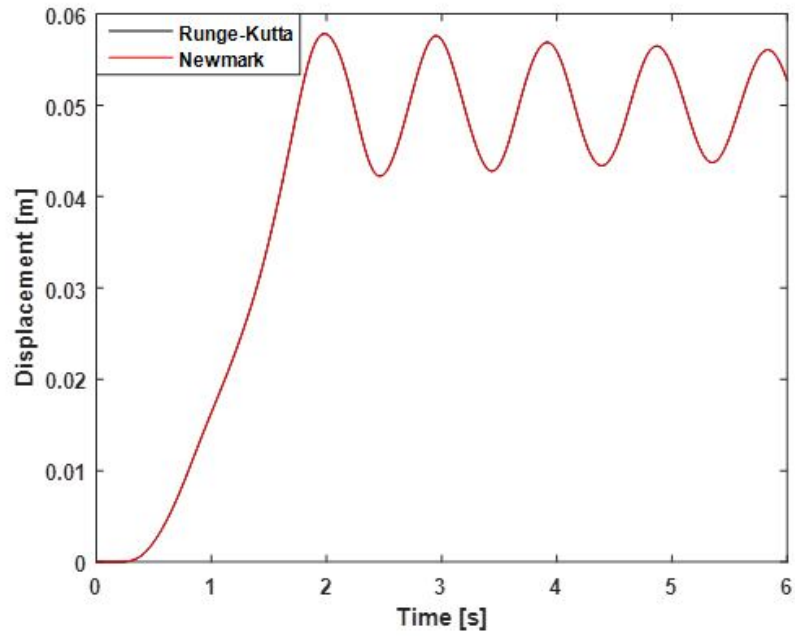
where

$$\begin{aligned} \mathbf{a}_0 &= \frac{1}{\alpha \Delta t^2}, & \mathbf{a}_1 &= \frac{\delta}{\alpha \Delta t}, & \mathbf{a}_2 &= \frac{1}{\alpha \Delta t}, & \mathbf{a}_3 &= \frac{1}{2\alpha} - 1, & \mathbf{a}_4 &= \frac{\delta}{\alpha} - 1, \\ \mathbf{a}_5 &= \frac{\Delta t}{2} \left(\frac{\delta}{\alpha} - 2 \right), & \mathbf{a}_6 &= \Delta t(1 - \delta), & \mathbf{a}_7 &= \delta \Delta t, \\ \alpha &= \frac{1}{4}(1 + \gamma)^2, & \delta &= \frac{1}{2} + \gamma \end{aligned} \quad (2.38)$$

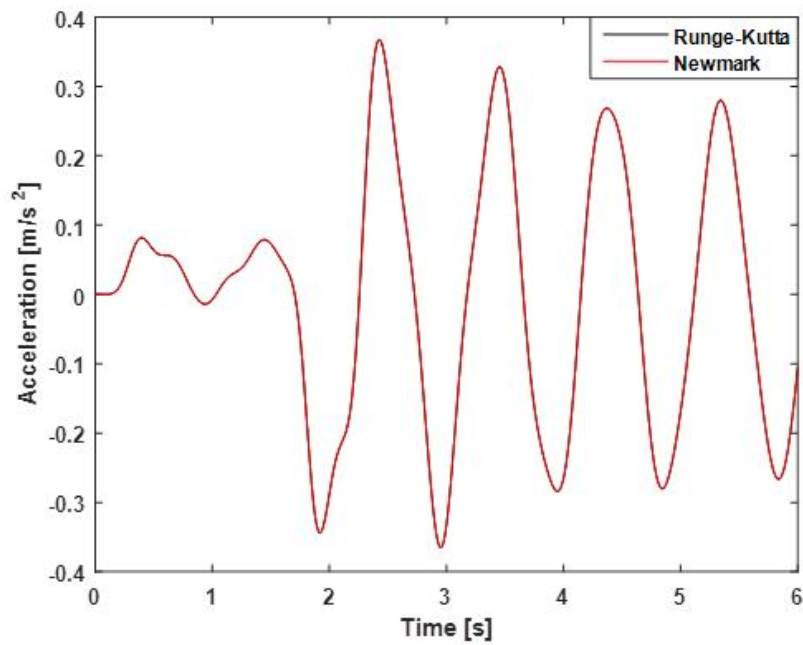
γ is the amplitude decay factor.

Mass \mathbf{M} , damping \mathbf{C} and stiffness \mathbf{K} matrices are defined for Newmark method. System matrices \mathbf{M} , \mathbf{C} and \mathbf{K} are $n \times n$ square matrices. For the system shown in Figure 2.1, $n=4$, because the system has four degrees of freedom. Input matrix \mathbf{u} which has $n \times 1$ column matrix is also defined.

Using the Equations (2.36-2.38), same triangular velocity profile given in Figure 2.4 is applied into Newmark solution and the results are compared with the results obtained by Runge-Kutta Method. The superposed results are given in Figure 2.8.

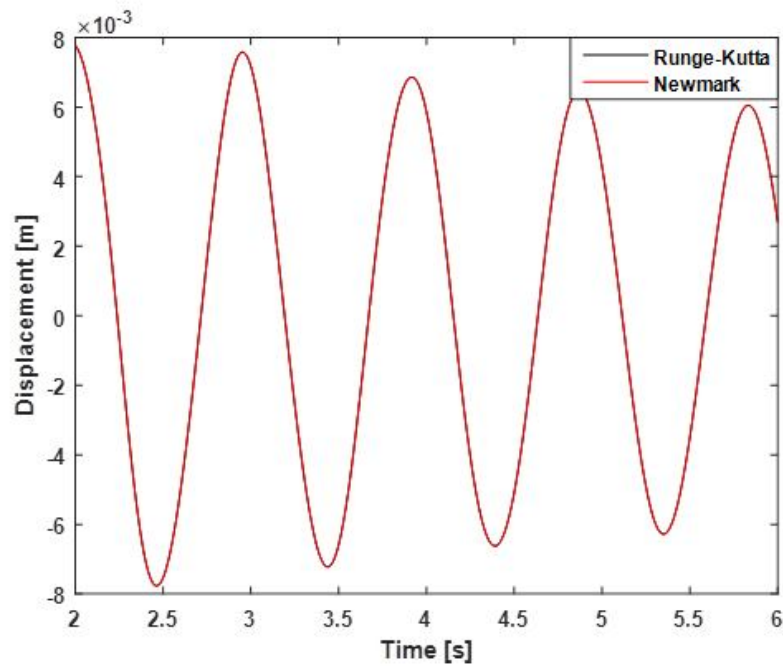


(a)

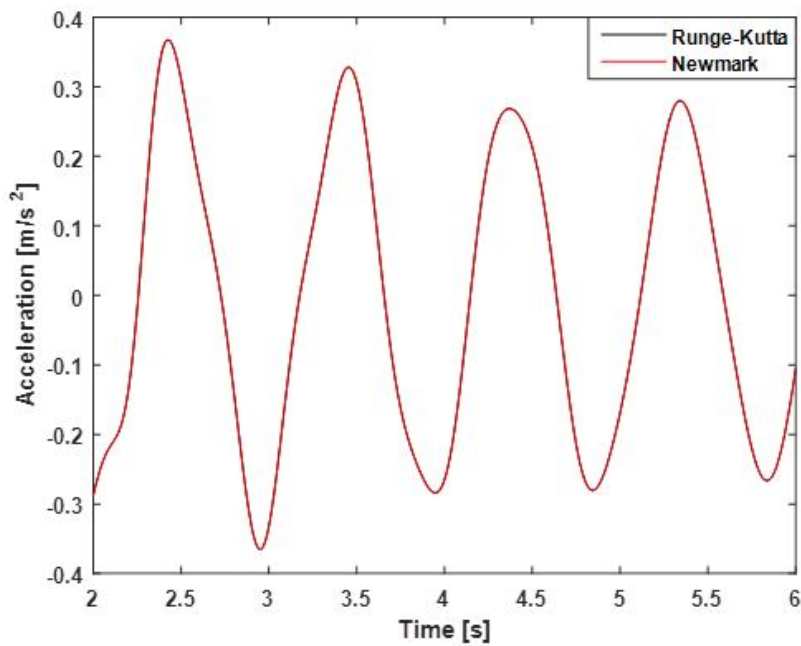


b)

Figure 2.8 Newmark and Runge-Kutta superposed for $[*,0,t_{1h},2]$ a) Displacement and b) Acceleration



a)



b)

Figure 2.9 Residual vibrations of Newmark and Runge-Kutta superposed for $[*,0,t_{th},2]$ a) Displacement and b) Acceleration

As shown in Figure 2.8 and Figure 2.9, the time responses obtained by Newmark and Runge-Kutta method are in good agreement. It is shown that dynamic responses

of the systems can be solved with numerical analysis such as Newmark or Runge-Kutta.

To emphasize the effect of multiples of t_{1h} in vibration control, the trapezoidal velocity input is also studied. Unlike the triangular velocity profile, different parameters can be considered for trapezoidal velocity input such as the acceleration time (t_{accel}), the deceleration time (t_{decel}) and the constant velocity time (t_{con}). The system can be reached the desired displacement with different time parameters in the same time duration.

Let the numerical values belong to motion inputs of the system be $d_0=0.05$ m, $t_{con}=t_{1h}$, $t_{decel}=t_{1h}$ and $t_m=4$ s. Acceleration time t_{accel} is determined as given in Equation (2.28). In the case of the system input is trapezoidal profile, velocity and displacement graphics are shown in Figure 2.10.

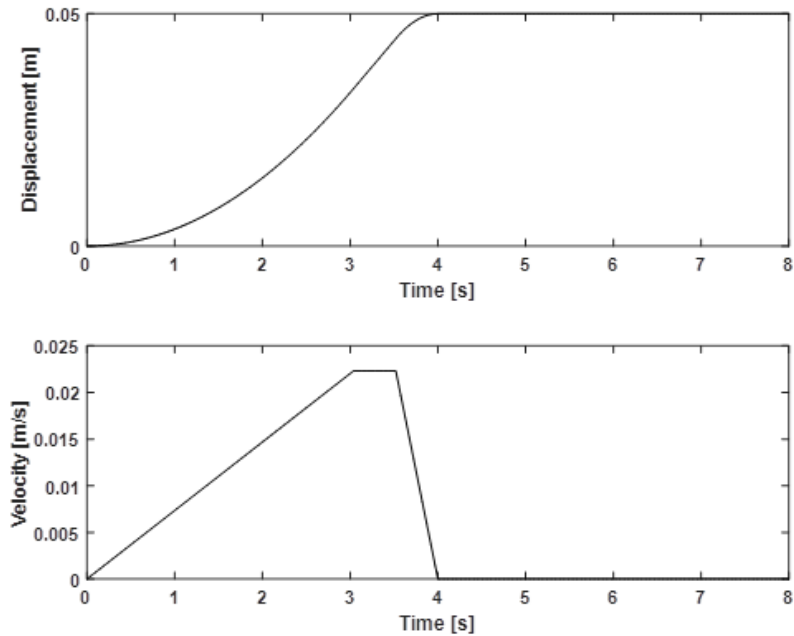
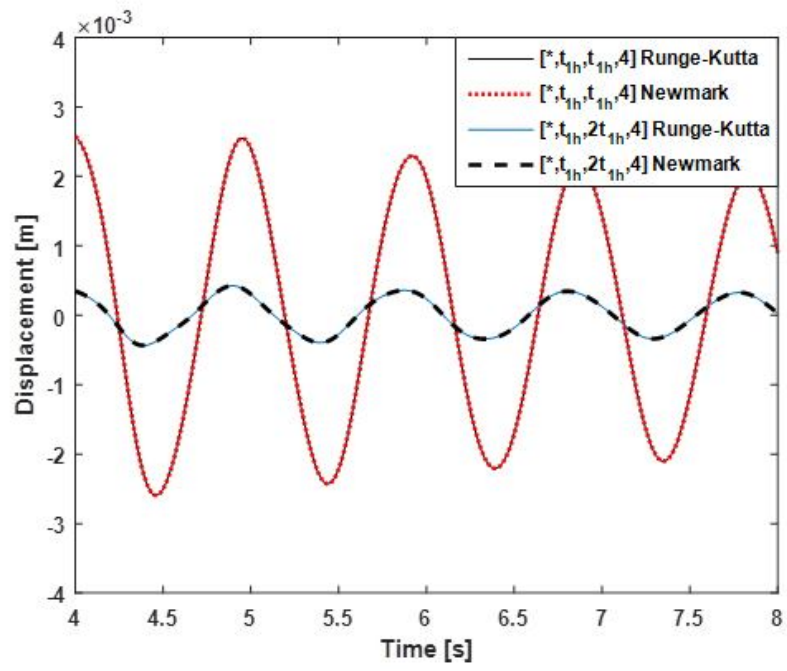
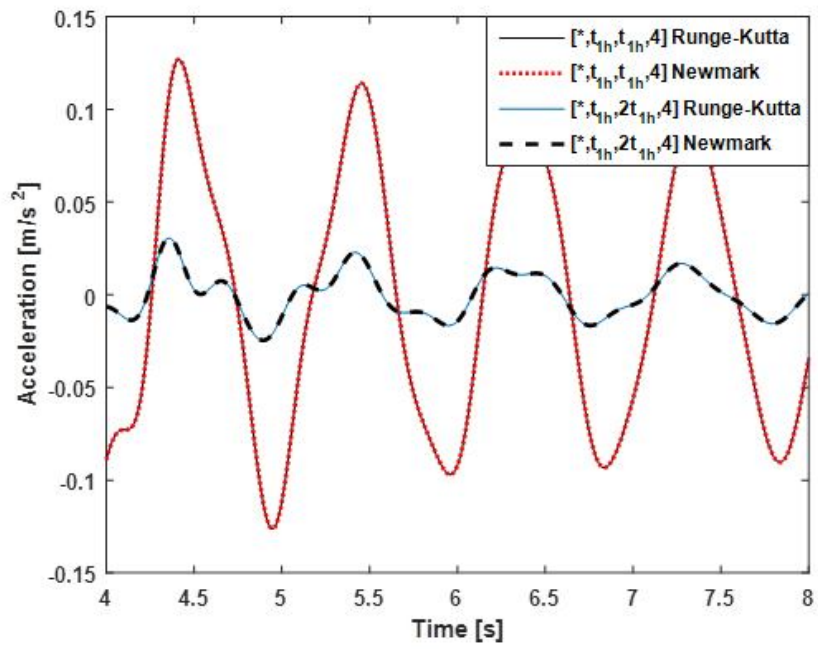


Figure 2.10 Trapezoidal velocity profile $t_i=[3.0403,0.4798,0.4798,4]$

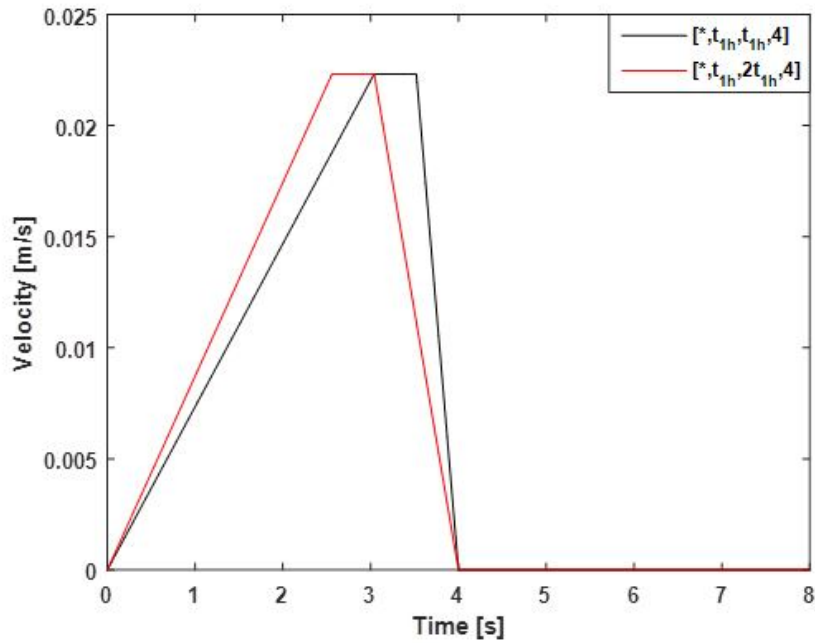
Arranging motion inputs as $t_i=[*,t_{1h},t_{1h},t_m]$ and $t_i=[*,t_{1h},2t_{1h},t_m]$ to reduce the residual vibrations, the responses are shown in Figure 2.11.



(a)



b)



c)

Figure 2.11 Residual vibrations of the end point for the trapezoidal velocity profile a) Displacement, b) Acceleration and c) Input profile

As seen in Figure 2.11 a) and b), for trapezoidal velocity profile, it is also observed that the residual vibration levels are high for $t_d=t_{1h}$, and residual vibration levels are significantly decreased for $t_d=2t_{1h}$. RMS values of residual vibration signals reduced from 0.00326 m for $t_d=t_{1h}$ to 3.4567e-4 m for $t_d=2t_{1h}$ and 86.70% reduction in vibration level has been achieved.

The results of different cases are given in Table 2.2 and Table 2.3 for the different time parameters.

Table 2.2 Motion input for Case-5

Motion	$t_i=[*, t_{1h}, t_{1h}, t_m]$	\dot{z}_{\max} (m/s)	RMS (m)	Reduction %	RMS (m/s ²)
Case5_a	$[*, t_{1h}, t_{1h}, t_m]$	0.0223	0.00326	-	0.0882
Case5_b	$[*, t_{1h}, 2t_{1h}, t_m]$	0.0223	3.4567e-04	86.70	0.0065
Case5_c	$[*, t_{1h}, 3t_{1h}, t_m]$	0.0223	7.2362e-04	72.17	0.0294
Case5_d	$[*, t_{1h}, 4t_{1h}, t_m]$	0.0223	5.3773e-04	79.32	0.0179

Table 2.3 Motion input for Case-6

Motion	$t_i=[*,2t_{1h},t_{1h},t_m]$	\dot{z}_{max} (m/s)	RMS (m)	Reduction %	RMS (m/s ²)
Case6_a	$[*,2t_{1h}, t_{1h},t_m]$	0.0202	0.0027	-	0.1005
Case6_b	$[*,2t_{1h}, 2t_{1h},t_m]$	0.0202	1.4489e-04	94.63	0.0153
Case6_c	$[*,2t_{1h}, 3t_{1h},t_m]$	0.0202	0.0013	51.85	0.0511
Case6_d	$[*,2t_{1h}, 4t_{1h},t_m]$	0.0202	2.106e-04	92.20	0.0116

Evaluating the results of Case-5 and Case-6, vibration reductions can be achieved for $2t_{1h}$ and $4t_{1h}$ as given in Table 2.2 and Table 2.3. It is seen that double times of t_{1h} is more effective to control vibration amplitudes. The reductions in Case-5 are 86.70% and 79.32% for $2t_{1h}$ and $4t_{1h}$, respectively. The reductions in Case-6 are 94.63% and 92.20% for $2t_{1h}$ and $4t_{1h}$, respectively. The response spectrum via the deceleration time for Case-5 and Case-6 is given in Figure 2.12.

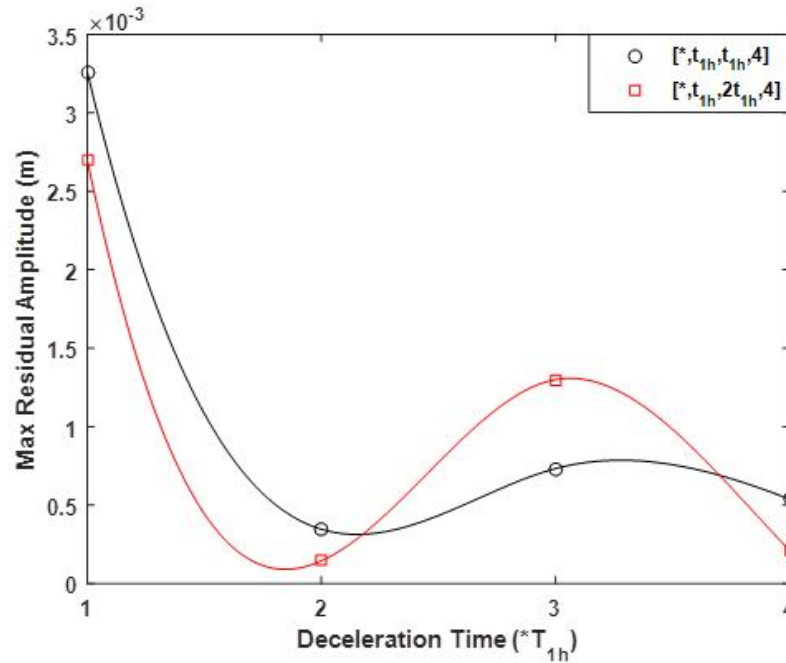


Figure 2.12 Change of the RMS values of the residual vibration signals versus the deceleration time for Case-3 and Case-4

2.4 Active Vibration Control of 4-DOF Mechanical System

2.4.1 Newmark Solution for Closed Loop Control

The block diagram for the integration of active vibration control action into the Newmark solution is shown in Figure 2.13. $x_r(t)$ is the reference input signal. x_{1n} , x_{2n} , x_{3n} and x_{4n} are the values of $x_1(t)$, $x_2(t)$, $x_3(t)$, and $x_4(t)$ at the time step n , respectively. x_{an} is the average at the time step n as given in Figure 2.13. x_{em} is the error value at the time step m , where $m=n+1$. K_p , K_i , and K_d are the proportional, integral, and derivative control action constants, respectively. z_m is the value of $z(t)$ at the time step m . Knowing the initial values of $\{q\}$ at the time step 1, the values of $\{q\}$ are found at the subsequent time steps as given below. Δt is the time interval between the time steps. $\{q\}_m$ is the value of $\{q\}$ at the time step m .

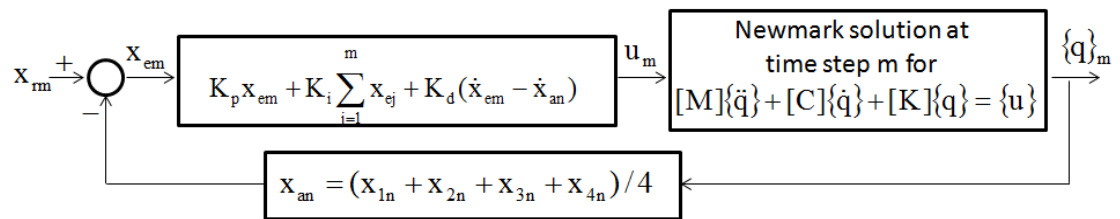


Figure 2.13 Block diagram for integration of closed loop control action into Newmark solution

A step function is considered for the input x_r . \dot{x}_r is then an impulse function. \ddot{x}_r is approximated with a trapezoidal velocity profile as shown in Figure 2.14 (b). The area under the profile equals to 1. Then, the samples of x_r and \ddot{x}_r are found as in Figure 2.14 (a), and (c), respectively.

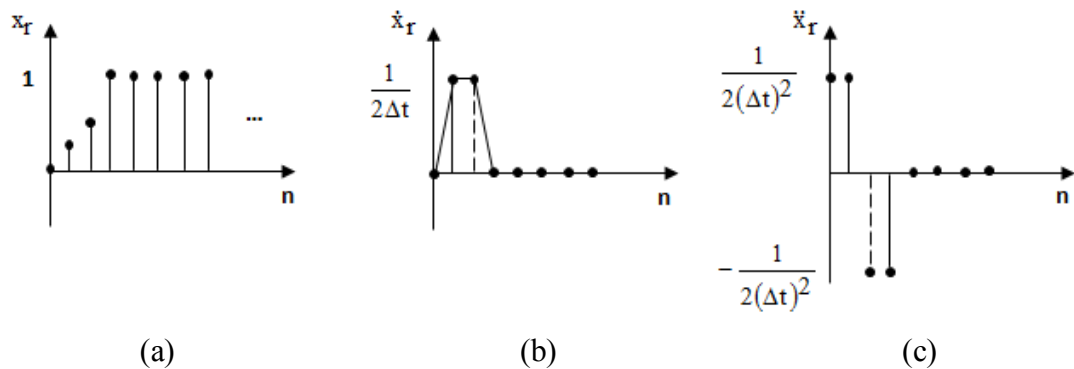


Figure 2.14 Approximate model of the step input, (a) displacement, (b) velocity and (c) acceleration.

The uncontrolled and controlled responses obtained by the Newmark method are shown in Figure 2.15 as an example result. The control action constants are selected by inspection. Here, the damping is ignored by taking $\mathbf{C}=\mathbf{0}$, to observe the effectiveness of the active vibration control.

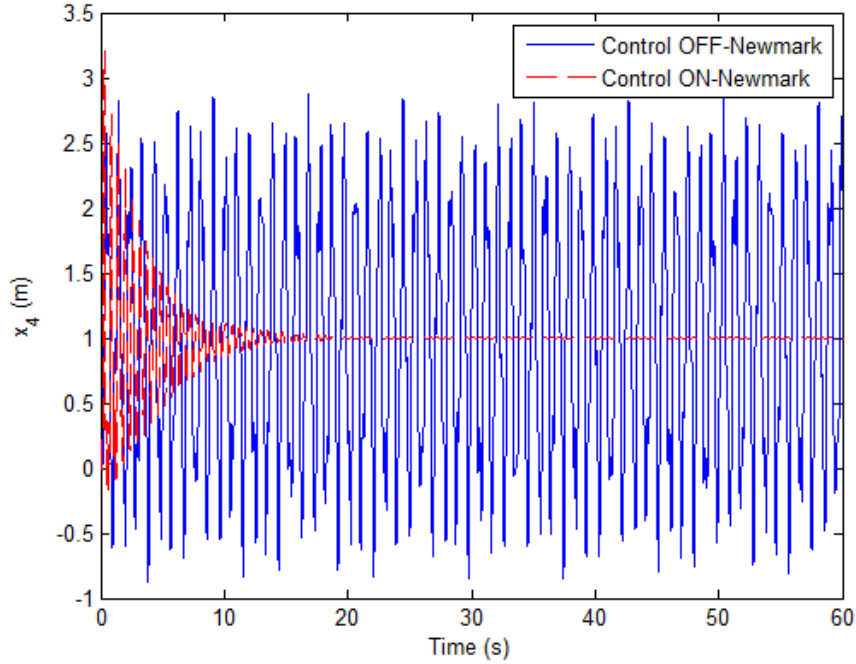


Figure 2.15 Solution by the Newmark method for undamped system, ($K_p=10$, $K_i=5$, $K_d=0.5$)

2.4.2 Analytical Solution

The analytical solution using the Laplace transform method is given in this section to verify the numerical results. The solution is found by using $\mathbf{Q}(s)=\mathbf{H}(s)\mathbf{U}(s)$, where $\mathbf{Q}(s)$ and $\mathbf{U}(s)$ are the Laplace transforms of $\mathbf{q}(t)$, and $\mathbf{u}(t)$, respectively. $\mathbf{H}(s)$ is the transfer function square matrix with a size of 4×4 . $H_{ij}(s)$ is the element of i^{th} row and j^{th} column of $\mathbf{H}(s)$. The following is found by using Equation (2.24) and the definition of the transfer function (Kuo & Golnaraghi, 2003):

$$\mathbf{H}(s)=[s^2\mathbf{M}+s\mathbf{C}+\mathbf{K}]^{-1}. \quad (2.39)$$

Then,

$$\mathbf{Q}(s)=\mathbf{H}(s)[c_1s+k_1,0,0,0]^T\mathbf{Z}(s), \quad (2.40)$$

where $Z(s)$ is the Laplace transform of $z(t)$.

The block diagram of the closed loop control system for the analytical solution is given in Figure 2.16. $G_1(s)$ is the transfer function of the control action, and it is taken as $G_1(s)=K_p+K_i/s+K_d s$.

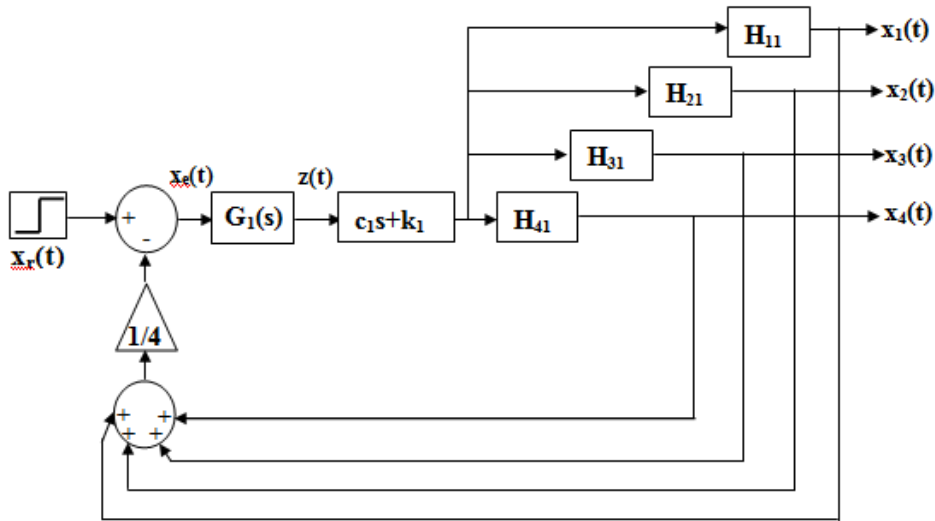


Figure 2.16 Block diagram of the system

Taking $\mathbf{C}=\mathbf{0}$, the transfer functions in Figure 2.16 can be found as

$$\begin{aligned}
 H_{11}(s) &= \frac{s^6 + 1200s^4 + 360000s^2 + 16000000}{D(s)} \\
 H_{21}(s) &= \frac{400s^4 + 240000s^2 + 16000000}{D(s)} \\
 H_{31}(s) &= \frac{80000s^2 + 16000000}{D(s)} \\
 H_{41}(s) &= \frac{16000000}{D(s)}
 \end{aligned} \tag{2.41}$$

where $D(s)=s^8 + 2200s^6 + 1400000s^4 + 280000000s^2 + 9600000000$.

Utilizing the block diagram given in Figure 2.16, the transfer function of the closed loop system $H_{CL}(s)$ is found as,

$$H_{CL}(s) = \frac{X_4(s)}{X_r(s)} = \frac{(c_1s + k_1)H_{41}(s)G_1(s)}{1 + (c_1s + k_1)G_1(s)[(H_{11}(s) + H_{21}(s) + H_{31}(s) + H_{41}(s))/4]} \quad (2.42)$$

Substituting $X_r(s)=1/s$ for the step input and the numerical values into the closed loop transfer function, by taking $c_1=0$, the Laplace transform of the displacement of the end mass can be found as

$$X_4(s) = \frac{96 \times 10^8 (K_d s^2 + K_p s + K_i)}{s^9 + 150 K_d s^8 + (2200 + 150 K_p) s^7 + (24 \times 10^4 K_d + 150 K_i) s^6 + (14 \times 10^5 + 24 \times 10^4 K_p) s^5 + (102 \times 10^6 K_d + 24 \times 10^4 K_i) s^4 + (28 \times 10^7 + 102 \times 10^6 K_p) s^3 + (96 \times 10^8 K_d + 102 \times 10^6 K_i) s^2 + (96 \times 10^8 K_p + 96 \times 10^8) s + 96 \times 10^8 K_i} \quad (2.43)$$

The controlled response of $x_4(t)$ can be found by taking the inverse Laplace transform of $X_4(s)$. The uncontrolled and controlled responses of $x_4(t)$ are shown in Figure 2.17.

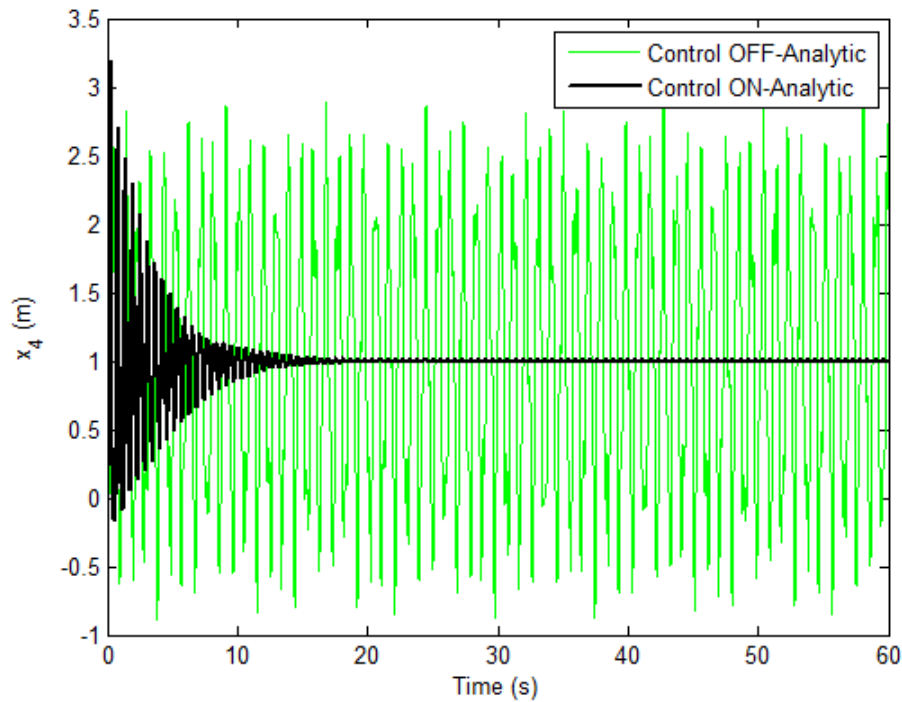


Figure 2.17 Analytic solution for the undamped system, ($K_p=10$, $K_i=5$, $K_d=0.5$)

The controlled responses obtained from the numerical and analytical solutions are shown on the same plot in Figure 2.18. It is observed from the figure that the numerical and analytical solutions are in good agreement.

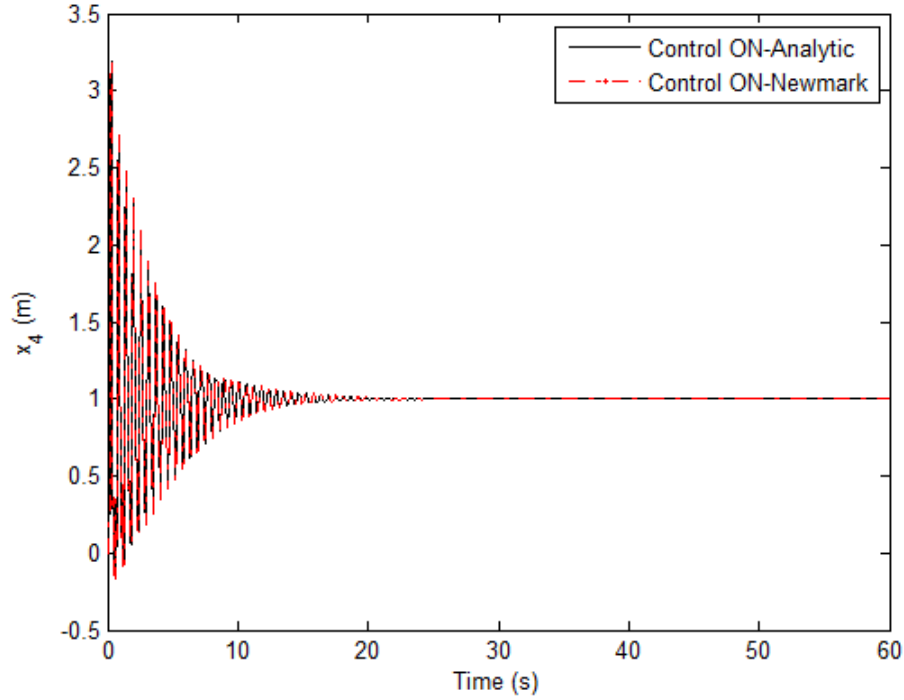


Figure 2.18 Comparison of the Control-ON results ($K_p=10$, $K_i=5$, $K_d=0.5$)

2.4.3 Effect of Damping and Effectiveness of Controller Gains

The system given in Figure 2.1 is considered to investigate the effect of damping on the active control problem. Analytical closed loop solution for the damped system can be done by considering the damping matrix C , and the transfer functions indicated in Figure 2.16 are given as

$$H_{11}(s) = \frac{250s^6 + 1100s^5 + 301200s^4 + 660192s^3 + 90160000s^2 + 44000000s + 400000000}{D(s)}$$

$$H_{21}(s) = \frac{300s^5 + 100720s^4 + 420192s^3 + 60160000s^2 + 44000000s + 400000000}{D(s)}$$

$$H_{31}(s) = \frac{240s^4 + 140192s^3 + 20160000s^2 + 44000000s + 400000000}{D(s)}$$

$$H_{41}(s) = \frac{192s^3 + 160000s^2 + 44000000s + 4000000000}{D(s)} \quad (2.44)$$

where

$$D(s) = 250s^8 + 1775s^7 + 553810s^6 + 2.333 \times 10^6 s^5 + 3.524 \times 10^8 s^4 + 7.074 \times 10^8 s^3 + 7.016 \times 10^{10} s^2 + 3.24 \times 10^{10} s + 2.4 \times 10^{12} \quad (2.45)$$

By using the controller gains $K_p=10$, $K_i=5$, $K_d=0.5$, the Laplace transform of the tip mass $X_4(s)$ for the damped system can be found by utilizing the block diagram given in Figure 2.16.

$$X_4(s) = \frac{144s^4 + 177600s^3 + 8.1107s^2 + 1.62 \times 10^{10} s + 1.2 \times 10^{12}}{s(250s^8 + 1775s^7 + 572560s^6 + 2.438 \times 10^6 s^5 + 3.825 \times 10^8 s^4 + 7.989 \times 10^8 s^3 + 8.296 \times 10^{10} s^2 + 4.56 \times 10^{10} s + 3.6 \times 10^{10})} \quad (2.46)$$

The time response of $x_4(t)$ can be found by taking the inverse Laplace transform of $X_4(s)$. The uncontrolled and controlled responses obtained with the analytical and numerical methods for the damped system are in good agreement as shown in Figure 2.19.

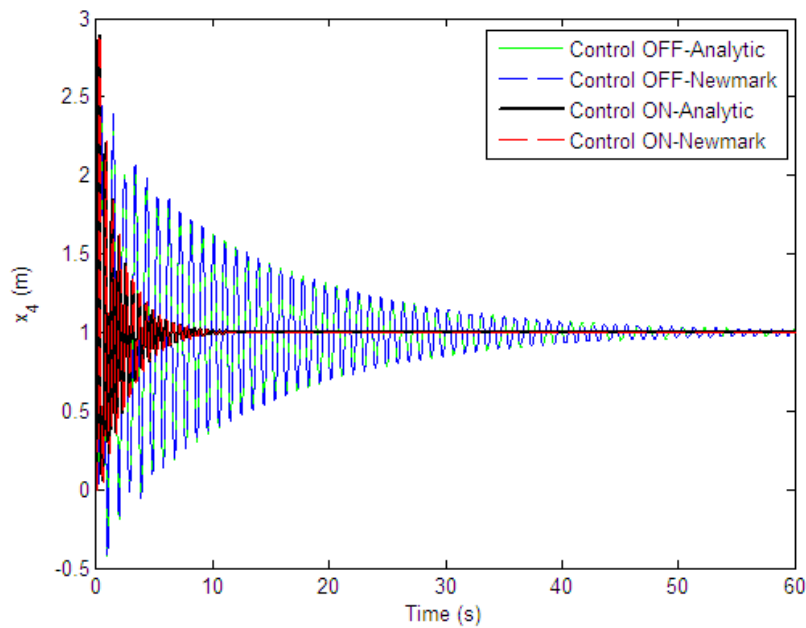


Figure 2.19 Comparison of controlled results for damped system. ($K_p=10$, $K_i=5$, $K_d=0.5$)

2.4.4 Setting Control Parameters

The effectiveness of the controller can be evaluated in terms of the performance parameters (Kuo & Golnaraghi, 2003). The performance parameters such as the settling time t_s , the steady state error e_{ss} , the overshoot, and RMS (root mean square) can be found for different PID control gains, which are listed below in Tables 2.4-2.5. The RMS can be used for the indication of the energy level in a vibration signal (Kelly, 1993). Analytical and numerical results for the damped system are given in Table 2.4. The comparison of the results for the undamped system is also given in Table 2.5. The closed loop responses of the damped and undamped systems obtained with analytical and numerical methods for the selected gains listed in the tables are compared in Figures 2.20-2.21.

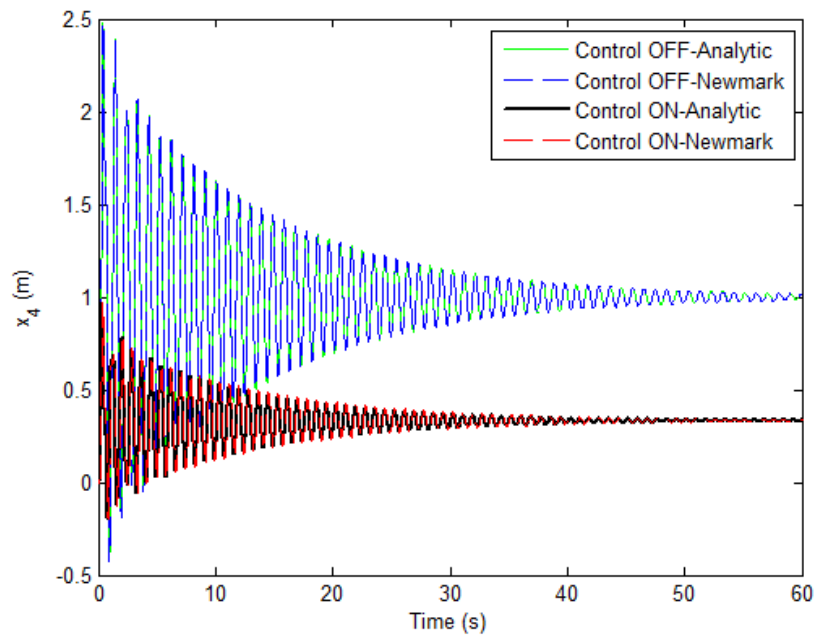
For the calculation of the settling time, it is assumed that the response decreases and stays within a 2 percent of its final value. The average of amplitudes in the last 5 s is also considered to find the final value or steady state value.

Table 2.4 Closed loop results for damped system

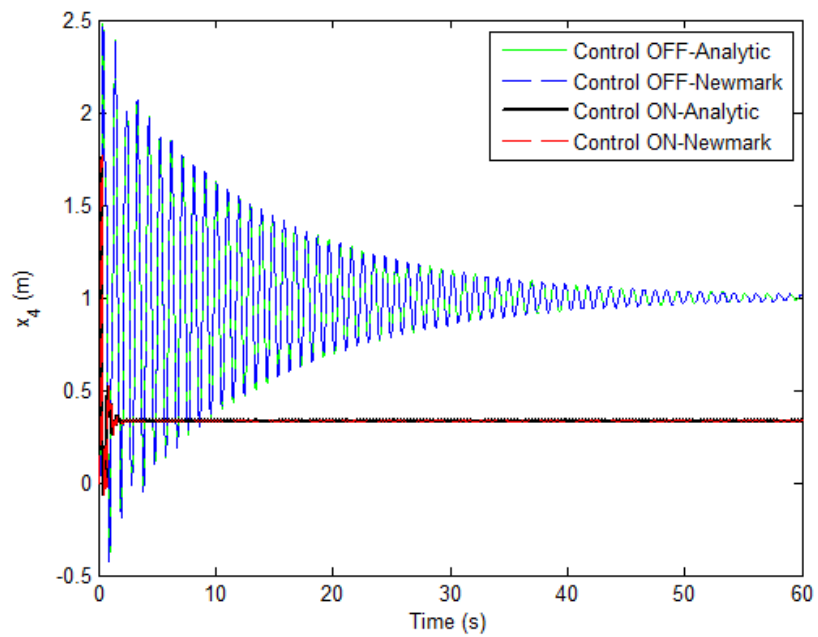
Control gains			t_s		e_{ss}		RMS		Overshoot %	
K_p	K_i	K_d	Newmark	Analytic	Newmark	Analytic	Newmark	Analytic	Newmark	Analytic
0	0	0	57.62	57.62	-7.38e-4	-7.47e-4	1.0483	1.0484	147.77	147.85
0.05	0	0	57.51	56.58	0.9523	0.9523	0.050	0.0499	-	-
0.5	0	0	54.78	50.64	0.6666	0.666	0.3511	0.3498	-	-
0.5	0	0.01	20.76	19.95	0.6667	0.6667	0.3406	0.3404	-	-
0.5	0	0.2	2.13	2.12	0.6667	0.6667	0.3414	0.3414	143.00	142.80
0.5	1	0.2	5.05	5.04	9.27e-14	5.66e-15	0.9880	0.9880	78.47	78.21
0.5	3	0.2	1.63	1.63	2.80e-13	-2.22e-16	0.9973	0.9973	82.80	82.43

Table 2.5 Closed loop results for undamped system

Control gains			t_s		e_{ss}		RMS		Overshoot %	
K_p	K_i	K_d	Newmark	Analytic	Newmark	Analytic	Newmark	Analytic	Newmark	Analytic
0	0	0	-	-	-	-	1.3959	1.3999	182.88	184.06
0.05	0	0.01	35.59	36.60	0.9524	0.9524	0.0521	0.0521	-	-
0.5	0	0.01	35.24	34.82	0.6667	0.6667	0.3465	0.3459	69.47	69.21
0.5	0	0.2	3.465	3.465	0.6667	0.6667	0.3436	0.3435	162.25	162.02
0.5	1	0.2	5.096	5.097	-5.91e-14	5.77e-15	0.9887	0.9887	97.77	97.49
0.5	3	0.2	2.632	2.636	-1.63e-13	-2.22e-16	0.9979	0.9979	102.21	101.81

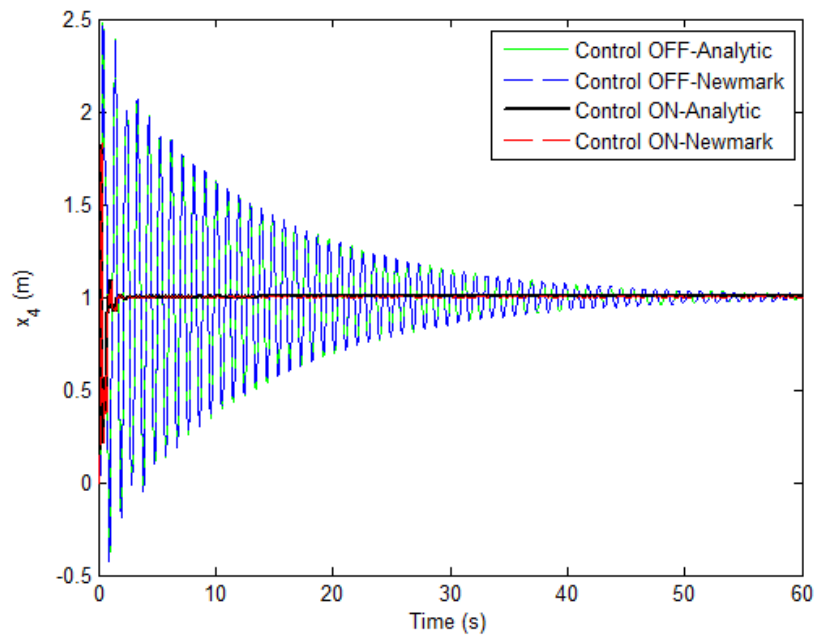


(a)



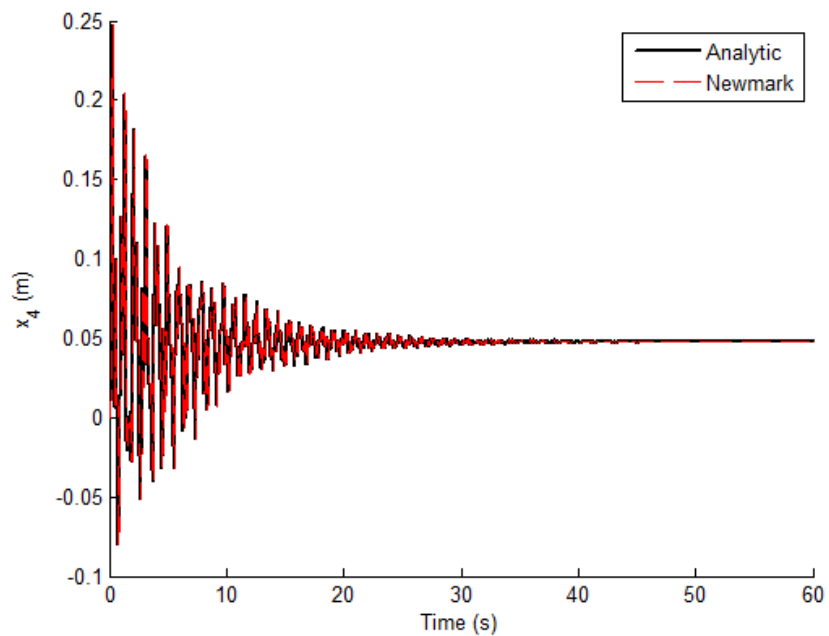
(b)

Figure 2.20 Comparison of open loop and closed loop results for the damped system, a) $K_p=0.5$, $K_i=0$, $K_d=0$, b) $K_p=0.5$, $K_i=0$, $K_d=0.2$, c) $K_p=0.5$, $K_i=3$, $K_d=0.2$.



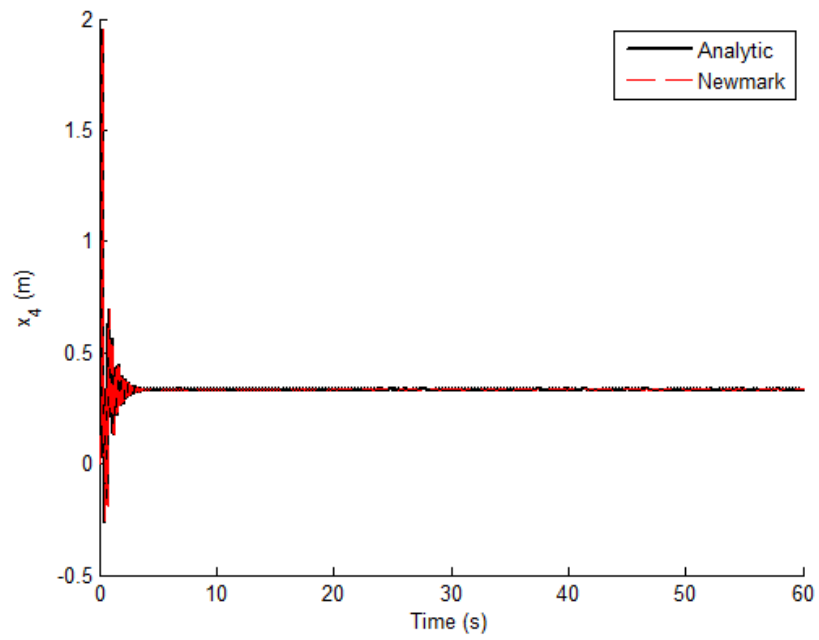
(c)

Figure 2.20 Comparison of open loop and closed loop results for the damped system, a) $K_p=0.5$, $K_i=0$, $K_d=0$, b) $K_p=0.5$, $K_i=0$, $K_d=0.2$, c) $K_p=0.5$, $K_i=3$, $K_d=0.2$. (cont.)

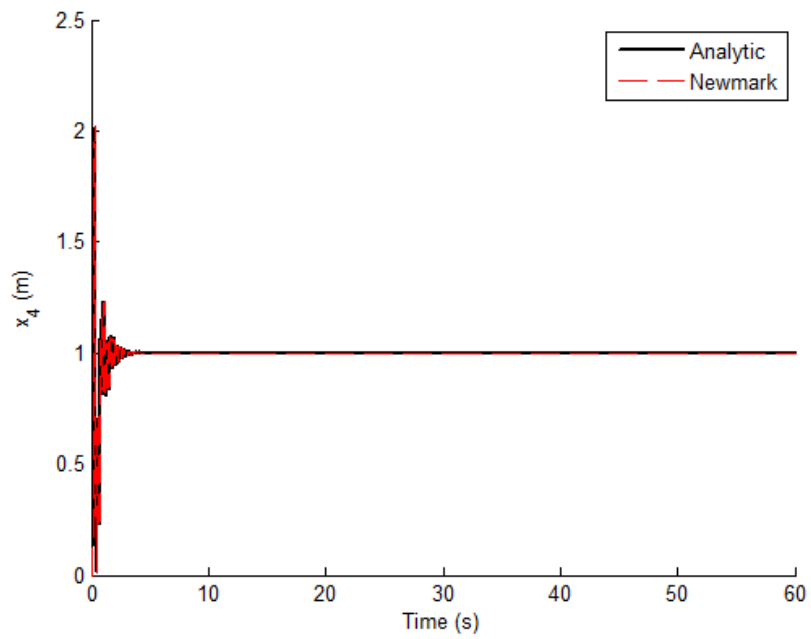


(a)

Figure 2.21 Comparison of closed loop results for undamped system, a) $K_p=0.05$, $K_i=0$, $K_d=0.01$, b) $K_p=0.5$, $K_i=0$, $K_d=0.2$, c) $K_p=0.5$, $K_i=3$, $K_d=0.2$.



(b)



(c)

Figure 2.21 Comparison of closed loop results for undamped system, a) $K_p=0.05$, $K_i=0$, $K_d=0.01$, b) $K_p=0.5$, $K_i=0$, $K_d=0.2$, c) $K_p=0.5$, $K_i=3$, $K_d=0.2$. (cont.)

As indicated in Table 2.4 for damped system and Table 2.5 for undamped system, the performance parameters obtained by the Newmark method match well those obtained by the analytical method.

As seen from Figure 2.20 (a) and Table 2.4, the control action starts with the proportional (P) control in the damped system. The proportional control decreases the values of the settling time and RMS of the signal as the gain increases. However, there is a large steady state error in the P control. The settling time decreases from 57.62 s to 2.13 s in the Newmark method and from 57.62 s to 2.12 s in the analytical solution, by adding differential (D) control. The PD control causes a large overshoot as shown in Figure 2.20 (b) although there is no change in the steady state error. The steady state error can be eliminated by adding the integral control. A better solution can be obtained with the PID control by selecting the gains $K_p=0.5$, $K_I=3$, $K_D=0.2$ as shown in Figure 2.20 (c).

As seen from Table 2.5, the P control is not sufficient for the reduction of the vibration amplitudes. The control actions start with the PD control in the undamped system as shown in Figure 2.21 (a). The value of the settling time decreases from 35.59 s to 3.465 s in the Newmark method and from 36.60 s to 3.465 s in the analytical solution, significantly as shown in Figure 2.21 (b) as the differential gain increases. The PID control eliminates the steady state error in undamped system as shown in Figure 2.21 (c).

The same controller gains are used in the closed loop solutions. The PID control can be successfully applied to both of the undamped and damped systems. Adding the damping to the open loop system affects the settling time and overshoot results in the closed loop system.

The settling time is the one of the key parameters in the evaluation of the controller effectiveness if the subject is the analysis of active vibration control. The overshoot limits the maximum vibration amplitudes. The existence of the damping decreases the value of the settling time from $t_s=2.632$ s to $t_s=1.63$ s in the Newmark

method and from 2.636 s to 1.63 s in the analytical solution, the damping reduces the value of the overshoot from 102.21 % to 82.80 % in the Newmark method and from 101.81 % to 82.43 % in the analytical solution.

2.5 Active Vibration Control of a Flexible Cantilever Beam by Newmark Method

The finite element models of complex mechanical systems can be established with computer programs, responses of the systems can be achieved with analytical or numerical methods. In this study, active vibration control of a flexible cantilever beam is analyzed with Newmark method. The finite element model of a flexible beam is obtained by Euler-Bernoulli theorem. An impulse input is applied to the end point of the flexible beam and also the open- and closed loop dynamic responses of the end point are found with Newmark solution. The values of the input are defined for the time intervals. PID control is applied to the error signal, which is calculated by subtracting the instantaneous value of displacement of the end point from the instantaneous reference value, to reduce the vibrations of the flexible system. This process is continued with the time step until steady state value is reached. In order to observe the effectiveness of the active vibration control, the damping is ignored. The effect of different PID control parameters and the element size in finite element method on active vibration control is studied.

2.5.1 Modelling of Flexible Beam

In this study, Euler-Bernoulli beam model is discussed. Considered beam model is shown in Figure 2.22. Here, F_D is input force, F_C is applied control force, y_r is reference input signal and L_C is the distance of the applied control force from the root-point of the beam. The material of the beam is aluminum. The material and geometrical properties of the beam are given in Table 2.6.

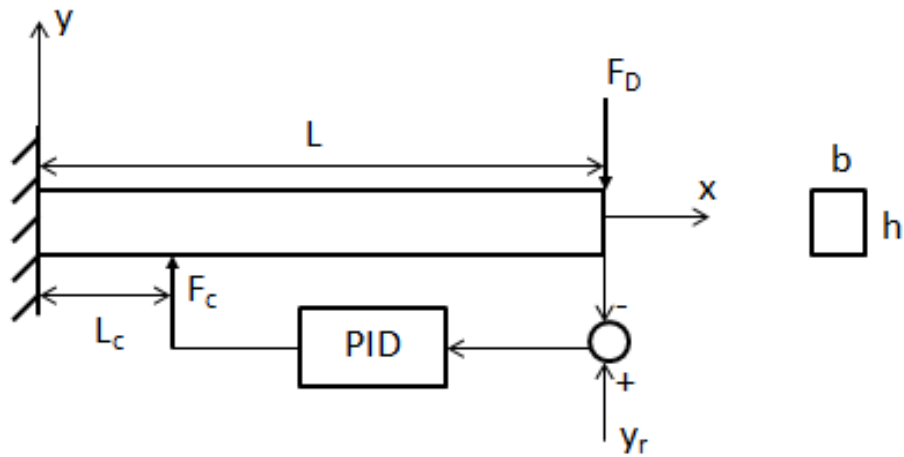


Figure 2.22 The model of cantilever beam

Table 2.6 Properties of the beam

	Aluminum Beam
Modulus of Elasticity, E (N/m^2)	68×10^9
Density, ρ (kg/m^3)	2800
Length, L (mm)	504
Height of the cross section, h (mm)	0.8
Width of the cross section, b (mm)	25.4

The finite element model of a flexible beam is obtained by Euler-Bernoulli theorem. The finite element model shown schematically in Figure 2.23 is divided into three elements and an impulse input is applied to the end point of the model, then control force is applied to the determined point to control the end point vibrations. Each elements of the flexible beam divided by finite elements have 2 nodes, and each nodes have translational degrees of freedom on x and y directions and rotational degree of freedom about z axis. As shown in Figure 2.23, the degrees of freedoms on nodes 10, 11 and 12 are zero due to having fixed boundary conditions of point A.

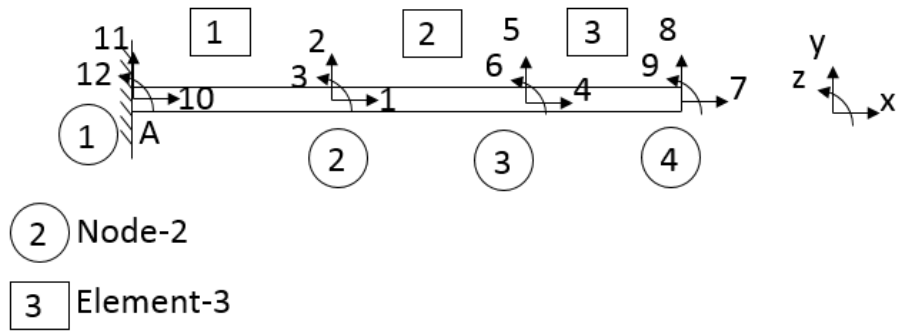


Figure 2.23 The finite element model of flexible beam

The mass and stiffness matrices for each finite element can be constructed in local coordinates. The mass and stiffness matrices in the local coordinates of a flexible beam having longitudinal and bending vibrations are given in Eq. 2.47. Here, l_{en} , A_n , E_n , I_n and ρ_n are the length, cross section area, the modulus of elasticity, the bending moment of inertia of the cross section and the density for each finite element, respectively.

$$m^e = \frac{\rho_n A_n l_{en}}{420} \begin{bmatrix} 140 & 0 & 0 & 70 & 0 & 0 \\ 0 & 156 & 22l_{en} & 0 & 54 & -13l_{en} \\ 0 & 22l_{en} & 4l_{en}^2 & 0 & 13l_{en} & -3l_{en}^2 \\ 70 & 0 & 0 & 140 & 0 & 0 \\ 0 & 54 & 13l_{en} & 0 & 156 & -22l_{en} \\ 0 & -13l_{en} & -3l_{en}^2 & 0 & -22l_{en} & 4l_{en}^2 \end{bmatrix}$$

$$k^e = \begin{bmatrix} \frac{A_n E_n}{l_{en}} & 0 & 0 & -\frac{A_n E_n}{l_{en}} & 0 & 0 \\ 0 & \frac{12E_n I_n}{l_{en}^3} & \frac{6E_n I_n}{l_{en}^2} & 0 & \frac{-12E_n I_n}{l_{en}^3} & \frac{6E_n I_n}{l_{en}^2} \\ 0 & \frac{6E_n I_n}{l_{en}^2} & \frac{4E_n I_n}{l_{en}} & 0 & \frac{-6E_n I_n}{l_{en}^2} & \frac{2E_n I_n}{l_{en}} \\ -\frac{A_n E_n}{l_{en}} & 0 & 0 & \frac{A_n E_n}{l_{en}} & 0 & 0 \\ 0 & \frac{-12E_n I_n}{l_{en}^3} & \frac{-6E_n I_n}{l_{en}^2} & 0 & \frac{12E_n I_n}{l_{en}^3} & \frac{-6E_n I_n}{l_{en}^2} \\ 0 & \frac{6E_n I_n}{l_{en}^2} & \frac{2E_n I_n}{l_{en}} & 0 & \frac{-6E_n I_n}{l_{en}^2} & \frac{4E_n I_n}{l_{en}} \end{bmatrix} \quad (2.47)$$

The natural frequencies of a cantilever beam can be calculated analytically as given in Eq 2.48.

$$\omega_n = \frac{\beta_n}{L^2} \sqrt{\frac{EI_{zz}}{\rho A}} \text{ (rad/s)} \quad (2.48)$$

Here, β_n , L , E , I_{zz} , ρ and A are the frequency parameter, the length of the beam, the modulus of elasticity, the bending moment of inertia of the cross section and the cross section area, respectively. For the cantilever beam, the frequency parameter β_n for first three natural frequency is 3.516, 22.03 and 61.7. The first three natural frequencies of the bending vibrations of the cantilever beam are calculated as 2.507 Hz, 15.71 Hz and 43.99 Hz, respectively.

2.5.2 Active Vibration Control with Newmark Method

In the flexible structures, high vibrations occur because of having low rigidity. In the literature, it is very important to reduce or eliminate residual vibrations. In this section, vibration control of a flexible beam by Newmark method is discussed. MATLAB is used to construct the finite element models of the system and to integrate the control strategy into Newmark method. The closed loop block diagram of the impulse input acting on the beam and the applying control force integrated into Newmark method is shown in Figure 2.24.

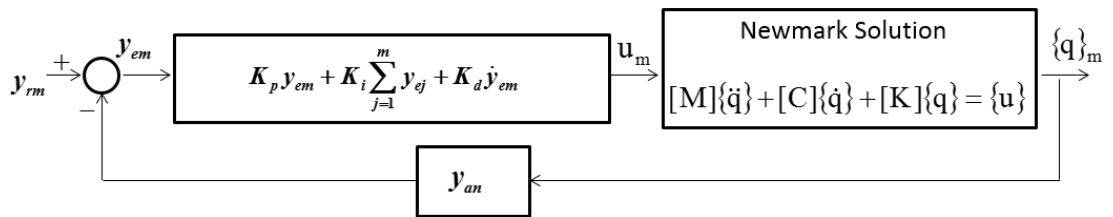


Figure 2.24 Closed loop block diagram

Here, y_{rm} is the reference input signal. The instantaneous impulse input is applied to the end point of the flexible beam and the displacement at the y-direction of the end point is taken as the feedback signal. The displacement y_{an} at the y-direction of the end point taken as the feedback signal is defined as the displacement at the y-

direction on the node related to the finite element number of the beam at the time step n . For the flexible beam divided into three finite elements as shown in Figure 2.23, y_{an} is the displacement at the y -direction on node-4 at the time step n . y_{em} is the error signal at the time step m and $m=n+1$. K_p , K_i , and K_d are the proportional, integral and derivative control action constants, respectively. An impulse input is applied to the end point of the flexible beam and the instantaneous displacement of the end point is subtracted from the reference input to find the error signal value at a time step in the Newmark solution. The PID control action is applied to find the actuator signal value in the time step. This input value is used to find the displacement of the end point for the subsequent time step. The process is continued with the time interval Δt until the steady-state value is approximately reached. After applying the impulse input, the reference value is taken as zero for each time interval in vibration control. A time step, Δt , is chosen for the solution as $\Delta t < 1/(20f_1)$, where f_1 is the first natural frequency considered. $\{q\}_m$ is the value of the translations at x and y directions and the rotation about z axis for each nodes at the time step m . U_m is the control input at the time step m .

Newmark method is the most preferred method among the numerical methods in the finite element analysis to achieve the system response by using the mass, stiffness and damping matrices. The displacements of the end point of the flexible beam obtained by Newmark method are shown in Figure 2.25 for open- and closed loop system. The control action constants are selected by inspection. Here, the damping is ignored by taking $C=0$, to observe the effectiveness of the active vibration control. The effectiveness of the vibration control can be evaluated in terms of the performance parameters such as the settling time t_s , the steady state error e_{ss} , the overshoot, and RMS (root mean square).

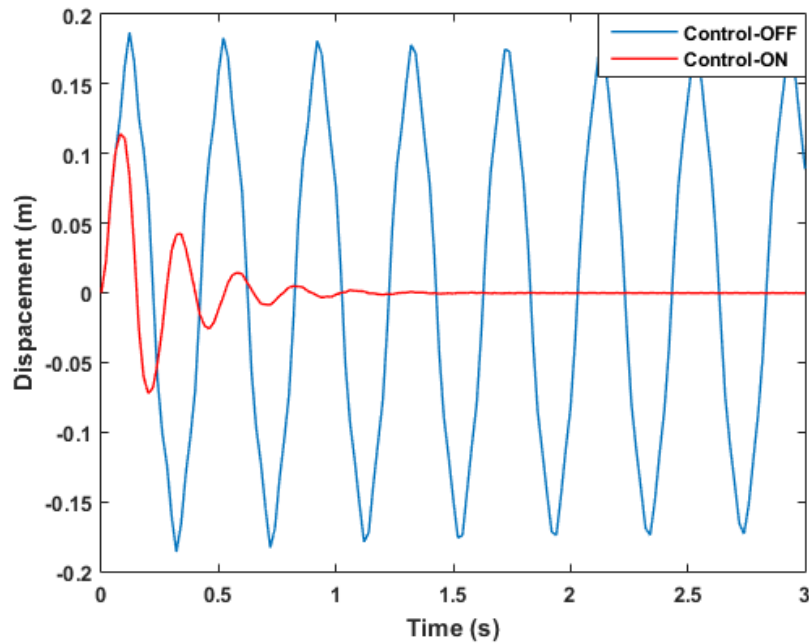


Figure 2.25 Control-OFF and Control-ON responses ($L_c=168\text{mm}$, $K_p=8$, $K_i=0.5$, $K_d=0.5$.)

The steady-state time, overshoot and RMS values obtained for different control gains are given in Table 2.7.

Table 2.7 Closed loop results for different control gains

Control gains			t_s	RMS	Overshoot %
K_p	K_i	K_d			
3	0	0.3	1.421	0.029	13.49
5	0	0.4	1.116	0.0247	12.39
8	0.5	0.5	0.985	0.0223	11.42

As shown in Table 2.7, the steady-state time, the overshoot and the amplitudes of the displacement of the end point of the flexible beam are changed for different control gains. It is observed that the best results are achieved by applying PID control.

The dynamic behavior of the end point is investigated when changing the number of element in finite element model and the results are given in Table 2.8.

Table 2.8 The effect of the number of element on dynamic behavior

The number of element	L_c (mm)	t_s	RMS	Overshoot
3	168	0.985	0.0223	0.114
4	126	1.77	0.0307	0.1332
9	112	2.229	0.035	0.1393
84	126	1.77	0.0307	0.1332
84	168	0.985	0.0223	0.1142
504	126	1.77	0.0307	0.1332
504	168	0.985	0.0223	0.1142
504	197	0.72	0.0192	0.1069

The results in Table 2.8 show that, as the point that the control force is applied changes, the steady-state time, the overshoot and the amplitudes of the displacement of the end point of the flexible beam also changes for the same control gains. It is observed that the number of element does not effect on the dynamic analysis as long as the distance at which the control force is applied. Based on these informations, it is intended to find optimal distance by changing the applying point of the control force on the flexible beam and the finite element program written in MATLAB is developed to optimize the distance at which the control force is applied by changing the number of element. The number of element is chosen as 504 to find the exact point of the distance. The point at which the control force is applied is increased by 1 mm from the distance of 1mm to 504 mm and the steady-state times and RMS values are obtained for each point by the program. It is requested from the developed program to suggest the optimum distance L_c . It is seen that, if the distance L_c which is suggested by the program is 197 mm, the end point vibration of the flexible beam is damped as soon as possible. When the control force is applied at the distance suggested by the program, the end point of the flexible beam reaches the steady-state time at 0.72 s.

2.6 Active Vibration Control of a Single Link Flexible Manipulator by Newmark Method

Residual vibrations occur after stopping the movement of flexible manipulators. Accuracy at the end-point positioning decreases if residual vibration amplitudes increase. Productivity decreases in the high speed applications since the settling time

required for this residual vibration delays subsequent operations. In this study, the active vibration control of a single-link flexible steel manipulator with a payload is studied numerically. The mathematical model of a manipulator is established by the finite element method (FEM). The FEM results in modal analysis are verified by the experimental results. Then, the transient analysis is realized by the Newmark method. Two different velocity profiles such as triangular and trapezoidal are applied to the manipulator. For active vibration control, the control action is integrated into Newmark solution. The proportional control gain is applied. Active control is activated after motion is done. The root mean square values calculated from the residual vibration signals, and reduction ratios are presented for the cases. It is observed from the results that the residual vibration amplitudes of the manipulators are successfully suppressed by the proportional control gain.

2.6.1 Modeling of Single Link Manipulator Based on Finite Element Method

A MATLAB code is developed based on the theory of the finite element method (FEM) (Bathe, 2014). The model of the single-link planar manipulator under study is shown in Figure 2.26 (a). Member-2 is the OB-beam. There is a revolute joint at O between Member-2 and the frame (Member-1). Member-2 is actuated by Motor-2 at O. The mass of Motor-2 is on the frame at O. There is a payload on Member-2 at B. The payload mass has a translational inertia of m_L and rotational inertia of I_L .

The instantaneous angular position of Member-2 is $\theta_2(t)$, where t is the time. The length of the link is $L_2=OB$. The global origin is at O. The global Cartesian coordinates are x , y and z .

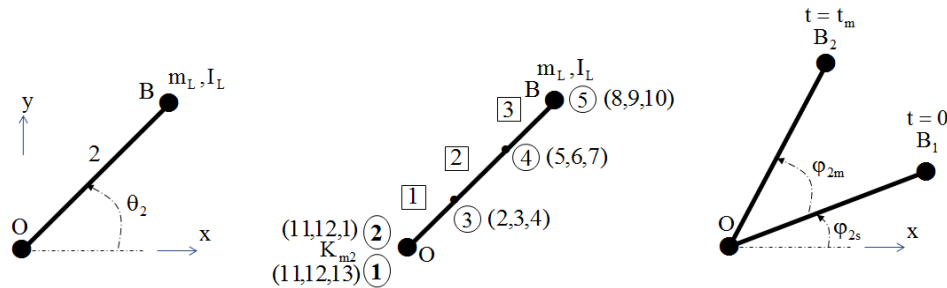


Figure 2.26 (a) Model, (b) FE model, (c) starting and stopping locations of the manipulator.

The finite element (FE) model of the system is shown in Figure 2.26 (b). The number of finite elements for Member-2 is n_{e2} . For Figure 2.26 (b), $n_{e2}=3$. The number for n_{e2} has been chosen as 3 for explanation. The model can be extended to different number of finite elements. The MATLAB code has been developed for any given n_{e2} .

The node numbers are shown in circles. The FE identification numbers are shown in squares. The plane frame analysis is considered and each node has 3 degrees of freedom. The identification numbers of 3 displacements for each node are given in the parentheses. For example, FE-2 has Node-3 at its origin and Node-4 at the far end. The displacements for Node-3 are d_{s2} , d_{s3} , and, d_{s4} , respectively. The local Cartesian coordinates of FE-2 are x_2 , y_2 and z_2 . The local origin of FE-2 is at Node-3 and x_2 axis is towards Node-4. The planar motion is considered, and thus z_2 axis is always parallel to z axis. The displacements in x and y directions for Node-3 are d_{s2} and d_{s3} , respectively. The flexural rotation of the cross-section for Node-3 is r_{s4} and $d_{s4}=h_2r_{s4}$, where h_2 is the length of FE-2. The instantaneous angle of orientation for x_2 is γ_3 , $\gamma_3= \theta_2$. Beam FE's and their parameters are shown in Table 2.9.

Table 2.9 Beam FE's on the system

FE-	On	FE	Length	γ_n	Identification numbers
	Member-	Nodes			for displacements at nodes
1	2	2,3	L_2/n_{e2}	θ_2	11,12,1,2,3,4
2	2	3,4	L_2/n_{e2}	θ_2	2,3,4,5,6,7
3	2	4,5	L_2/n_{e2}	θ_2	5,6,7,8,9,10

The theory of the FE analysis is given in many textbooks (Bathe, 2014). The displacement (\mathbf{d}_{eln}), force (\mathbf{f}_{eln}), stiffness (\mathbf{k}_{eln}), and mass (\mathbf{m}_{eln}) matrices in local coordinates of a finite element (FE-n) are given below (Bathe, 2014). The node numbers are j at the local origin, and k at the far end of FE-n. Flexural bending is about the z axis.

$$\mathbf{d}_{eln} = \begin{Bmatrix} \mathbf{u}_{jn} \\ \mathbf{v}_{jn} \\ h_n r_{jn} \\ \mathbf{u}_{kn} \\ \mathbf{v}_{kn} \\ h_n r_{kn} \end{Bmatrix} \mathbf{k}_{eln} = \begin{bmatrix} \frac{A_n E_n}{h_n} & 0 & 0 & -\frac{A_n E_n}{h_n} & 0 & 0 \\ 0 & \frac{12E_n I_n}{h_n^3} & \frac{6E_n I_n}{h_n^2} & 0 & \frac{-12E_n I_n}{h_n^3} & \frac{6E_n I_n}{h_n^2} \\ 0 & \frac{6E_n I_n}{h_n^2} & \frac{4E_n I_n}{h_n} & 0 & \frac{-6E_n I_n}{h_n^2} & \frac{2E_n I_n}{h_n} \\ -\frac{A_n E_n}{h_n} & 0 & 0 & \frac{A_n E_n}{h_n} & 0 & 0 \\ 0 & \frac{-12E_n I_n}{h_n^3} & \frac{-6E_n I_n}{h_n^2} & 0 & \frac{12E_n I_n}{h_n^3} & \frac{-6E_n I_n}{h_n^2} \\ 0 & \frac{6E_n I_n}{h_n^2} & \frac{2E_n I_n}{h_n} & 0 & \frac{-6E_n I_n}{h_n^2} & \frac{4E_n I_n}{h_n} \end{bmatrix} \quad (2.49)$$

$$\mathbf{f}_{eln} = \begin{Bmatrix} F_{jnx'} + q_{nx'} \frac{h_n}{2} \\ F_{jny'} + q_{ny'} \frac{h_n}{2} \\ T_{jn} + q_{ny'} \frac{h_n^2}{12} \\ F_{knx'} + q_{nx'} \frac{h_n}{2} \\ F_{kny'} + q_{ny'} \frac{h_n}{2} \\ T_{kn} + q_{ny'} \frac{h_n^2}{12} \end{Bmatrix} \mathbf{m}_{eln} = \frac{\rho_n A_n h_n}{420} \begin{bmatrix} 140 & 0 & 0 & 70 & 0 & 0 \\ 0 & 156 & 22h_n & 0 & 54 & -13h_n \\ 0 & 22h_n & 4h_n^2 & 0 & 13h_n & -3h_n^2 \\ 70 & 0 & 0 & 140 & 0 & 0 \\ 0 & 54 & 13h_n & 0 & 156 & -22h_n \\ 0 & -13h_n & -3h_n^2 & 0 & -22h_n & 4h_n^2 \end{bmatrix} \quad (2.50)$$

Here, h_n is the length of FE-n. It has a uniform cross section and A_n is the cross-sectional area. The nodal displacement at Node-m in the x_n direction is u_{mn} , where $m=j$ or k . The nodal displacement in the y_n direction is v_{mn} . The flexural rotation of the cross section at Node-m is r_{mn} . The external load forces at Node-m in the x_n and y_n directions are $F_{mnx'}$ and $F_{mny'}$, respectively. The external bending moment at Node-m is T_{mn} . The distributed external loads on the FE-n in the x_n and y_n directions are $q_{nx'}$ and $q_{ny'}$, respectively. The modulus of elasticity is E_n , I_n is the bending moment of inertia of the cross section and ρ_n is the density.

The displacement (\mathbf{d}_{egn}), force (\mathbf{f}_{egn}), stiffness (\mathbf{k}_{egn}), and mass (\mathbf{m}_{egn}) matrices in global coordinates of FE-n are given below (Bathe, 2014).

$$\mathbf{d}_{egn} = \mathbf{T}_n \mathbf{d}_{eln} \quad \mathbf{k}_{egn} = \mathbf{T}_n^T \mathbf{k}_{eln} \mathbf{T}_n \quad \mathbf{f}_{egn} = \mathbf{T}_n \mathbf{f}_{eln} \quad \mathbf{m}_{egn} = \mathbf{T}_n^T \mathbf{m}_{eln} \mathbf{T}_n \quad (2.51)$$

where, \mathbf{T}_n is the transformation matrix and \mathbf{T}_n^T is the transpose of \mathbf{T}_n . The transformation matrix is given as

$$\mathbf{T}_n = \begin{bmatrix} c_n & s_n & 0 & 0 & 0 & 0 \\ -s_n & c_n & 0 & 0 & 0 & 0 \\ 0 & 0 & 1 & 0 & 0 & 0 \\ 0 & 0 & 0 & c_n & s_n & 0 \\ 0 & 0 & 0 & -s_n & c_n & 0 \\ 0 & 0 & 0 & 0 & 0 & 1 \end{bmatrix} \quad \begin{aligned} c_n &= \cos \gamma_n \\ s_n &= \sin \gamma_n \end{aligned} \quad (2.52)$$

Node-1 and Node-2 are coincident in Figure 2.26 (b), but their flexural rotations are different due to the revolute joint at O. There is a rotational spring between Node-1 and Node-2 (K_{m2}). The rotational spring K_{m2} is for Motor-2. There is a mass representing the payload at Node-5. The Node-1 is fixed. So, $d_{s11}=0$, $d_{s12}=0$, and $d_{s13}=0$. The reaction torque required to fix the rotation is provided by Motor-2.

The mathematical model of the system is obtained as

$$\mathbf{m}_s \ddot{\mathbf{d}}_s + \mathbf{c}_s \dot{\mathbf{d}}_s + \mathbf{k}_s \mathbf{d}_s = \mathbf{f}_s \quad (2.53)$$

Here, \mathbf{m}_s is the system mass matrix, \mathbf{c}_s is the system damping matrix, \mathbf{k}_s is the system stiffness matrix, \mathbf{d}_s is the system displacement matrix, and \mathbf{f}_s is the system force matrix. The sizes of \mathbf{d}_s and \mathbf{f}_s are 10×1 , and the sizes of \mathbf{m}_s , \mathbf{c}_s , and \mathbf{k}_s are 10×10 for the configuration in Figure 2.26 (b). For example, $\mathbf{d}_s(6,1)=d_{s6}$, which is the displacement of Node-4 in the y direction. $\mathbf{f}_s(6,1)=f_{s6}$, which is the external force at Node-4 in the y direction.

Global FE matrices with a size of 6×6 are assembled to obtain the system stiffness (\mathbf{k}_s) and the mass (\mathbf{m}_s) matrices. For example,

$$\mathbf{k}_s(6,5) = \mathbf{k}_{eg2}(5,4) + \mathbf{k}_{eg3}(2,1) \quad \text{and} \quad \mathbf{m}_s(6,5) = \mathbf{m}_{eg2}(5,4) + \mathbf{m}_{eg3}(2,1) \quad (2.54)$$

The combination of (6,5) exists in FE-2 and FE-3 as observed in Table 2.9. The combination of (6,5) is the combination of (5,4) for the FE-2 matrix, and the combination of (2,1) for FE-3 matrix.

Considering the kinetic energy, m_L and I_L are added to the system mass matrix as the following

$$\mathbf{m}_s(8,8)=\mathbf{m}_{eg3}(4,4)+m_L, \quad \mathbf{m}_s(9,9)=\mathbf{m}_{eg3}(5,5)+m_L, \quad \mathbf{m}_s(10,10)=\mathbf{m}_{eg3}(6,6)+I_L \quad (2.55)$$

Considering the potential energy, K_{m2} is added to the system stiffness matrix as the following

$$\mathbf{k}_s(1,1)=\mathbf{k}_{eg1}(3,3)+K_{m2} \quad (2.56)$$

2.6.2 Damping

The Rayleigh damping is considered as

$$\mathbf{c}_s = \eta \mathbf{m}_s + \beta \mathbf{k}_s \quad (2.57)$$

where, η and β are damping coefficients (Rao, 2011).

2.6.3 Motion

The trapezoidal motion profile for the manipulator is considered as shown in Figure 2.26 (c). The manipulator moves from a starting position (OB_1) at $t=0$ to an end position (OB_2) at $t=t_m$, where t_m is the motion time. The initial angular position is given as $\theta_2=\varphi_{2s}$ at $t=0$. The angular position at the stopping time is given as $\theta_2= \varphi_{2s}+ \varphi_{2m}$ at $t=t_m$.

The motor follows the trapezoidal velocity profile. The area under the velocity curve gives the corresponding the motor rotation, φ_{2m} .

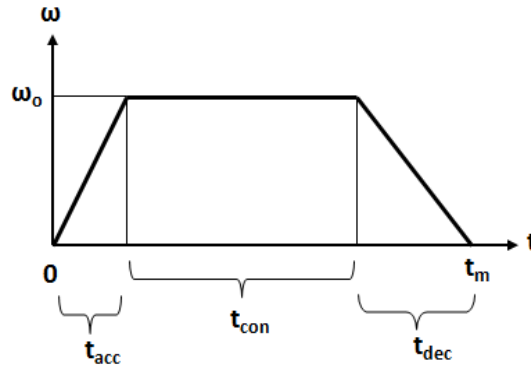


Figure 2.27 The angular trapezoidal velocity profile of the motor.

The accelerations of the mid-points of the FE's are calculated to consider the distributed inertia forces. The rigid body kinematics is considered for the calculation. Let L_{nm} be the distance of a mid-point of FE-n on Member-2 from the point O. Then, the position vector of the mid-point is written with complex numbers as $\mathbf{R}_{nm} = L_{nm} e^{i\theta_2}$, where $i = \sqrt{-1}$. The real part of \mathbf{R}_{nm} is the x component and the imaginary part is the y component. The second derivative of \mathbf{R}_{nm} gives the acceleration as $\mathbf{a}_{nm} = (i\ddot{\theta}_2 - \dot{\theta}_2^2)L_{nm} e^{i\theta_2}$. The real part of \mathbf{a}_{nm} is a_{nmx} , and the imaginary part of \mathbf{a}_{nm} is a_{nmy} .

Considering the velocity profile of the motor, the following equations can be obtained.

$$\omega_{02} = \frac{\Phi_{2m}}{(0.5t_{acc} + t_{con} + 0.5t_{dec})} \quad (2.58)$$

$$\dot{\theta}_2 = \frac{\omega_{02}t}{t_m} \quad \ddot{\theta}_2 = \frac{\omega_{02}}{t_{acc}} \quad \text{for } 0 \leq t < t_{acc} \quad (2.59)$$

$$\dot{\theta}_2 = \omega_{02} \quad \ddot{\theta}_2 = 0 \quad \text{for } t_{acc} \leq t < t_m - t_{dec} \quad (2.60)$$

$$\dot{\theta}_2 = \frac{\omega_{02}(t_m - t)}{(t_m - t_{dec})} \quad \ddot{\theta}_2 = -\frac{\omega_{02}}{t_{dec}} \quad \text{for } t_m - t_{dec} \leq t < t_m \quad (2.61)$$

$$\dot{\theta}_2 = \ddot{\theta}_2 = 0 \quad \text{for } t \geq t_m \quad (2.62)$$

2.6.4 Forces

There are distributed inertia and gravity forces. Let q_{nx} , and q_{ny} be the distributed forces for FE-n. The following can be written:

$$q_{nx} = -(\rho_n A_n h_n) a_{nmx} \quad \text{and} \quad q_{ny} = -(\rho_n A_n h_n) (a_{nmy} + g) \quad \text{where } g = 9.81 \text{ m/s}^2. \quad (2.63)$$

For example, the nodal forces for Node-6 are formed due to the distributed forces for FE-2 and FE-3. So, the following can be written for the elements of the nodal force vector, \mathbf{f}_s , corresponding to Node-6.

$$\mathbf{f}_s(5,1) = q_{2x} h_2 / 2 + q_{3x} h_3 / 2, \quad \mathbf{f}_s(6,1) = q_{2y} h_2 / 2 + q_{3y} h_3 / 2, \quad \mathbf{f}_s(7,1) = q_{2y} h_2^2 / 12 + q_{3y} h_3^2 / 12. \quad (2.64)$$

The inertia forces due to the payload mass are added for $\mathbf{f}_s(8,1)$, $\mathbf{f}_s(9,1)$ and $\mathbf{f}_s(10,1)$.

2.6.5 Vibration Signals

The vibration at the sensor point is analyzed. The vibration direction perpendicular to the line-BC in the x-y plane (motion plane) is considered. Let the displacement of the receiving point in the vibration direction be d_R . The second derivative of d_R is the acceleration signal and denoted by a_R . The gravity is in the z direction, and thus is not included.

2.6.6 Modal Analysis

In order to find the undamped natural frequencies of the manipulators, modal analyses are performed by MATLAB. The following eigenvalues equation obtained from the mathematical model based on the FEM is solved by MATLAB for the single link manipulator.

$$|-\omega^2 \mathbf{m}_s + \mathbf{k}_s| = 0 \quad (2.65)$$

The values of eigenvalues ω_i are found by MATLAB in rad/s. Let f_1 be the first natural frequency of the manipulators. Then, the period T_1 corresponding to the first natural frequency is calculated as $T_1 = 1/f_1$. The half of the period, $T_{1h} = 0.5T_1$, is used to define the motion parameters t_{acc} , t_{con} , t_{dec} .

2.6.7 Numerical Values

A revolute joint is defined at O for the manipulators. The global origin is at O. The manipulators are actuated by a servo motor, which is used in the experiments and rotates around z axis, which is the global coordinate of the link. Since the servo-motor has a joint flexibility, its rotational spring constant K_m is defined for the revolute joint at O. The value of K_m is provided as given in Table 2.10. The wireless accelerometer sensor which will be introduced in the experimental system is considered as a pay-load at B, where vibration responses are obtained from.

The FE model of the planar manipulator has 100 elements and 301 nodes. The material and geometrical properties of the manipulators are given in Table 2.10.

Table 2.10 Properties of the manipulator

Description	Value	Description	Value
Modulus of elasticity	$E = 200 \text{ GPa}$	Density	$\rho = 7800 \text{ kg/m}^3$
Length	$L = 500 \text{ mm}$	Width	$b = 20 \text{ mm}$
Thickness	$h = 3.2 \text{ mm}$	Cross section area	$A = 64 \text{ mm}^2$
Distance of the payload from the end point	$d_{\text{payload}} = 15 \text{ mm}$	Inertia of cross section	$I = 54.61 \text{ mm}^4$
Distance of the receiving point from the center of the payload	$d_{\text{sensor}} = 55 \text{ mm}$	Newmark amplitude decaying factor	$\gamma = 0.005$
Number of finite elements	$n_e = 100$	Rayleigh damping coefficient	$\beta = 3.8 \times 10^{-4}$
Motor rotational spring constants	$K_{m2} = 16000 \text{ Nm/rad}$	Time step	$\Delta t = 0.005 \text{ s}$
Weight of the sensor	$m_s = 0.054 \text{ kg}$	Weight of the payload	$m_L = 0.62 \text{ kg}$

2.6.8 Experimental System

The experimental system used in this study is shown in Figure 2.28.

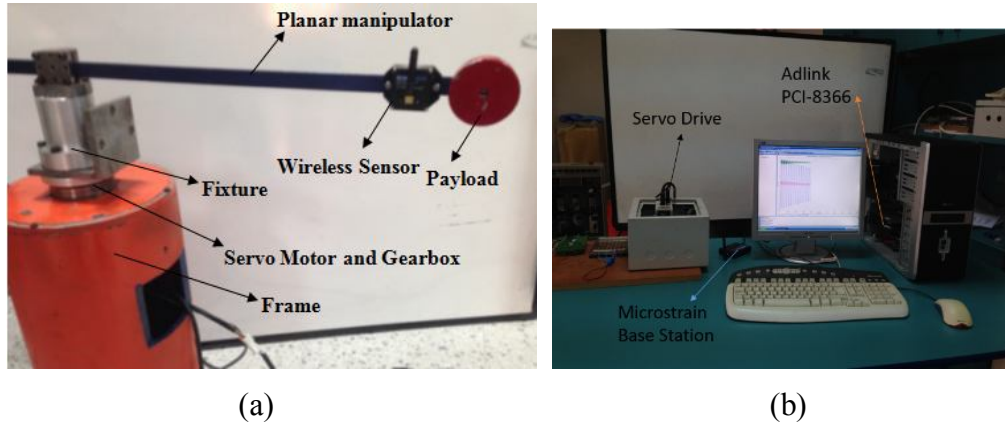


Figure 2.28 Experimental system, (a) planar manipulator, (b) pc-based motion and measurement system.

The manipulator is produced for the experiments. The experimental set-up consists of single-link flexible manipulator, a servo motor and a driver, a motion control card, a wireless accelerometer sensor (WAS), a wireless data acquisition system (WDA) and a PC. The WAS is located at the end of the manipulators in the experiments. The WAS is also modeled as another payload in the simulations since it affects the dynamic behavior of the manipulators.

Mitsubishi Electric servo motor and driver with 200 W, Model HC-KFS23B/MR-J2S-20A, are used. Harmonic Drive gearbox with the gear ratio of 100, Model HFUC-32-100/100 is used for the motor. A PC-based motion control card, Adlink PCI-8366 is used. The motion control card and driver are connected in serial by SSCNET network. The driver is programmed by Visual Basic commands using Adlink-ActiveX component. The motion control units which produce pulses according to the profile given in Figure 2.27 are readily available in the market.

MicroStrain WDA is used to measure acceleration signals at the end point of the manipulators. The WDA system uses three main components; the WAS, the USB base station to receive and pass the data to a host, and software which operates the

system and records the data. The WAS combines triaxial accelerometers and measures vibrations in three directions with their embedded accelerometers. The sampling rate is set as 617 Hz. The low-pass filter is set as and 5 Hz in case of the planar manipulator.

2.6.9 Simulation and Experimental Results

The single-link flexible manipulator is considered in the numerical and experimental analyses. The natural frequencies of the manipulators corresponding to the first three modes are listed in Table 2.11.

Table 2.11 Natural frequencies of the manipulator

Order of Frequency	Planar manipulator	
	FEM (Hz)	Experiment (Hz)
1.	3.166	3.163
2.	-	17.850
3.	48.250	43.080

The second natural frequencies of the planar manipulator obtained by the simulation and experiment correspond to the mode in out of plane. Since the solution by FEM gives the results in plane, the value of its second mode is not listed in the table.

Different stopping positions of the manipulators, which are defined by the vector $\mathbf{q}_p = [\theta_s, \theta_m]$ are studied with the trapezoidal and triangular velocity motion profiles. θ_s is always taken as zero since their value indicates starting position and is not important at rest position. θ_m indicates incremental value of the angular position. Time parameters of the trapezoidal velocity profile is defined by the vector $\mathbf{q}_m = [t_{acc}, t_{con}, t_{dec}, t_m]$. Three time parameters are chosen and the other time parameter is calculated by the equation below.

$$t_m = t_{acc} + t_{con} + t_{dec} \quad (2.66)$$

The calculated parameter is indicated with “*” in \mathbf{q}_m . The units are degree for angles and second for the time parameters unless otherwise stated. The triangular velocity profile, which can be assumed as a special case of a trapezoidal motion profile, is defined by the vector, $\mathbf{q}_m=[t_{acc}, 0, t_{dec}, t_m]$. The constant time parameter is $t_{con}=0$ for the triangular velocity profile. The manipulator moves from a rest position (OB1) at $t=0$ to a stopping position (OB2) at $t=t_m$.

2.6.10 Active Vibration Control of the Manipulator

It is known that, flexibility causes residual vibrations after motion is done. The aim of this study is to reduce the end point vibrations of the beam with active control action. MATLAB is used to construct the finite element models of the system and to integrate the control strategy into Newmark method. The closed loop block diagram is shown in Figure 2.29.

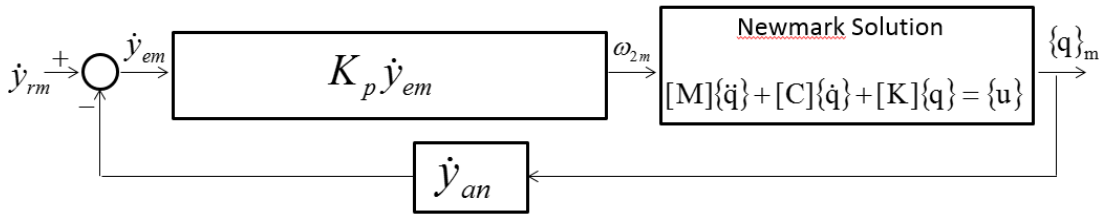


Figure 2.29 Closed loop block diagram

Since the flexible beam is driven by a servo motor in velocity mode, average velocity feedback is used in the closed loop block diagram. Here, \dot{y}_{rm} is the reference velocity signal at the time step m . It is desired to reduce the residual vibrations of the flexible beam, therefore reference velocity signal is taken as zero at each step. The average velocity defined as \dot{y}_{an} at the y -direction of all nodes is taken as the velocity feedback signal at the time step n . \dot{y}_{erm} is the error velocity signal at the time step m and $m=n+1$. K_p is the proportional control action constant. Trapezoidal and triangular velocity profiles are applied to the flexible beam. Closed loop control is activated after motion is done and the instantaneous average velocity of all nodes is subtracted from the reference velocity input to find the error signal

value at a time step in the Newmark solution. The proportional control action is applied to find the actuator signal value in the time step. This input value is used to find the acceleration of the end point for the subsequent time step. The process is continued with the time interval Δt until the steady-state value is approximately reached. A time step, Δt , is chosen for the solution as $\Delta t < 1/(20f_1)$, where f_1 is the first natural frequency considered. $\{q\}_m$ is the value of the translations at x and y directions and the rotation about z axis for each nodes at the time step m. ω_{2m} is the control input at the time step m.

Arbitrary trapezoidal and triangular velocity profiles with the stopping position $\theta_m = 90^\circ$ are applied to the flexible beam and the effect of proportional gain is investigated in active vibration control. Examples signals of vibration responses obtained by Newmark are shown in Figure 2.30 and 2.31.

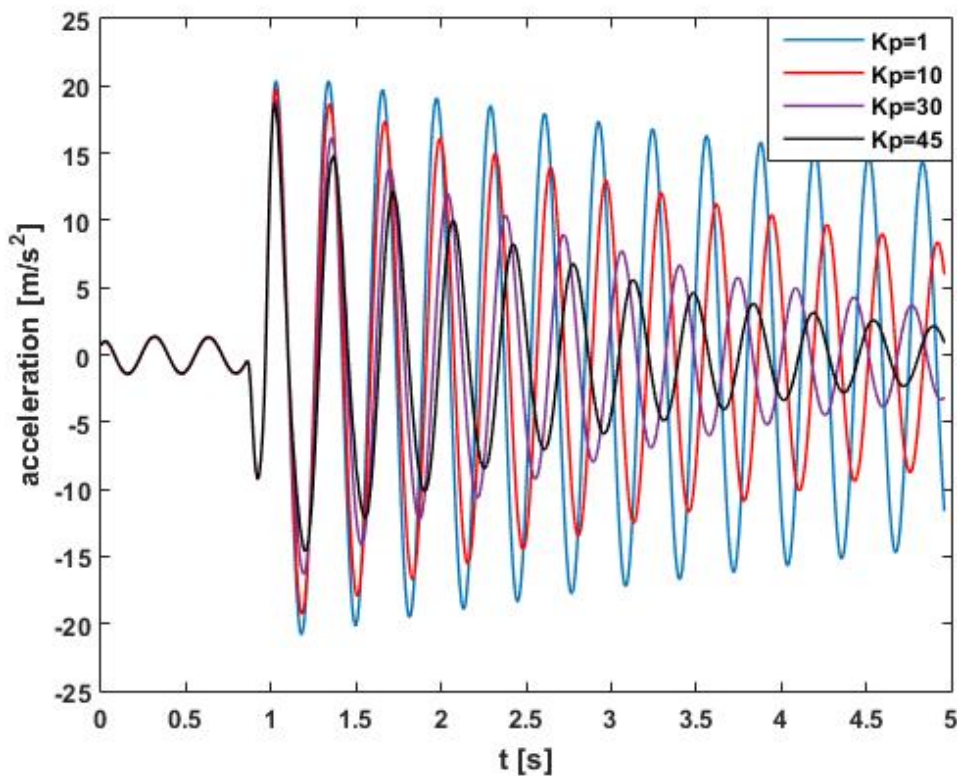


Figure 2.30 Vibration responses for $\theta_m = 90^\circ$ and $\mathbf{q}_m = [* , 0, 0.1, 1]$

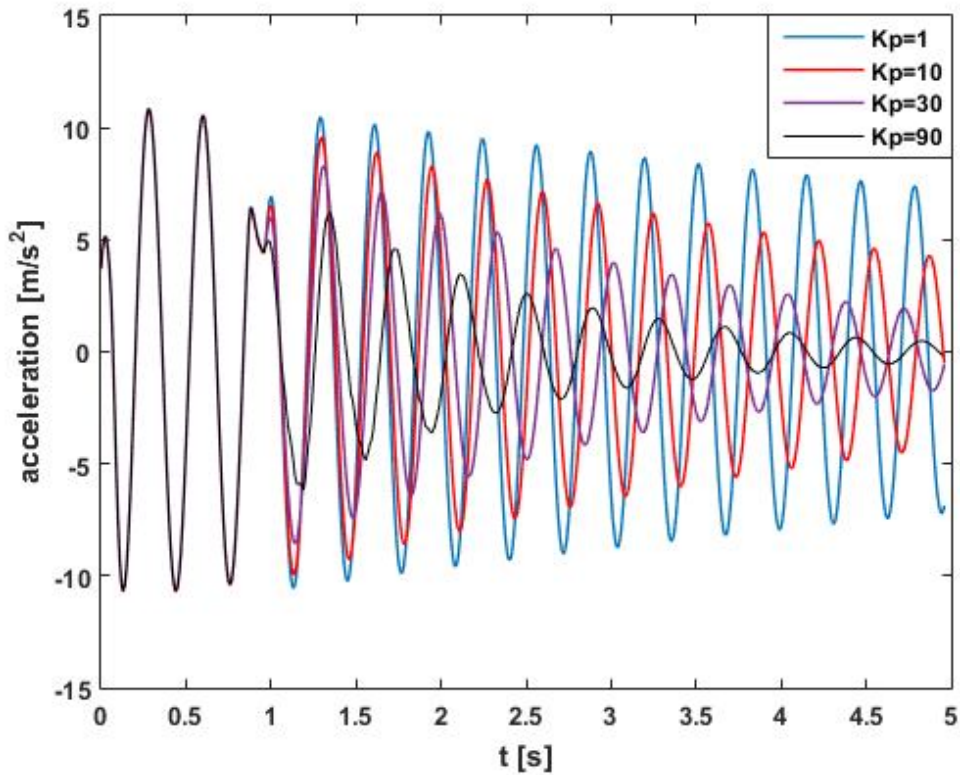


Figure 2.31 Vibration responses for $\theta_m = 90^\circ$ and $\mathbf{q}_m = [*, 0.1, 0.1, 1]$

The window of the vibration signals for $t_m < t < t_m + t_{res}$ is considered to analyze residual vibrations, where t_{res} is the chosen time for residual vibrations. The time value is taken as $t_{res} = 4s$ for the window. The root mean square (RMS) value of the windowed signal is computed for the cases. The computed RMS values for the cases are listed in Table 2.12.

Table 2.12 Case results for the manipulator

Motion parameters	K_p	RMS (m/s ²) Control-OFF	RMS (m/s ²) Control-ON	Reduction %
[* , 0,0.1, 1]	10	12.5301	9.8642	21.28
	30		7.0428	43.79
	45		5.9737	52.33
[* , 0, 0.05, 1]	10	14.4543	11.2576	22.12
	30		7.8813	45.47
	45		6.5966	54.36
[* , 0.1, 0.1, 1]	10	6.2974	4.9633	21.18
	30		3.4890	44.60
	90		2.1187	66.36
[* , 0.05, 0.1, 1]	10	3.4	2.6681	21.53
	30		1.8563	45.40
	90		1.0972	67.73

In case of the triangular velocity profile with $\mathbf{q}_m=[*, 0, 0.1, 1]$; the RMS value for Control-OFF result is 12.5301 and the reductions are 21.28 %, 43.79 % and 52.33 % for $K_p= 10, 30$ and 45, respectively. In case of the triangular velocity profile with $\mathbf{q}_m=[*, 0, 0.05, 1]$; the RMS value for Control-OFF result is 14.4543 and the reductions are 22.12 %, 45.47 % and 54.36 % for $K_p= 10, 30$ and 45, respectively.

In case of the trapezoidal velocity profile with $\mathbf{q}_m=[*, 0.1, 0.1, 1]$; the RMS value for Control-OFF result is 6.2974 and the reductions are 21.18 %, 44.60 % and 66.36 % for $K_p= 10, 30$ and 90, respectively. In case of the trapezoidal velocity profile with $\mathbf{q}_m=[*, 0.1, 0.05, 1]$; the RMS value for Control-OFF result is 3.4 and the reductions are 21.53 %, 45.40 % and 67.73 % for $K_p= 10, 30$ and 90, respectively.

The response spectrum via the deceleration time for triangular and trapezoidal cares is given in Figure 2.32-2.33.

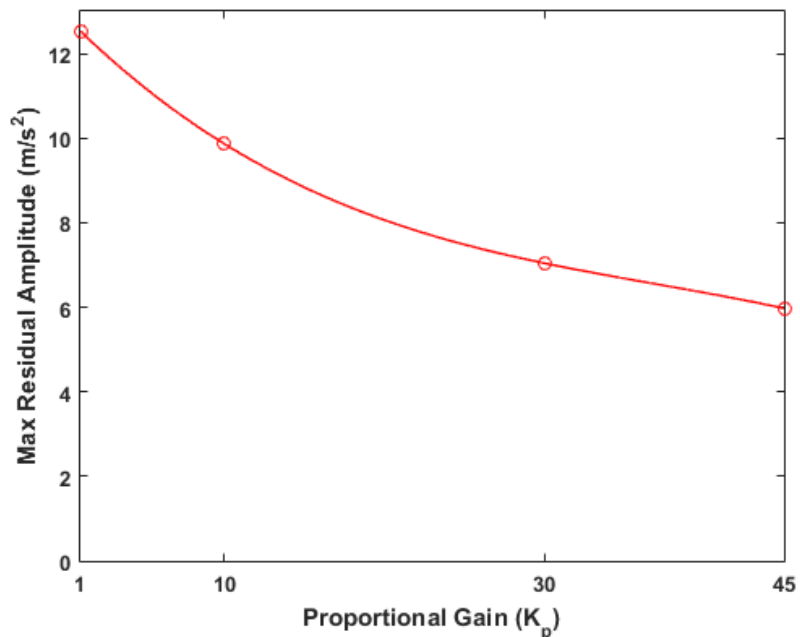


Figure 2.32 Change of the RMS values of the residual vibration signals versus the proportional gain for $\mathbf{q}_m=[*, 0, 0.1, 1]$.

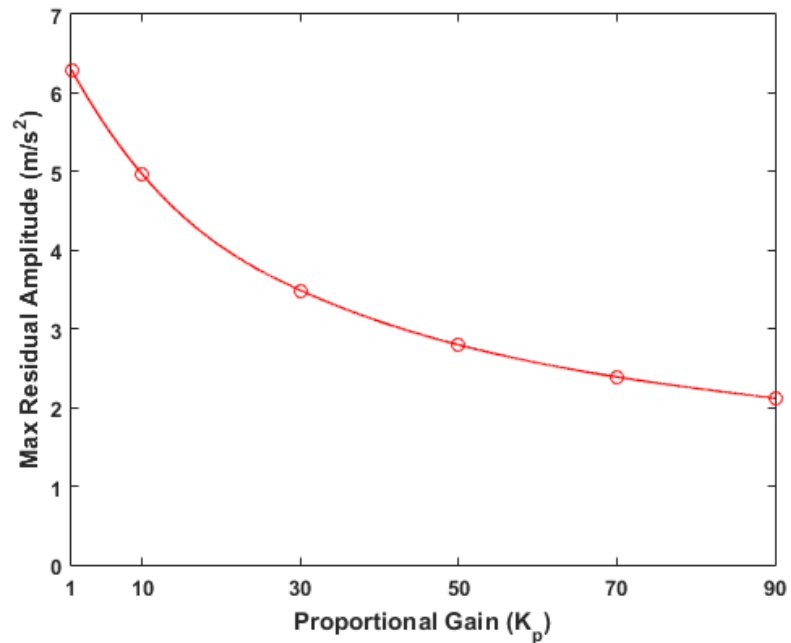


Figure 2.33 Change of the RMS values of the residual vibration signals versus the proportional gain for $\mathbf{q}_m=[*, 0.1, 0.1, 1]$.

2.7 Conclusion

Flexible robot manipulators have smaller actuators and consume less energy. Active vibration control is important to control the vibrations due to the flexibility. Robot arms and flexible mechanical systems in general can be modeled as a multi-degree of freedom vibratory system. The mathematical model of such systems can be solved by the Runge-Kutta and Newmark method.

In this chapter, the modeling and dynamic analysis of the multi-degree-of-freedom system are performed and the dynamic responses are obtained with Runge-Kutta and Newmark method. Passive vibration control is applied to the system and the results are compared with both numerical methods. It is observed that both numerical methods are in good agreement.

For the other study of this chapter, a procedure is developed to integrate proportional-integral-derivative (PID) control action into the Newmark solution for four-degree-of-freedom system. The numerical control action is applied to the error

signal value at a time step to find the actuator signal value and the Newmark algorithm is applied to find the output values at the subsequent time step. A step function is considered as the reference input signal for the closed loop system. An approximate model for the samples of the step function is used to obtain bounded derivatives. The numerical results are compared with analytical solutions obtained by the Laplace transform method. Various results are given for undamped or damped system by setting PID parameters. It is observed that the numerical and analytical results are in good agreement. The results of this study can be used to simulate the active vibration control of flexible mechanical systems which are more complex and have their finite element models.

Finite element model of a cantilever flexible beam is created in MATLAB by Euler-Bernoulli beam theorem. Active vibration control by Newmark method is achieved by applying a control force to a determined distance from the created model's end point under impulse input. Effect of various controller parameters on end-point vibrations is examined. When the number of elements in the finite element model of the flexible beam is increased, it is observed that dynamic behavior does not change as long as the feedback point and the point that the control force is applied stayed the same. The distance which the control force has to be applied for damping the end point vibrations of the finite element model of the flexible beam in the least amount of time is optimized in MATLAB. With this approach more complex systems can be modelled and actively controlled.

The finite element model of a rotating flexible manipulator can also be created in MATLAB and transient results can be observed by the Newmark method. In this study, triangular and trapezoidal velocity profiles are applied to the manipulator. The proportional control gain is applied which is integrated into Newmark solution. Active control is activated after motion is done. The root mean square values calculated from the residual vibration signals, and reduction ratios are presented for the cases. It is observed from the results that the residual vibration amplitudes of the manipulators are successfully suppressed by the proportional control gain.

CHAPTER THREE

VIBRATION CONTROL OF SINGLE-LINK FLEXIBLE COMPOSITE MANIPULATOR

The use of lighter manipulators reduces the power consumption and increases payload-to-weight ratio. Composite manipulators can be preferred for this aim due to their properties such as light weight and high strength. Using lighter manipulators causes vibrations due to their flexibility. Flexibility affects the end-point positioning accuracy and repeatability of manipulators in high speed engineering applications. In this section, a single-link flexible composite manipulator is considered to analyze in ANSYS and reduce end-point vibrations. The finite element vibration analysis is performed and an experimental system is introduced to verify simulation results. [0/90] and [45/-45] lay-ups, trapezoidal and triangular velocity profiles are studied by creating cases for different stopping positions and motion times. The time intervals of the motion profiles are determined from the natural frequency of the composite manipulator. Residual vibrations which are occurred after stopping the movement of the manipulator are obtained and the root mean square (RMS) values of these signals are calculated. It is observed from the results that the first vibration mode dominates to reduce the residual amplitudes. The lowest RMS values are achieved for various cases if the time interval is selected so that the deceleration time equals to the inverse of the first natural frequency.

3.1 Introduction

Manipulators having lighter arms, lower power consumption and higher payload-to-weight ratio are currently in demand in industry. Manipulators can be produced with composite materials for these demands. However, the use of lightweight arms causes flexibility and vibrations. Vibrations affect the accuracy of the end point and repeatability of the flexible manipulators. There are challenging problems in design, modeling, analysis and control due to the nature of the flexible manipulators (Gao et al., 2012).

Suppressing the vibrations with active or passive control techniques become important to increase productivity of the flexible manipulators. Passive control techniques do not require additional equipment and hardware in practice while active control techniques require a closed loop control with additional equipment in practice.

The vibration control of single-link metal manipulators is studied extensively with active or passive techniques. Limited studies on the passive vibration control of flexible composite manipulators have been observed and literature survey of the single-link flexible manipulators composed of metal and composite materials are summarized here.

A survey on control of flexible manipulators is presented in (Benosman & LeVey, 2004). Control objectives for the flexible manipulators are classified as end effector regulation problem, end effector to rest motion in a desired fixed time, joint-trajectory tracking, and end-effector trajectory tracking. Studies related to four control objectives are cited.

A literature review for dynamic analysis of flexible manipulators is given in the reference (Dwivedy & Eberhard, 2006). Modeling, control, and experimental studies on single link flexible manipulators are reviewed in detail. The studies related to the modeling of single flexible manipulators are grouped as assumed mode method, finite element method, lumped parameter models and other studies. One of the conclusions of the review is that the necessity of more experimental investigations to validate the simulation modeling.

Residual vibrations of flexible manipulators are reduced by changing the motion commands. In references (Mimmi & Pennachi, 2001; Pereira et al., 2012; Shan et al., 2005; Yang et al., 2006) input shaping control is applied to single flexible manipulators. Simulation and experiments are performed by planning motion of a flexible single link with a piezoelectric actuation in the reference (Reis & da Costa, 2012). Free vibration of a rotating beam with nonlinear spring-mass system is

investigated and natural frequency results are given in the reference (Das et al., 2007). Two methods based on the shock response spectrum is presented in the reference (Shin & Brennan, 2008) for suppressing of the residual vibrations of a rotating flexible beam without considering any control algorithms. The procedure is summarized to eliminate residual vibration. The results have showed that the residual response is zero if the duration of the pulse is appropriately chosen. Vibration control of residual vibration of an elastic manipulator is performed using the mode summation techniques in the reference (Ankarali & Diken, 1997). Zero residual vibration results are obtained for certain values of the cycloidal motion input. The study is extended by Diken and Alghamdi (2003) conducting experiments to verify the simulation results for a rotating aluminum beam. A response spectrum obtained from residual vibrations of a flexible shaft-beam for a cycloidal motion input is presented by Ankarali et al. (2012) using the same method in the reference (Ankarali & Diken, 1997).

Although there are many studies on vibration analysis of composite beams in the literature, limited works has included vibration control of composite structures. In references (Abramovic, 1992; Abramovic & Livshits, 1994; Kapania & Raciti, 1989; Singh & Abdelanser, 1992), vibration analysis has been studied on stationary composite beams by reasearchers. For rotating composite structures, different methods have been used to analyze the vibrations (Aksencer & Aydogdu, 2015; Arvin & Lacarbonara, 2014; Arvin & Nejad, 2013; Arvin et al., 2013; Chandiramani et al., 2002; DeValve & Pitchumani, 2014; Jiang et al., 2014; Ozdemir & Kaya, 2006; Rand, 1995; Yoo et al., 2005). In control techniques, passive control is used as changing the damping ratio by using different orientation angles (Kang et al., 2002). Bandopadhyaya et al. (2008) have used ionic polymer metal composite (IPMC) as an active damper to control a single-link flexible manipulator. They proposed the suitable positions to fix two IPMC actuators based on modal approach to suppress vibrations efficiently. Ji et al. (2009) have improved synchronized switch damping on voltage (SSDV) approach to control the vibrations of a composite beam. The proposed approach adjusted the voltage coefficient which controls the damping

efficiency adaptively and they showed that the improved SSDV approach is the most stable compared with previous SSDV techniques.

In the present work, the vibration control of a single-link flexible composite manipulator with [0/90] and [45-45 lay-ups] is studied using the trapezoidal and triangular motion profiles. Theoretical vibration results are obtained using the FE method and experiments are conducted to verify the FE vibration results. Cases are created for different stopping positions and motion times of the composite manipulator. The effect of the time intervals such as the acceleration time, the constant velocity time, and especially the deceleration time on the residual vibration of the end point is analyzed. The deceleration time based on the fundamental frequency of the manipulator is effective to reduce vibrations as the proposed studies in the references (Ankarali & Diken, 1997; Ankarali et al., 2012; Diken & Alghamdi, 2003). Satisfactory reduction ratios are achieved theoretically and experimentally in the residual vibration amplitudes of the composite manipulator with a passive control approach.

3.2 Finite Element Vibration Analysis

The system under study is shown in Figure 3.1. The manipulator is the OB beam. There is a revolute joint at O. The manipulator is actuated by a servo motor, which is used in the experiments and rotates around z axis, which is the global coordinate of the link. The global origin is at O. The mass of the servo motor is on the frame at O. Since the servo-motor has a joint flexibility, its rotational spring constant K_m is defined for the revolute joint at O. The value of K_m is given by the manufacturer as 16000 Nm/rad. The wireless accelerometer sensor which will be introduced in the experimental system is considered as a pay-load. The pay-load is defined at the distance of 320 mm from O.

The FE model the manipulator is created using shell elements in ANSYS/Workbench. The FE model has 80 elements and 123 nodes as shown in Figure 3.1.

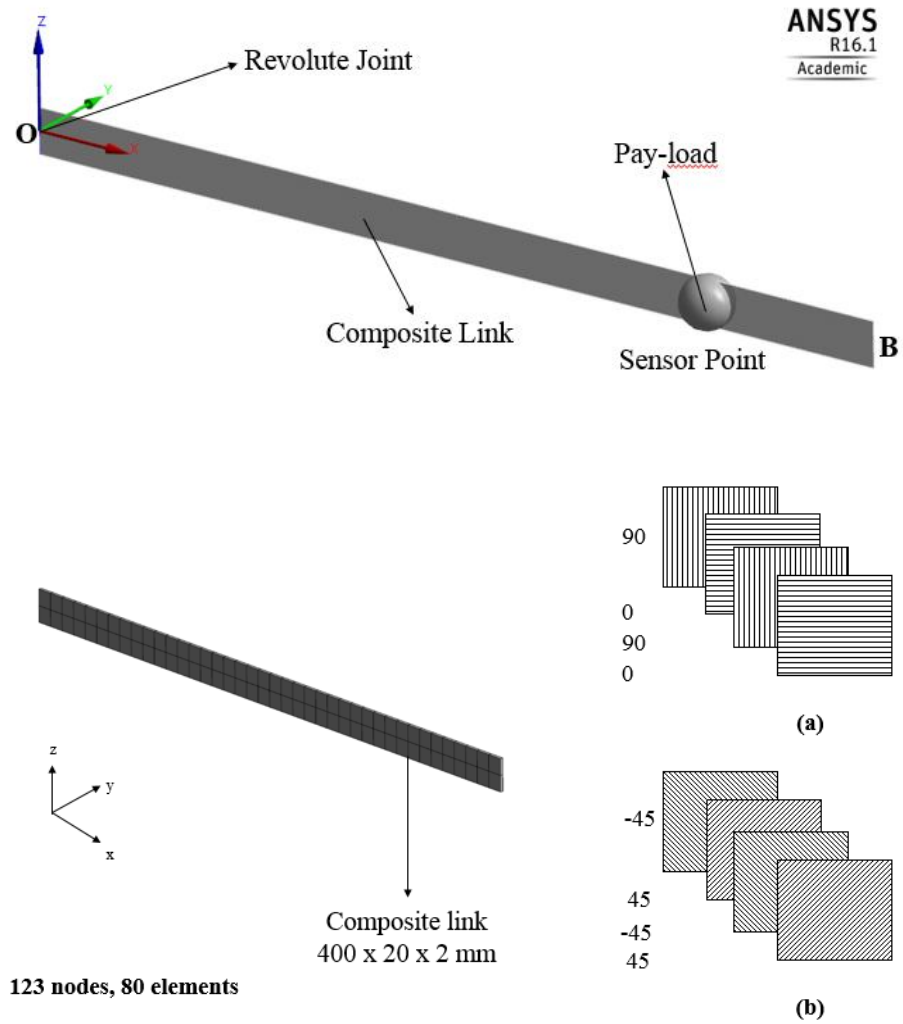


Figure 3.1 The FE model of the composite manipulator.

The composite link consists of eight layers and the orientations are defined for each layer. Two lay-ups such as $[0/90]$ and $[45/-45]$ are considered for the composite manipulator. The material and geometrical properties of the composite manipulators are given in Table 3.1.

Table 3.1 Properties of the composite manipulator

Description	Value	Description	Value
Longitudinal Modulus	$E_1 = 23800$ MPa	Manipulator Length	$L=400$ mm
Transverse Modulus	$E_2 = 22900$ MPa	Rectangular Cross Section	$b=20$ mm, $h=2$ mm
Poison ratio	$\nu_{12} = 0.16$	Cross Section Area	$A=40$ mm ²
Shear Modulus	$G_1=3400$ MPa $G_2 = 3250$ MPa	Inertia of Cross Section	$I=13.33$ mm ⁴
Density	$\rho = 1.78$ g/cm ³	Wight of pay-load	$m_p=54$ g

After modeling the composite manipulator, modal analysis is performed to find natural frequencies. Then transient analysis is realized for the FE vibration analysis of the single-link manipulator. The motion is assigned to the revolute joint in the FE model.

The servo motor is derived by the trapezoidal velocity profile as shown in Figure 3.2.

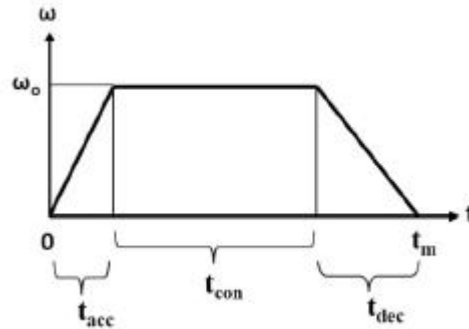


Figure 3.2 Trapezoidal velocity profile.

The maximum angular velocity for this profile can be calculated with the equation below.

$$\omega_0 = \frac{\theta_m \frac{\pi}{180}}{0.5t_a + t_c + 0.5t_d} \quad (3.1)$$

where t_{acc} is the acceleration time, t_{con} is the constant time, t_{dec} is the deceleration time, t_m is motion time, θ_m is the angular displacement in rad and ω_0 is the angular velocity in rad/s.

In simulations, the time step is chosen as 0.001 s by considering first three natural frequencies of the system. Rayleigh damping is used to take into account the damping of composite manipulator. The Rayleigh damping coefficient (β) is taken as 0.0004.

3.3 Experimental System

The experimental system used in this study is shown in Figure 3.3.

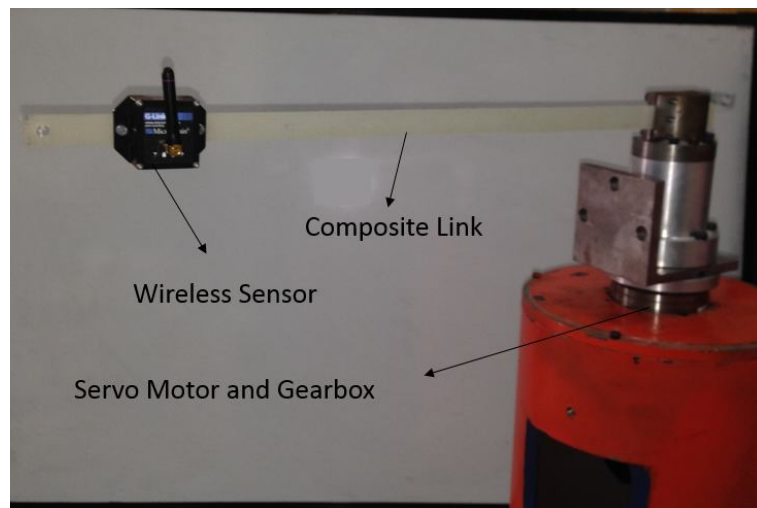


Figure 3.3 Experimental system

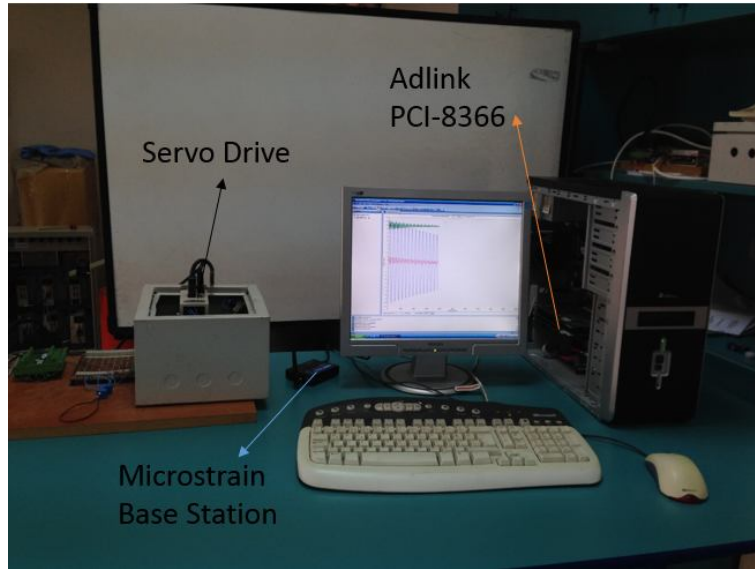


Figure 3.3 Experimental system (cont.)

The experimental set-up consists of a single-link flexible composite manipulator, a servo motor and a driver, a motion control card, a wireless accelerometer sensor (WAS), a wireless data acquisition system (WDA) and a PC. The WAS is fixed with bolts to the manipulator in the experiments. The WAS is considered as a pay-load in the simulations as explained in section 2 since it affects the dynamic behavior of the composite manipulator.

The composite manipulators with $[0/90]$ and $[45/-45]$ lay-ups are produced from a woven glass fiber/epoxy composite plate. The area density of woven fabric glass fibers is 500 g/m^2 . An epoxy system consisted of Araldite LY 564 and Aradur 3487 BD is used as matrix material. For the curing process, the laminated plates are kept at $80 \text{ }^\circ\text{C}$ for 8 h.

Mitsubishi Electric servo motor and driver with 200 W, Model HC-KFS23B/ MR-J2S-20A, are used. Harmonic Drive gearbox with the gear ratio of 100, Model HFUC-32-100/100 is used for the motor. A PC-based motion control card, Adlink PCI-8366 (Adlink Technology Inc, 2015) is used. The motion control card and driver are connected in serial by SSCNET network. The driver is programmed by Visual Basic commands using Adlink-ActiveX component.

MicroStrain WDA (MicroStrain Inc., 2015) is used to measure acceleration signals at the end point of the composite manipulator. The WDA system uses three main components; the WAS, the USB base station to receive and pass the data to a host, and software which operates the system and records the data. The WAS combines triaxial accelerometers and measures vibrations in three directions with their embedded accelerometers. The sampling rate and low-pass filter are set as 617 Hz and 5 Hz in the software, respectively.

3.4 Simulation and Experimental Results

Two different lay-ups such as [0/90] and [45/-45] for the single-link composite manipulator are considered in simulation and experimental analyses. The natural frequencies of the composite manipulator corresponding to the first three modes are found and listed in Table 3.2.

Table 3.2 Natural frequencies of the composite manipulator

Order of Frequency	[0/90]		[45/-45]	
	Simulation (Hz)	Experiment (Hz)	Simulation (Hz)	Experiment (Hz)
1.	3.2283	3.2386	2.6351	2.5608
2.	32.08	30.88	24.812	23.5743
3.	45.27	43.68	34.997	57.3165

It is observed from the table that ply orientations affect the dynamic properties of the manipulator and the natural frequencies of [0/90] lay-up are higher than those of [45/-45] lay-up. The composite manipulator becomes more flexible as the first natural frequency decreases. The first natural frequencies for the two lay-ups are considered in the transient analyses since the effect of the higher frequency modes is very small. So, it is expected that their first vibration modes are dominated for vibration reduction.

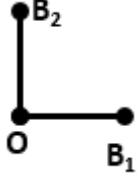
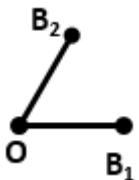
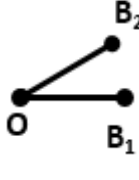
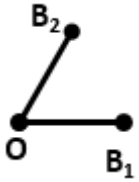

Different stopping positions of the composite manipulator, which are defined by the vector $\mathbf{q}_p=[\theta_s, \theta_m]$ are studied with the trapezoidal and triangular velocity motion

profiles. θ_s is always taken as zero since their value indicates starting position and is not important at rest position. θ_m indicates incremental value of the angular position. Time parameters of the trapezoidal velocity profile is defined by the vector $\mathbf{q}_m=[t_{acc}, t_{con}, t_{dec}, t_m]$. Three time parameters are chosen and the other time parameter is calculated by the equation below.

$$t_m = t_{acc} + t_{con} + t_{dec} \quad (3.2)$$

The calculated parameter is indicated with “*” in \mathbf{q}_m . The units are degree for angles and second for the time parameters unless otherwise stated. The triangular velocity profile, which can be assumed as a special case of a trapezoidal motion profile, is defined by the vector, $\mathbf{q}_m=[t_{acc}, 0, t_{dec}, t_m]$. The constant time parameter is $t_{con}=0$ for the triangular velocity profile. The manipulator moves from a rest position (OB1) at $t=0$ to a stopping position (OB2) at $t=t_m$. Five cases with the trapezoidal and triangular velocity motion profiles are considered for different stopping positions and motion times of the composite manipulator as given in Table 3.3.

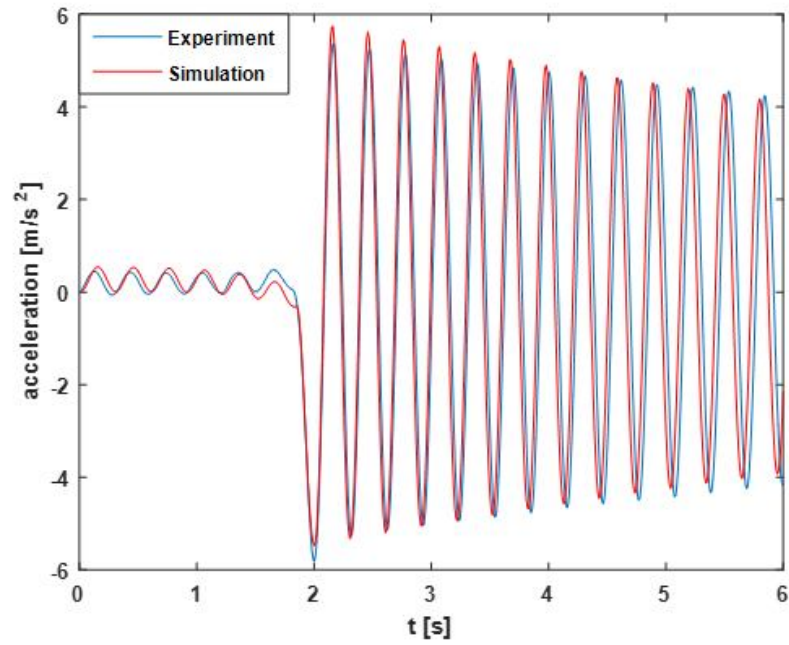
Table 3.3 Motion cases

Cases	$[\Theta_s, \Theta_m]$	t_m	Pictorial	[0/90]		[-45/45]	
				T_{1h} for simulation ^a	T_{1h} for experiment ^a	T_{1h} for simulation ^a	T_{1h} for experiment ^a
Case-1	[0,90]	2		1/3.2283/2	1/3.2386/2	1/2.6351/2	1/2.5608/2
Case-2	[0,60]	2		1/3.2283/2	1/3.2386/2	1/2.6351/2	1/2.5608/2
Case-3	[0,30]	2		1/3.2283/2	1/3.2386/2	1/2.6351/2	1/2.5608/2
Case-4	[0,60]	1		1/3.2283/2	1/3.2386/2	1/2.6351/2	1/2.5608/2
Case-5	[0,60]	4		1/3.2283/2	1/3.2386/2	1/2.6351/2	1/2.5608/2

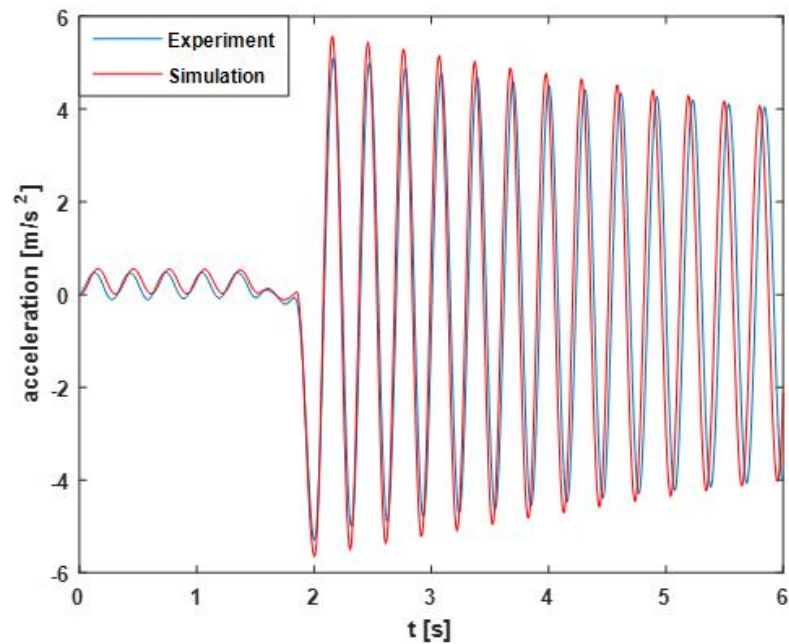
^a T_{1h} is determined from the value of the fundamental frequency of the manipulator.

The effect of θ_m is studied in Case-1, Case-2 and Case-3. The effect of t_m is studied in Case-4, Case-5. The stopping positions and motion time are taken as $\theta_m=90^\circ$, $\theta_m=60^\circ$, $\theta_m=60^\circ$ and $t_m=2$ s for Case-1, Case-2 and Case-3, respectively. The stopping position and motion time are taken as $\theta_m=60^\circ$, and $t_m=1$ s for Case-4. The stopping position and motion time are taken as $\theta_m=60^\circ$, and $t_m=4$ s for Case-5.

Examples signals of vibration responses obtained by simulation and experimental analyses are shown in Figure 3.4 and Figure 3.5.

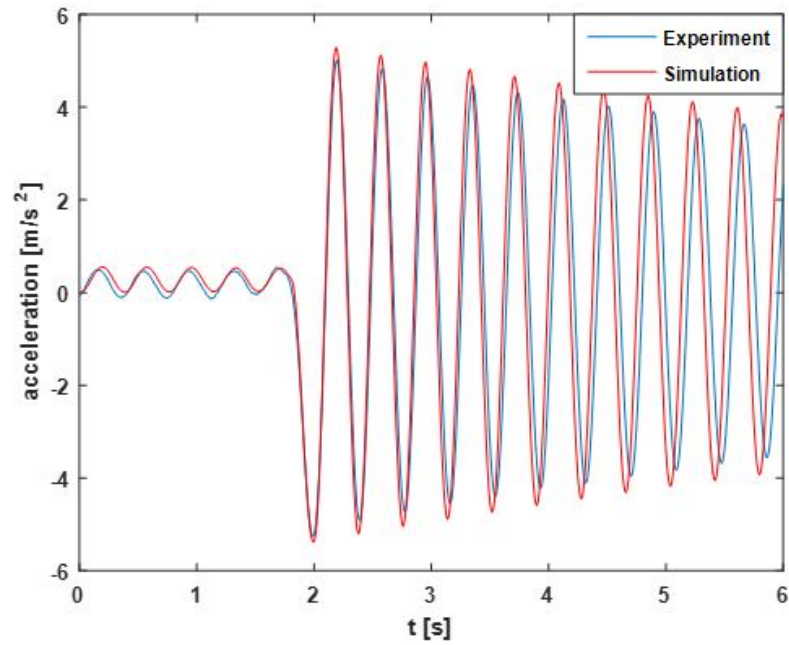


(a)

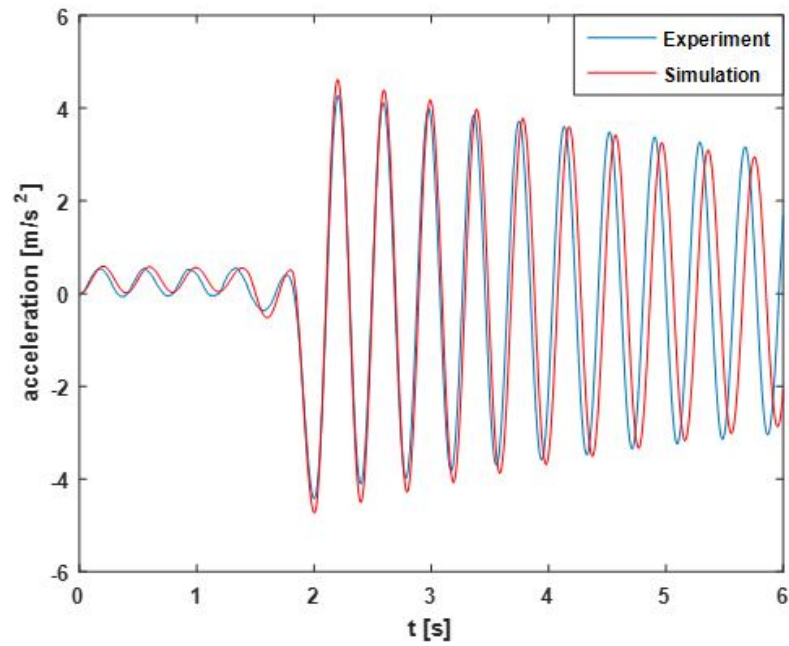


(b)

Figure 3.4 Vibration responses for Case-1 for [0/90] lay-up (a) $\mathbf{q}_m = [* , 0, t_{1h}, t_m]$, (b) $\mathbf{q}_m = [* , 2t_{1h}, t_{1h}, t_m]$ and [45/-45] lay-up (c) $\mathbf{q}_m = [* , 0, t_{1h}, t_m]$, (d) $\mathbf{q}_m = [* , 2t_{1h}, t_{1h}, t_m]$.

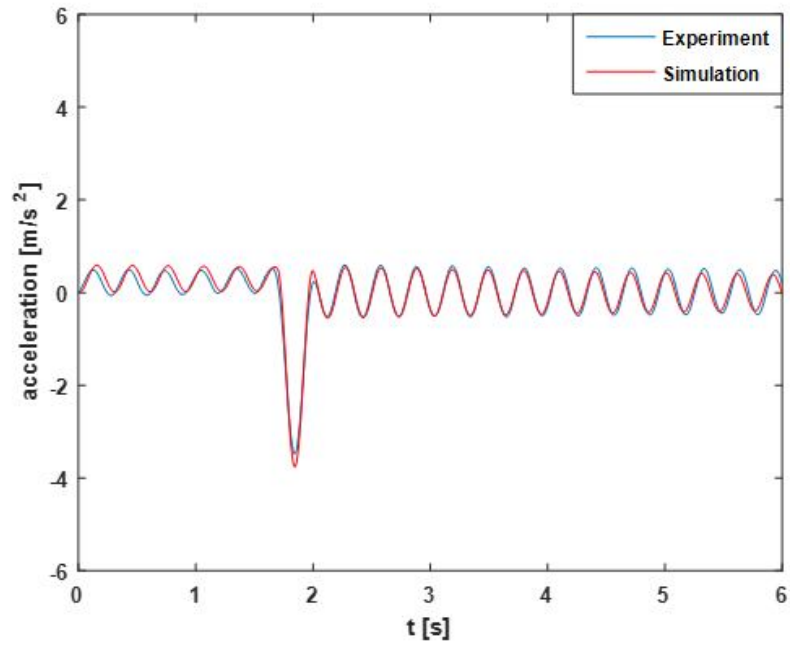


(c)

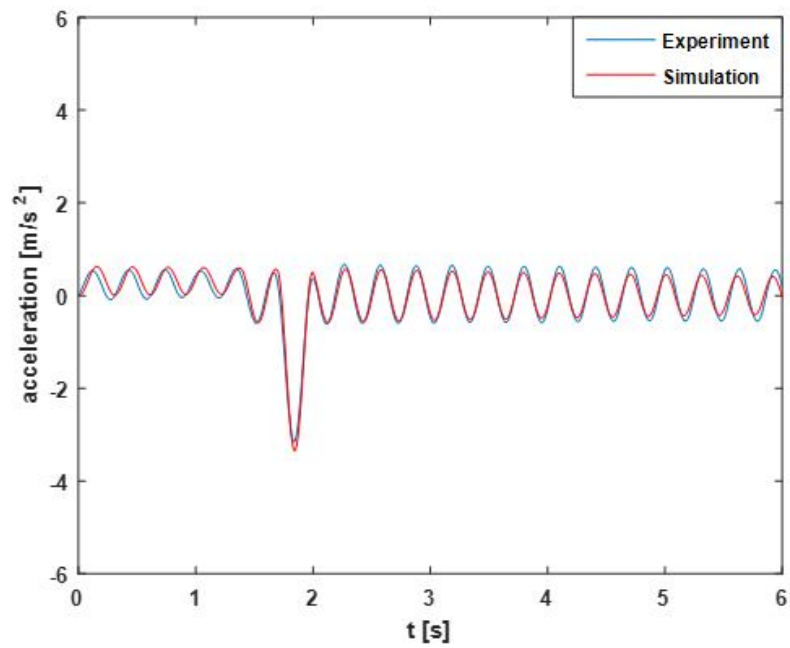


(d)

Figure 3.4 Vibration responses for Case-1 for [0/90] lay-up (a) $\mathbf{q}_m = [* , 0, t_{1h}, t_m]$, (b) $\mathbf{q}_m = [* , 2t_{1h}, t_{1h}, t_m]$ and [45/-45] lay-up (c) $\mathbf{q}_m = [* , 0, t_{1h}, t_m]$, (d) $\mathbf{q}_m = [* , 2t_{1h}, t_{1h}, t_m]$. (cont.)

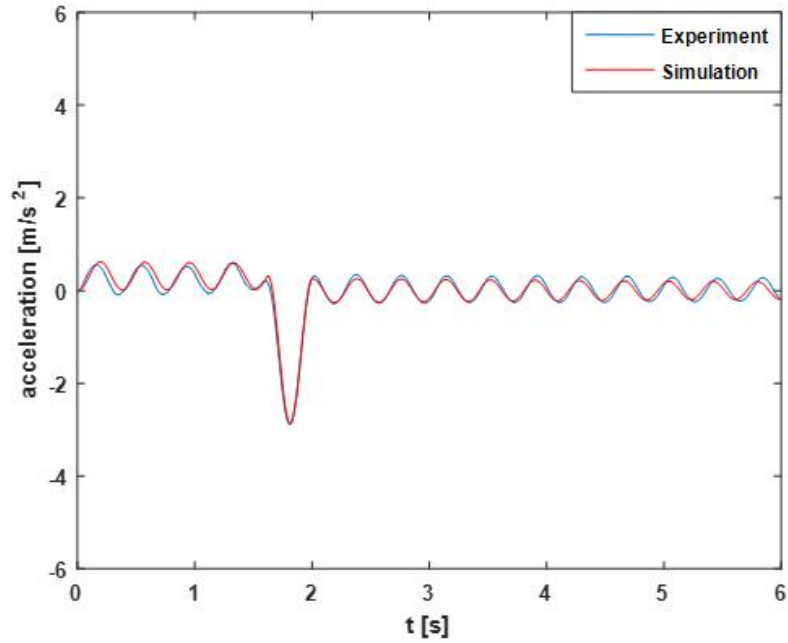


(a)

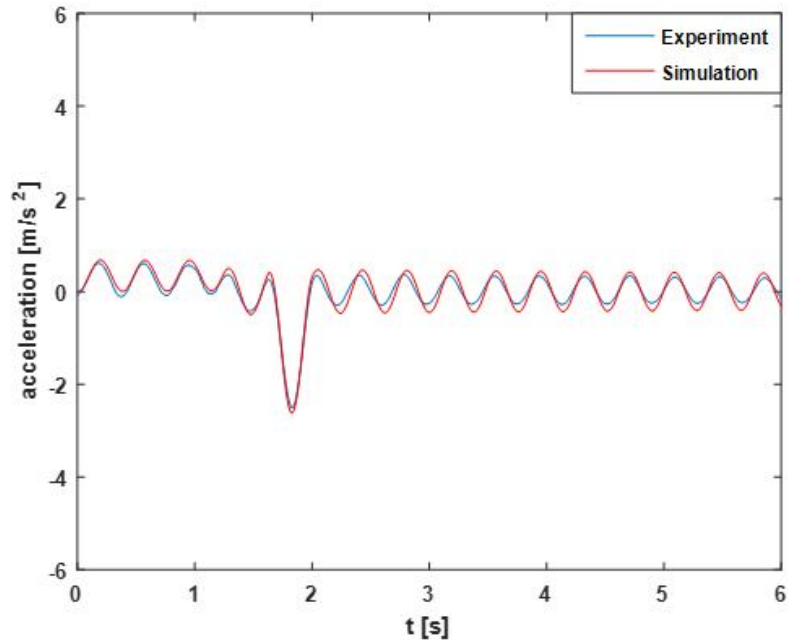


(b)

Figure 3.5 Vibration responses for Case-1 for [0/90] lay-up (a) $\mathbf{q}_m = [* , 0, 2t_{1h}, t_m]$, (b) $\mathbf{q}_m = [* , 2t_{1h}, 2t_{1h}, t_m]$ and [45/-45] lay-up (c) $\mathbf{q}_m = [* , 0, 2t_{1h}, t_m]$, (d) $\mathbf{q}_m = [* , 2t_{1h}, 2t_{1h}, t_m]$.



(c)



(d)

Figure 3.5 Vibration responses for Case-1 for $[0/90]$ lay-up (a) $\mathbf{q}_m = [*,0,2t_{1h},t_m]$, (b) $\mathbf{q}_m = [*,2t_{1h}, 2t_{1h},t_m]$ and $[45/-45]$ lay-up (c) $\mathbf{q}_m = [*,0, 2t_{1h},t_m]$, (d) $\mathbf{q}_m = [*,2t_{1h}, 2t_{1h},t_m]$. (cont.)

Residual vibrations are important to discuss the effect of vibration control and observe especially the reduction in the amplitudes. The window of the vibration

signals for $t_m < t < t_m + t_{res}$ is considered to analyze residual vibrations, where t_{res} is the chosen time for residual vibrations. The time value is taken as $t_{res} = 4s$ for the window. The root mean square (RMS) value of the windowed signal is computed for the cases. The computed RMS values for the five cases are listed in Table 3.4-3.8.

It is observed from the figures that simulation and experimental result matches well each other. The RMS value is the highest when deceleration time equals to T_{1h} . The constant velocity time parameter is chosen as $t_{con} = 2T_{1h}$ for the trapezoidal motions in all cases.

Table 3.4 RMS and reduction ratios for Case-1.

Lay-up	Motion parameters	ω_{max} (rad/s)	RMS (m/s ²) Experiment	Reduction %	RMS (m/s ²) Simulation	Reduction %	
[0/90]	[*,0, t_{1h}, t_m]	1.5708	3.3822	-	3.4070	-	
	[*,0, $2t_{1h}, t_m$]	1.5708	0.3660	89.18	0.3302	90.31	
	[*,0, $3t_{1h}, t_m$]	1.5708	1.2713	62.41	1.3157	61.38	
	[*,0, $4t_{1h}, t_m$]	1.5708	0.4681	86.16	0.3973	88.34	
	[*,0, $5t_{1h}, t_m$]	1.5708	0.7882	76.70	0.7870	76.90	
	[*,0, $6t_{1h}, t_m$]	1.5708	0.5904	82.54	0.5029	85.24	
	[* , $2t_{1h}, t_{1h}, t_m$]	1.3607	3.2170	-	3.4082	-	
	[* , $2t_{1h}, 2t_{1h}, t_m$]	1.3607	0.4214	86.90	0.3483	89.78	
	[* , $2t_{1h}, 3t_{1h}, t_m$]	1.3607	1.1183	65.24	1.1377	66.62	
	[* , $2t_{1h}, 4t_{1h}, t_m$]	1.3607	0.5103	84.14	0.4408	87.07	
	[* , $2t_{1h}, 5t_{1h}, t_m$]	1.3607	0.6911	78.52	0.6791	80.07	
	[* , $2t_{1h}, 6t_{1h}, t_m$]	1.3607	0.6409	80.08	0.6053	82.24	
	[45/-45]	[*,0, t_{1h}, t_m]	1.5708	3.0127	-	3.2621	-
		[*,0, $2t_{1h}, t_m$]	1.5708	0.1988	93.40	0.1579	95.19
[*,0, $3t_{1h}, t_m$]		1.5708	1.1638	61.37	1.2348	62.15	
[*,0, $4t_{1h}, t_m$]		1.5708	0.2324	92.29	0.1920	94.11	
[*,0, $5t_{1h}, t_m$]		1.5708	0.8859	70.59	0.9344	71.36	
[*,0, $6t_{1h}, t_m$]		1.5708	0.3041	89.91	0.2618	91.97	
[* , $2t_{1h}, t_{1h}, t_m$]		1.3142	2.5769	-	2.6775	-	
[* , $2t_{1h}, 2t_{1h}, t_m$]		1.3142	0.2133	91.72	0.2356	91.20	
[* , $2t_{1h}, 3t_{1h}, t_m$]		1.3142	1.0539	59.10	1.1543	56.87	
[* , $2t_{1h}, 4t_{1h}, t_m$]		1.3142	0.2680	89.60	0.2547	90.48	
[* , $2t_{1h}, 5t_{1h}, t_m$]		1.3142	0.9313	63.86	1.0683	60.09	
[* , $2t_{1h}, 6t_{1h}, t_m$]		1.3142	0.4265	83.45	0.4420	83.49	

Table 3.5 RMS and reduction ratios for Case-2

Lay-up	Motion parameters	ω_{\max} (rad/s)	RMS (m/s ²) Experiment	Reduction %	RMS (m/s ²) Simulation	Reduction %
[0/90]	[*, 0, t _{1h} , t _m]	1.0472	2.4853	-	2.6208	-
	[*, 0, 2t _{1h} , t _m]	1.0472	0.2797	88.75	0.2214	91.55
	[*, 2t _{1h} , t _{1h} , t _m]	0.9071	1.9615	-	2.1339	-
	[*, 2t _{1h} , 2t _{1h} , t _m]	0.9071	0.2885	85.29	0.2335	89.06
[45/-45]	[*, 0, t _{1h} , t _m]	1.0472	2.0408	-	2.1767	-
	[*, 0, 2t _{1h} , t _m]	1.0472	0.1323	93.52	0.1055	95.15
	[*, 2t _{1h} , t _{1h} , t _m]	0.8761	1.6815	-	1.8415	-
	[*, 2t _{1h} , 2t _{1h} , t _m]	0.8761	0.1336	92.05	0.1130	93.86

Table 3.6 RMS and reduction ratios for Case-3

Lay-up	Motion parameters	ω_{\max} (rad/s)	RMS (m/s ²) Experiment	Reduction %	RMS (m/s ²) Simulation	Reduction %
[0/90]	[*, 0, t _{1h} , t _m]	0.5236	1.2369	-	1.3081	-
	[*, 0, 2t _{1h} , t _m]	0.5236	0.1454	88.24	0.1126	91.39
	[*, 2t _{1h} , t _{1h} , t _m]	0.4536	0.9709	-	1.0646	-
	[*, 2t _{1h} , 2t _{1h} , t _m]	0.4536	0.1493	84.62	0.1183	88.89
[45/-45]	[*, 0, t _{1h} , t _m]	0.5236	1.0476	-	1.0888	-
	[*, 0, 2t _{1h} , t _m]	0.5236	0.0657	93.73	0.0532	95.11
	[*, 2t _{1h} , t _{1h} , t _m]	0.4381	0.8846	-	0.9211	-
	[*, 2t _{1h} , 2t _{1h} , t _m]	0.4381	0.0626	92.92	0.0568	93.83

Table 3.7 RMS and reduction ratios for Case-4

Lay-up	Motion parameters	ω_{\max} (rad/s)	RMS (m/s ²) Experiment	Reduction %	RMS (m/s ²) Simulation	Reduction %
[0/90]	[*, 0, t _{1h} , t _m]	2.0944	5.0065	-	5.2005	-
	[*, 0, 2t _{1h} , t _m]	2.0944	0.7907	84.21	0.7361	85.85
	[*, 2t _{1h} , t _{1h} , t _m]	1.6003	3.9831	-	3.8011	-
	[*, 2t _{1h} , 2t _{1h} , t _m]	1.6003	1.0641	73.28	1.0164	73.26
[45/-45]	[*, 0, t _{1h} , t _m]	2.0944	3.9405	-	4.0680	-
	[*, 0, 2t _{1h} , t _m]	2.0944	1.2206	69.02	1.2491	69.29
	[*, 2t _{1h} , t _{1h} , t _m]	1.5062	3.0008	-	3.1908	-
	[*, 2t _{1h} , 2t _{1h} , t _m]	1.5062	2.1651	27.85	2.4422	23.46

Table 3.8 RMS and reduction ratios for Case-5

Lay-up	Motion parameters	ω_{\max} (rad/s)	RMS (m/s ²) Experiment	Reduction %	RMS (m/s ²) Simulation	Reduction %
[0/90]	[*, 0, t _{1h} , t _m]	0.5236	1.2568	-	1.3295	-
	[*, 0, 2t _{1h} , t _m]	0.5236	0.0459	96.37	0.0222	98.33
	[*, 2t _{1h} , t _{1h} , t _m]	0.4681	1.0508	-	1.0707	-
	[*, 2t _{1h} , 2t _{1h} , t _m]	0.4681	0.045	95.72	0.0218	97.96
[45/-45]	[*, 0, t _{1h} , t _m]	0.5236	1.0118	-	1.0422	-
	[*, 0, 2t _{1h} , t _m]	0.5236	0.0711	92.97	0.0629	93.96
	[*, 2t _{1h} , t _{1h} , t _m]	0.4770	0.9158	-	0.9487	-
	[*, 2t _{1h} , 2t _{1h} , t _m]	0.4770	0.0821	91.04	0.0635	93.31

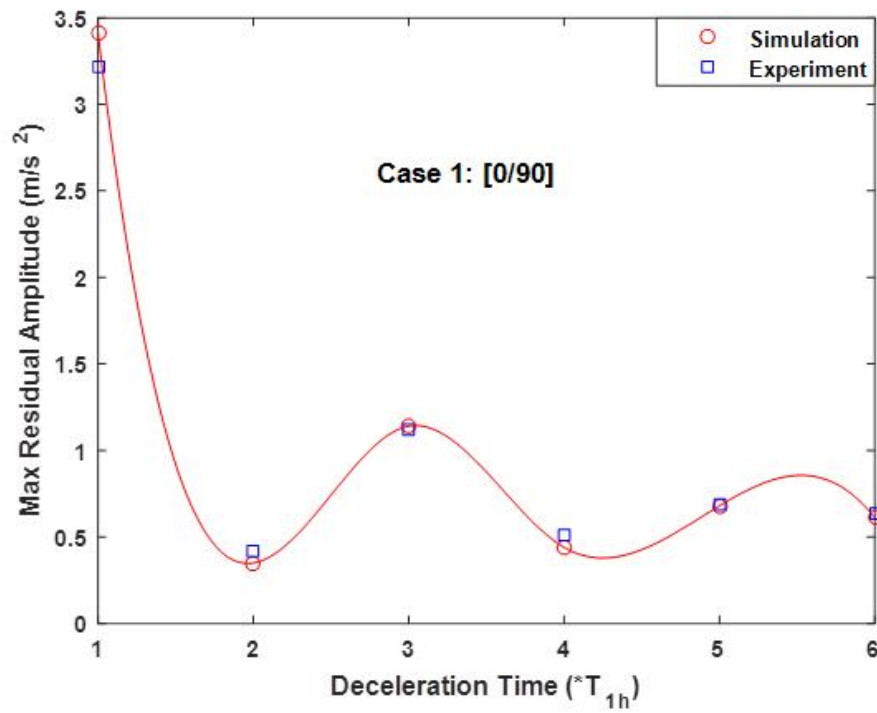
The results of Case-1 show that vibration reductions can be achieved for 2T_{1h}, 4T_{1h}, 6T_{1h} as given in Table 4. It is seen that double times of T_{1h} is more effective to control vibration amplitudes.

In case of the lay-up [0/90] and triangular velocity profile; the reductions are 90.31 %, 88.34 % and 85.24 % for 2T_{1h}, 4T_{1h} and 6T_{1h} in the simulation, respectively and the reductions are 89.18 %, 88.34 % and 82.54 % for 2T_{1h}, 4T_{1h} and 6T_{1h} in the experiment, respectively.

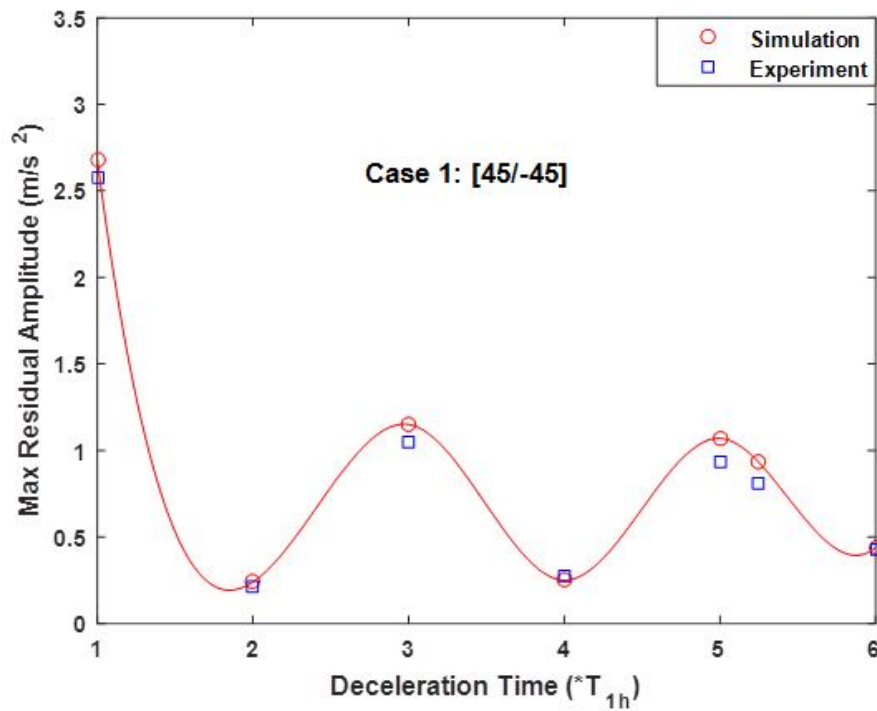
In case of the lay-up [0/90] and trapezoidal velocity profile; the reductions are 89.78 %, 87.07 % and 82.24 % for 2T_{1h}, 4T_{1h} and 6T_{1h} in the simulation, respectively and the reductions are 86.90 %, 84.14 % and 80.08 % for 2T_{1h}, 4T_{1h} and 6T_{1h} in the experiment, respectively.

In case of the lay-up [45/-45] and triangular velocity profile; the reductions are 95.19 %, 94.11 % and 91.97 % for 2T_{1h}, 4T_{1h} and 6T_{1h} in the simulation, respectively and the reductions are 93.40 %, 92.29 % and 89.91 % for 2T_{1h}, 4T_{1h} and 6T_{1h} in the experiment, respectively.

In case of the lay-up [45/-45] and trapezoidal velocity profile; the reductions are 91.20 %, 90.48 % and 83.49 % for 2T_{1h}, 4T_{1h} and 6T_{1h} in the simulation, respectively and the reductions are 91.72 %, 89.60 % and 83.45 % for 2T_{1h}, 4T_{1h} and 6T_{1h} in the experiment, respectively. The response spectrum via the deceleration time for Case-1 is given in Figure 3.6.



(a)



(b)

Figure 3.6 Change of the RMS values of the residual vibration signals versus the deceleration time for Case-1 (a) [0/90] and (b) [45/-45].

The reduction ratios for the simulation and experiment are very close as seen in Table 4. It is also observed from the table that the deceleration time for $t_{dec} = 2T_{1h}$ is the most effective parameter to reduce vibration amplitudes. The other cases are studied by taking the deceleration time as $t_{dec} = 2T_{1h}$. The results show that better reduction ratios are achieved when the flexibility of composite manipulator increases. So, the reduction ratios of the lay-up [45/-45] are higher than those of the lay-up [0/90].

Table 3.4, 3.5 and 3.6 reveals that the RMS values decrease when the stopping position of the composite manipulator decreases for the same motion times. Higher reduction ratios are achieved for the lay-up [45/-45].

The effect of the motion time on the vibration control for the same stopping positions is investigated in Case 4 and 5. The results for these cases are given in Tables 3.7 and 3.8. The composite manipulator moves same stopping positions at different motion times in Cases 2, 4 and 5. When the results in Tables 3.5, 3.7 and 3.8 are compared, the best reduction ratios are achieved when the composite manipulator moves slowly. On the contrary, the lowest reduction ratios are achieved when the composite manipulator moves rapidly. Better reduction ratios are obtained for the triangular motion even if it is not always useful in practice.

The results in all tables reveal that the vibration control is achieved for different stopping positions, motion times, motion velocity profiles and lay-ups. The experimental results encourage that the method can be used for practical implementations of composite manipulators in case of high speed applications.

3.5 Conclusion

Passive control of flexible systems has been studied in the literature extensively. Command input pre-shaping has been used to control the residual vibrations. The use of pulse sequence superimposed on the motion input by considering the system frequency and damping reduces the end point vibrations. Another approach is to

select the deceleration time in the velocity profile considering the natural frequency of the system. This approach was developed for a one-link flexible manipulator. The vibration control of single-link flexible manipulators was explored in the literature. It was observed that the deceleration time of the cycloidal velocity profile was important to suppress the residual vibration of the single-link. However, there are very limited studies on the passive control of composite manipulators.

This study presents the vibration control of a single-link flexible composite manipulator using motion profiles. The trapezoidal and triangular velocity profiles are considered for the motion commands. The time intervals of the trapezoidal motion input such as the acceleration time, the constant time, and the deceleration time are expressed in relation to the fundamental frequency of the composite manipulator. The constant time is taken as zero for the triangular motion input since the triangular motion can be assumed as a special case of the trapezoidal motion. The finite element vibration analyses are performed and the experiments are realized to verify simulation results. The residual vibration results are given as the acceleration signals. The RMS values of these signals are calculated to evaluate the effectiveness of the vibration control. It is observed that simulation and experimental results for the composite manipulator are in good agreement. The residual vibrations of single-link flexible composite manipulators can be controlled by selecting an appropriate deceleration time in the trapezoidal and triangular motion inputs.

The trapezoidal motion inputs are widely used to drive servo motors of industrial and manufactured robots. The results obtained in this study encourage that the proposed method can be used in practice, especially in pick and place applications to control residual vibrations. It is expected that the proposed method can be successful in the vibration control of complex and realistic composite manipulators.

CHAPTER FOUR

MODELING AND VIBRATION CONTROL OF SIX-AXIS SERIAL ROBOT WITH ANSYS APDL AND EXPERIMENTAL RESULTS

In this chapter, vibration control is applied to a six-axis serial robot. First, the six-axis robot with rigid members is considered. The robot is modeled as beam model in ANSYS by using APDL (Ansys Parametric Design Language). The end point vibration signals are simulated by transient analysis performing in ANSYS based on the finite element theory. Experimental results are also presented and compared with simulation results. Second, vibration control is applied to a six-axis serial robot and experimental results are presented. Triangular and trapezoidal velocity profiles for the actuating motors are used. The acceleration, constant velocity and deceleration time intervals of the trapezoidal velocity profile are selected by considering the lowest natural frequency of the manipulator structure at the stopping position. Arbitrary starting and stopping positions are considered. The root mean square (RMS) acceleration values of the vibration signals after stopping are calculated. It is observed that the residual vibration is sensitive to the deceleration time. The RMS values are lowest if the inverse of the deceleration time equals to the first natural frequency. It is highest if the inverse of the deceleration time equals to the half of the first natural frequency. It is observed that simulation and experimental results are in good agreement.

4.1 Introduction

Flexibility of robot manipulators depends on the parameters such as the weight, the dimension, the payload and speed of manipulators. The effect of flexibility in manipulators is observed as vibrations both during the motion and after the motion has finished. Vibrations caused after finishing the motion are called as residual vibrations. Residual vibrations also affect the accuracy and settling time at the end point. The performance of such manipulators or repeatability decreases in high speed engineering applications. Suppressing residual vibrations are important and possible by applying different control strategies such as passive or active.

The first step is to develop the mathematical models of manipulators. The mathematical models of manipulators can be constructed by the finite element method or analytical methods. Control of multi-link flexible manipulators reviewed in reference (Benosman & LeVey, 2004) by considering the control objectives of end-effector position and trajectory tracking. The governing differential equations of dynamic systems can be solved by using numerical methods (Fung, 1997; Owren & Simonsen, 1995; Zhang et al., 1999) or commercial engineering programs (Karagülle and Malgaca, 2004). Dynamic analysis of flexible manipulators reviewed in detail by classifying single-link, two-link, and multi-link manipulators in (Dwivedy & Eberhard, 2006).

Active or passive control techniques can be applied to flexible robot manipulators to suppress their residual vibrations. A passive control technique can be carried out with motion commands without using any additional hardware while an active control technique requires an actuator, a sensor and a control system. A passive control can be achieved as open loop while an active control can be achieved as closed loop.

Active control of flexible manipulator with both single-link and two-link has been studied in the literature (Shin & Choi, 2001; Gurses et al., 2009, Mirzaee et al., 2010). Most of these studies used piezoelectric (PZT) actuators to reduce the vibration amplitudes of flexible manipulators. Shin and Choi (2001) studied position control of a two-link flexible manipulator with PZT actuators and sensors. They established a nonlinear model including inertial effects by using Lagrange's equation and a sliding mode controller. Gurses et al. (2009) studied vibration control of single-link flexible manipulator with PZT actuators based on the finite element theory. They proposed PD based hub and velocity control techniques providing a feedback with a fiber optic sensor. Mirzaee et al. (2010) investigated active control of a two-link manipulator with PZT actuator and sensor by using Lyapunov based controller for maneuver tracking.

Some studies are related to designing and selecting appropriate trajectories to reduce residual vibrations. Park (2004) studied control of residual vibration of two-link manipulator by designing and optimizing a path under torque constraints. Abe (2009) also proposed an optimal trajectory planning for residual suppression of a two-link rigid-flexible link by using the Lagrangian approach and the assumed modes method. Green and Sasiadek (2004) presented control methods such as LQR and fuzzy logic for end point tracking of a trajectory by a two-link manipulator.

The passive control of flexible systems was studied in the literature extensively (Singhose, 2009). Command input pre-shaping has been used to control the residual vibration. The use of pulse sequence superimposed on the motion input by considering the system frequency and damping reduces the end point vibration. Singer and Seering (1990) applied this method to the aerospace field and improved the robustness of the method by increasing the number of pulses. Command shaping research advancements and application examples are reviewed in detail by Singhose (2009).

The passive control of single-link flexible manipulators was studied in the literature extensively (Ankaralı & Diken, 1997; Mimmi and Pennacchi, 2001; Shan et al., 2005; Shin & Brennan, 2008). However, there are limited studies regarding the passive control of two-link or multi-link manipulators. Özer and Semercigil (2008) demonstrated the effectiveness of the variable stiffness control technique on a two-link manipulator with passive components to implement control action.

In the references (Ankaralı & Diken, 1997; Shin and Brennan, 2008), it was shown that by selecting an appropriate deceleration time, the residual vibrations of single-link manipulators can be controlled. Ankaralı and Diken (1997) solved the transient vibration problem of a single elastic link, which was modeled by using Euler-Bernoulli beam theory and mode summation techniques. They drove the link with a cycloidal motion to eliminate its residual vibrations. Shin and Brennan (2008) proposed two simple methods to control residual vibrations of translating or rotating

Euler-Bernoulli beam reducing the problem to the base excitation of a single-freedom system without considering any control algorithms.

In this chapter, vibration control is applied to the six-axis serial robot. First, a Karagulle et al. (2015) have studied on the vibration control of two-link flexible manipulator. They have simulated the end point vibration signals by developing a MatLAB code based on the finite element theory and Newmark solution. Differently, the end point vibration of the robot is simulated by using ANSYS (Ansys, 2016). The simulation results are compared with experimental. Triangular velocity profile inputs for the three actuators are used. The effect of the acceleration, constant velocity, and deceleration time intervals on the residual vibration of the end point is studied simulation and experimentally.

4.2 Analysis by ANSYS APDL Code based on Finite Element Theory

4.2.1 Finite Element Model

The six-axis serial robot is modeled in ANSYS by using APDL which allows you typing commands in text file and running analysis without using graphical interface. In graphical interface study, it is very difficult to fix when there is a mistake on the model. Therefore, APDL is much easier and faster way to create a model and make changes on the model. BEAM188 element is used as a flexible beam. BEAM188 element is based on Timoshenko beam theory. The element has six degrees of freedom at each node: translations in the nodal x, y and z directions and rotations about the nodal x, y and z-axis. The element is defined by two nodes, the cross-sectional area, the dimensions of the cross-section, the area moment of inertia, the height, and the material properties. The materials of the links are steel and the properties of the links are given in Table 4.2.

The easiest way of FE analysis after constructing solid model of the system is using solid finite elements. ANSYS uses SolidWorks models, considers contacting surfaces, and performs meshing to generate solid finite elements. The user defines the boundary conditions and obtains the solution.

The disadvantages of this approach for complex systems are the resulting number of elements and degrees of freedom are very large, meshing problems may arise, solution times are long, high performance computers are necessary, solutions may not be obtained, and analysis may not be practical. Considering the disadvantages of the solid FE modeling, beam finite elements are used. In this approach, lines are assigned for beams, first. Section attributes are defined for the lines. The solid model and line model of the six-axis robot are shown in Figure 4.1.

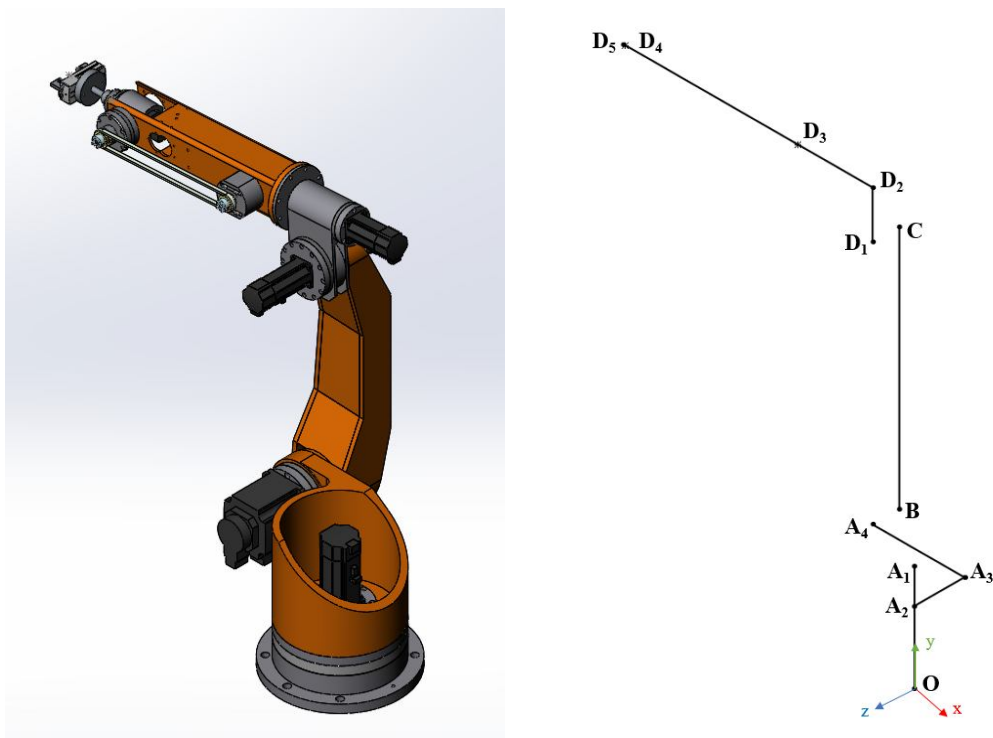


Figure 4.1 (a) Solid model and (b) line model of the robot.

The six-axis robot shown in the figure has six servo motors, first three motors define the location of the end-point in the global x, y and z axis, other three motors define the orientations of the end-point about x, y and z axis. The axes which define the locations are important for the vibration control, thus the robot is modeled as three degree of freedom. Member-1 is the $OA_1A_2A_3A_4$ -beam, Member-2 is the BC -beam and Member-3 is $D_1D_2D_5$ -beam. There are revolute joints at O , A_4-B and $C-D_1$. Member-1 is actuated by Motor-1 at O , Member-2 is actuated by Motor-2 at B and Member-3 is actuated by Motor-3 at C . The mass of Motor-1 is on the frame

(Member-1) at O. The mass of Motor-2 is on Member-1 at B. The mass of Motor-3 is on Member-3 at D₁. The mass of Motor-4 is on Member-3 at D₂. The mass of Motor-5 is on Member-3 at D₃. The mass of Motor-6 is on Member-3 at D₄. The end point is at D₅. The instantaneous angular positions of Member-1, Member-2 and Member-3 are θ_1 , θ_2 and θ_3 , respectively. The lengths of the links are $L_2=OB$ and $L_3=BC$. The global origin is at O. The global Cartesian coordinates are x, y and z. The instantaneous position of the manipulator is defined by θ_1 , θ_2 and θ_3 .

The node numbers are defined in APDL as parametric. The number of finite elements for Member-1, Member-2 and Member-3 are n_{e1} , n_{e2} and n_{e3} , respectively. For Member-1, Member 2 and Member-3, the element size is chosen 1 mm to coincide the nodes with the located mass points, thus n_{e2} , n_{e2} and n_{e3} are changed related to the member lengths. The numbers which are chosen for analysis can be extended to different number of finite elements.

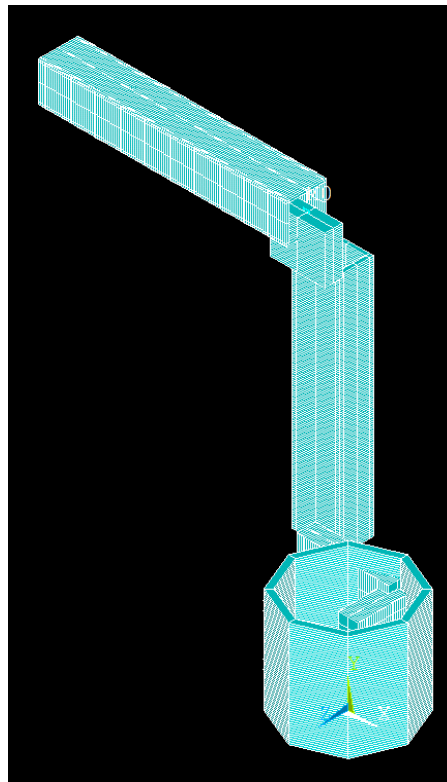
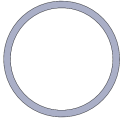






Figure 4.2 Beam model of the robot in ANSYS

Different cross-sections are defined in APDL, because Member-1, Member-2 and Member-3 have different cross-sections as given in Table 4.1. Beam188 elements

with different cross-sections are assigned between nodes related to Member-1, Member-2 and Member-3.

Table 4.1 Cross-sections of the members

Section	Member	Dimensions	Area (cm ²)	Moment of inertia	
				I _x (cm ⁴)	I _y (cm ⁴)
	Member-11	R ₀ =13.25 cm R ₁ =15 cm	155.3	15553	15553
	Member-13	8.75x4.8 cm	42	80.64	267.97
	Member-2	12x8.54x1 cm	37.08	389.7	684.76
	Member-31	13.75x4.5 cm	61.3	101.62	965.34
	Member-32	10x10x0.6 cm	22.56	333.59	333.59

Since there are three revolute joints at the points O, B and D₁ corresponding to Motor-1, Motor-2 and Motor-3, respectively, pilot nodes are defined and assigned at these points with TARGE170 elements. TARGE170 is used to represent various 3-D target surfaces for the associated contact elements. It can be imposed any translational or rotational displacements on the target segment elements. Each target segment of a rigid surface is a single element with a specific shape or segment type. The segment types are defined by several nodes and a target shape code TSHAP. The TSHAP command indicates the geometry (shape) of the element. Eight different segment types are supported for TARGE170 element by changing TSHAP definition: 3 node triangle, 4 node quadrilateral, 6 node triangle, 8 node quadrilateral, cylinder, cone, sphere and pilot node. Only pilot nodes have rotational degrees of freedom about the x, y and z axis. The detailed information can be found in ANSYS Theory Reference.

The other element type used in APDL is MPC184 element to define revolute joint. The MPC184 family of elements serves to connect the flexible and rigid

component to each other in a multibody mechanism. An MPC184 joint element is defined by two nodes with six degrees of freedom at each node. The relative motion between the two nodes is characterized by six relative degrees of freedom. Depending on application, different kinds of joint elements can be configured by imposing appropriate kinematic constraints on any or some of these six relative degrees of freedom. For example, to simulate a revolute joint, the three relative displacement degrees of freedom and two relative rotational degrees of freedom are constrained, leaving only one relative rotational degree of freedom available. Some joint types of MPC184 elements are given in Table 4.2.

Table 4.2 Properties of MPC184 element

Joint Element Type	Keyoption (1)	Keyoption (4)	Constraints
Revolute	6	-	5
Z-axis Revolute	6	1	5
Universal	7	-	4
Translational	10	-	5
Spherical	5	-	3
Cylindrical	11	-	4
Z-axis Cylindrical	11	1	4

MPC184 element allows to rotate the beam on the x-axis by defining this element type as a revolute joint with Keyoption (1) as 6 and Keyoption (4) as 1. Thus, MPC184 elements are assigned between two pilot nodes which are assigned to the nodes related to the points O and B. Due to having joint flexibility of the motor, motor rotational spring constant is defined as 28000 Nm/rad.

The flow chart for the analysis in ANSYS is summarized below.

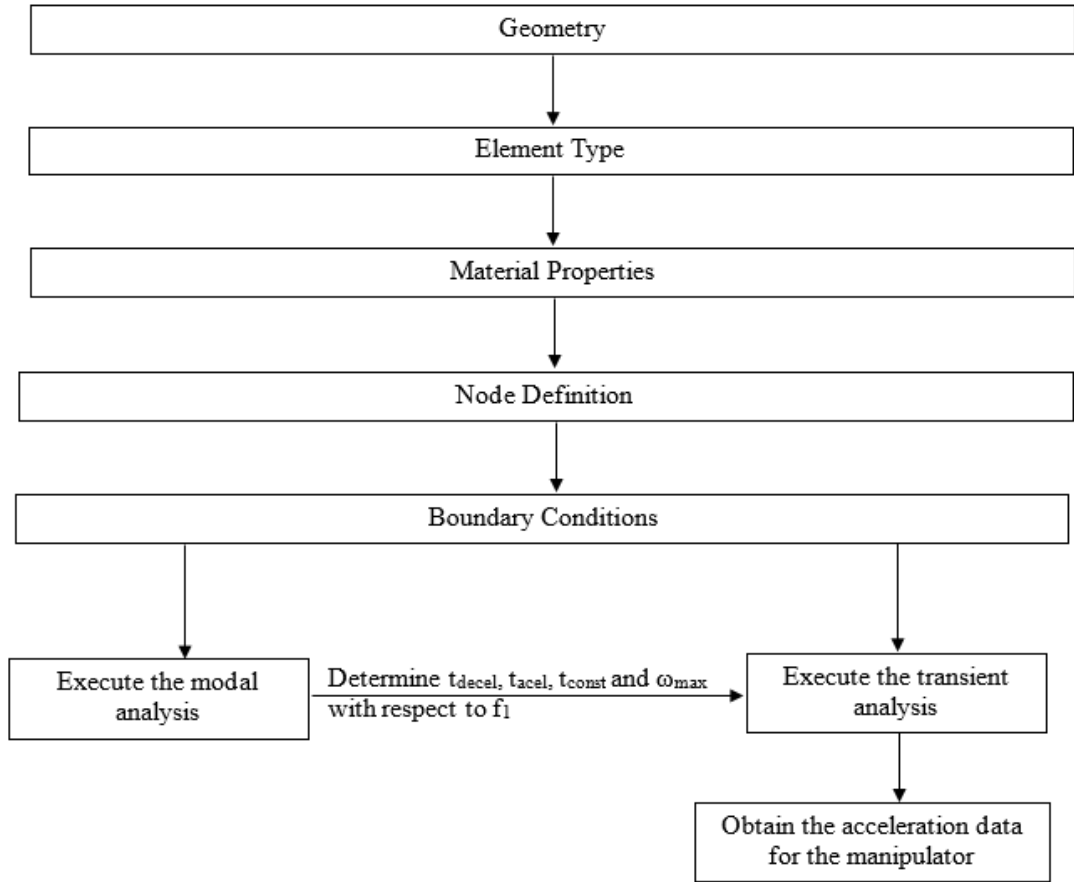


Figure 4.3 The flow chart for the analysis in ANSYS.

4.2.2 Damping

The Rayleigh damping is considered as

$$\mathbf{c}_s = \eta \mathbf{m}_s + \beta \mathbf{k}_s \quad (4.1)$$

where, η and β are damping coefficients (Thomson and Dahleh, 1988).

4.2.3 Motion

The motion of the six-axis robot is considered as shown in Figure 4.8. The manipulator moves from a starting position (Figure 4.8 (a)) at $t=0$ to an end position (Figure 4.8 (b)) at $t=t_m$, where t is time and t_m is the motion time. The initial angular positions are given as $\theta_2 = \phi_{2s}$, and $\theta_3 = \phi_{2s} + \phi_{3s}$ at $t=0$. The angular positions at the

stopping time are given as $\theta_1 = \phi_{1s} + \phi_{1m}$, $\theta_2 = \phi_{2s} + \phi_{2m}$ and $\theta_3 = \phi_{2s} + \phi_{2m} + \phi_{3s} + \phi_{3m}$ at $t = t_m$.

The motors follow the trapezoidal velocity profile given in Figure 4.4. The motion control units which produce pulses according to the profile given in Figure 4.4 are readily available in the market. The area under the velocity curve gives the corresponding motor rotations, ϕ_{1m} , ϕ_{2m} and ϕ_{3m} .

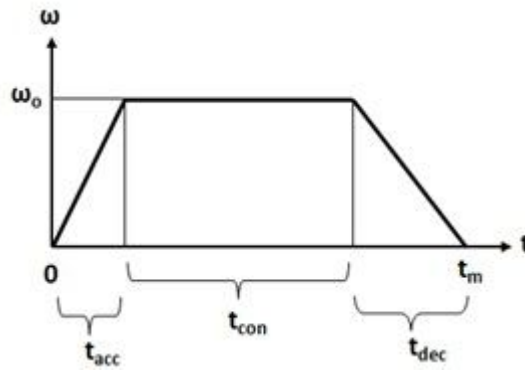


Figure 4.4 The angular velocity profile of motors.

4.2.4 Vibration Signals

The vibration of the receiving point located at a distance of d_{sensor} from the end-point, C, is analyzed. The vibration direction perpendicular to the line-BC in the x-y plane (motion plane) is considered. Let the displacement of the receiving point in the vibration direction be d_R . The second derivative of d_R is the acceleration signal and denoted by a_R . The gravity is in the z direction, and thus is not included.

4.2.5 Modal Analysis

The following eigenvalue equation is solved for the modal analysis.

$$\left| -\omega^2 \mathbf{m}_s + \mathbf{k}_s \right| = 0 \quad (4.2)$$

The values of ω are the un-damped natural frequencies of the system. Let ω_1 be the first natural frequency in rad/sec and T_1 be the period corresponding to the first natural frequency. Then, $\omega_1 T_1 = 2\pi$ and $T_1 = 1/f_1$, where f_1 is the first natural frequency in Hz. The half of the period, $T_{1h} = 0.5T_1$, will be used to define t_{acc} , t_{con} , or t_{dec} below.

It is noted that the angles θ_1 , θ_2 and θ_3 are changing during the motion of the two-link system, and thus the natural frequencies are changing depending on the position of the system.

4.2.6 Numerical Values

The values given in Table 4.3 are taken for the simulation results obtained by ANSYS in this study. The experimental system given in Section 4.2.7 is considered for assigning the numerical values. The material, geometric, inertia and rotational spring values approximately correspond to the experimental system.

Table 4.3 Properties of experimental system

Description	Value	Description	Value
Elasticity Module	210 GPa	Density	$\rho_{11} = 9217 \text{ kg/m}^3$
Density	$\rho_{12} = 1 \text{ kg/m}^3$	Density	$\rho_{13} = 9884 \text{ kg/m}^3$
Density	$\rho_2 = 12783 \text{ kg/m}^3$	Density	$\rho_{31} = 7861 \text{ kg/m}^3$
Density	$\rho_{32} = 4556 \text{ kg/m}^3$	Number of finite elements	$n_{e11} = 267, n_{e13} = 230$
Number of finite elements	$n_{e2} = 616$	Number of finite elements	$n_{e31} = 119, n_{e32} = 625$
Rayleigh Damping Coefficient	$\eta = 0$ (mass matrix coefficient)	Rayleigh Damping Coefficient	$\beta = 0.001$ (stiffness matrix coefficient)
Member Length	$L_{11} = 267 \text{ mm}$	Member Length	$L_{12} = 125 \text{ mm}$
Member Length	$L_{13} = 230 \text{ mm}$	Member Length	$L_2 = 616 \text{ mm}$
Member Length	$L_{31} = 119 \text{ mm}$	Member Length	$L_{32} = 625 \text{ mm}$
Weight of the Motor-1	$m_3 = 13.94 \text{ kg}$	Weight of the Motor-2	$m_3 = 5.34 \text{ kg}$
Weight of the Motor-3	$m_3 = 2.42 \text{ kg}$	Weight of the Motor-4	$m_3 = 3.48 \text{ kg}$
Weight of the Motor-5	$m_3 = 1.53 \text{ kg}$	Weight of the Motor-6	$m_3 = 3.29 \text{ kg}$
Motor rotational spring constants	$K_{m1} = K_{m2} = K_{m3} = 28000 \text{ Nm/rad}$	Time interval	$\Delta t = 0.0025 \text{ s}$

The time interval where the residual vibration is observed after the stopping time is denoted by t_{res} . The time until which the simulation results are obtained in the transient analysis is denoted by t_s . Then, $t_s = t_m + t_{res}$. For the transient results given below, t_{res} is taken as 1 s.

4.3 Experimental Results of Vibration Control of Six-Axis Serial Robot

The photo of the experimental system of the six axis serial robot is shown in Figure 4.5. The experimental set-up consists of a six servo motors. Mitsubishi Electric servo motors and drivers with 1 kW, Model HC-KFS053B/ MR-J2S-100A, 750 W, Model HC-KFS13B/ MR-J2S-70A, 400 W, Model HC-KFS43B/ MR-J2S-40A, 200 W, Model HC-KFS23B/ MR-J2S-20A, 100 W Model HC-KFS7B/ MR-J2S-10A, 50 W Model HC-SFS102B/ MR-J2S-10A are used for Motor-1, Motor-2, Motor-3, Motor-4, Motor-5 and Motor-6, respectively. Harmonic Drive gearboxes, Model HFUC-32-100/100 (gear ratio: 100), Model HFUC-32-100/100 (gear ratio: 100), Model HFUC-32-100/100 (gear ratio: 100), Model HFUC-32-100/100 (gear ratio: 100), Model HFUC-32-100/100 (gear ratio: 100) and HFUC-20-80/80 (gear ratio: 80) are used for Motor-1, Motor-2, Motor-3, Motor-4, Motor-5 and Motor-6, respectively. The six axis are driven with ADLINK/PCI-8366 control card. The velocity profile is given to servomotors with a developed VisualBASIC program which is used ADLINK-ActiveX components (ADLINK Technology Inc., 2015).

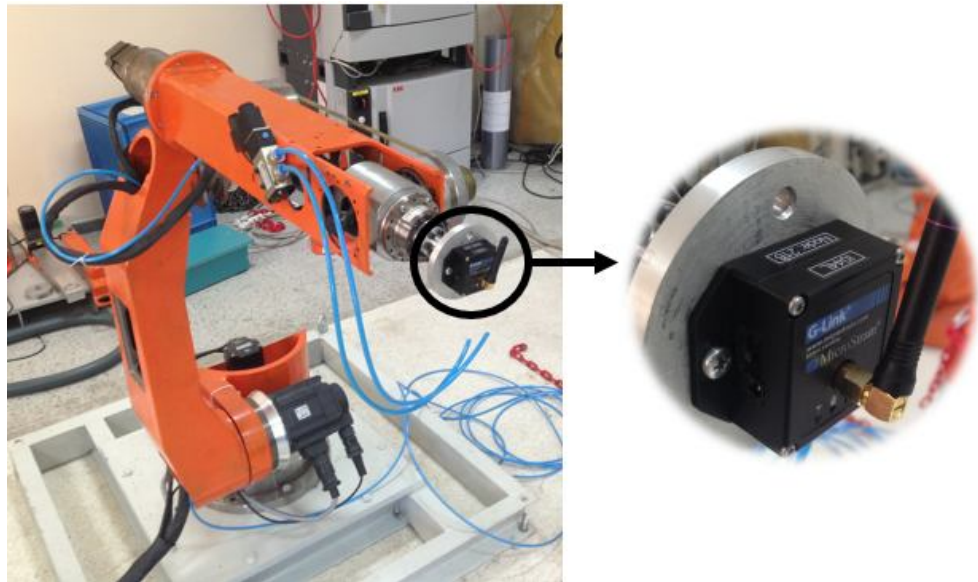


Figure 4.5 Experimental system of the robot.

The measurement system for obtaining experimental results are shown in Figure 4.6.



Figure 4.6 Measurement system.

MicroStrain wireless data acquisition (WDA) system is used to get the experimental acceleration signals at the receiving point.

A motion case is examined for the vibration control where the robot moves from rigid to flexible position. Motion parameters are shown in Figure 4.7.

```

initial position
axis1,0
axis2,-30
axis3,-30

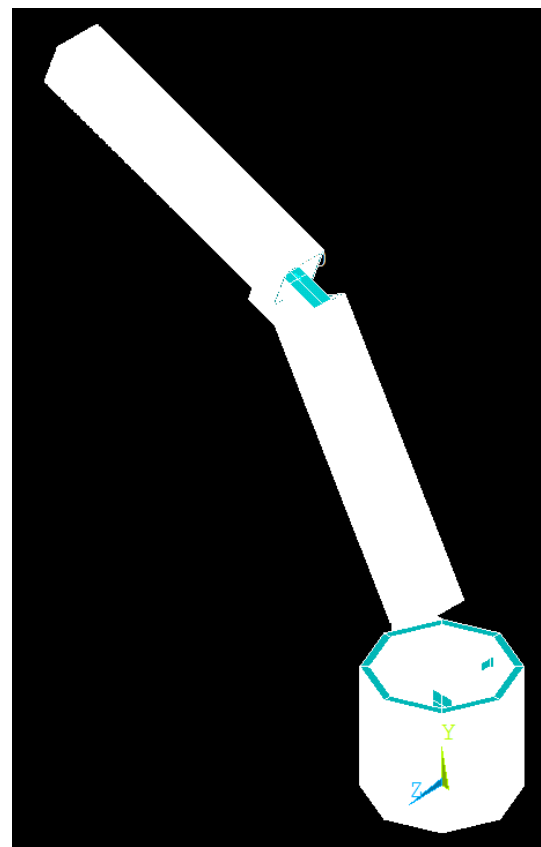
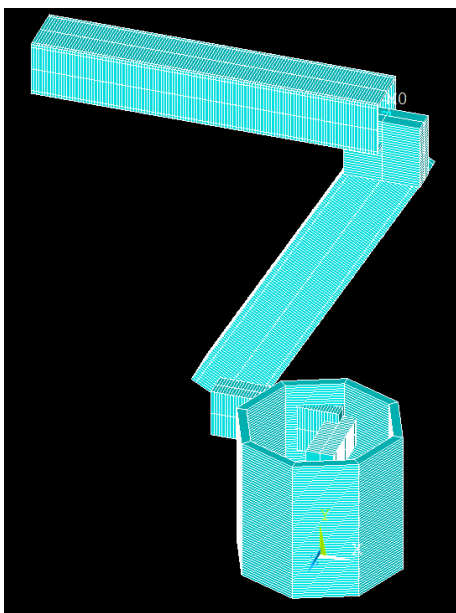
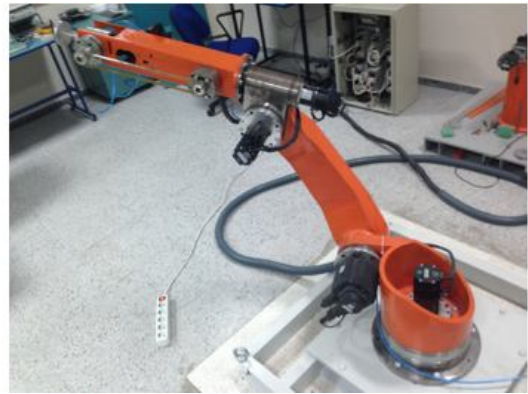
wait,1

move
axis,tacel,tdecel,td,disp
axis1,1.3929,0.1071,1.5000,60
wait,0
axis2,1.3929,0.1071,1.5000,60
wait,0
axis3,1.3929,0.1071,1.5000,80

```

Figure 4.7 Motion parameters.

The motion is given to three axis which represent the location of the end-point of the robot in the workspace. The motion parameters of the robot can be described in the text box and the motion of the six axis robot is provided by the VisualBASIC. The starting position is written under “initial position” label and the motion is written under “move” label in the text box. Let the starting position of the robot be $\mathbf{q}_s=[0,-30,-30]$ and the stopping position of the robot be $\mathbf{q}_f=[60,30,50]$. So, the axis of the robot rotate 0, -30 and -30 degrees from rest position for Motor-1, Motor-2 and Motor-3, respectively. Then, the robot moves 60, 60 and 80 degrees for Motor-1, Motor-2 and Motor-3 from starting position to reach rest position after waiting 1 s. The starting position and stopping position of the robot are shown in Figure 4.8.



(a)

(b)

Figure 4.8 (a) The starting position and (b) the stopping position.

For example motion, motion time is selected as 1.5 s and the residual vibration is examined for 1 s after motion is done. Triangular velocity profile is applied to the servo motors. Acceleration and deceleration time are determined by the program based on multiples of half the period of the first natural frequency of the system

where the motion is done. The results are given in Table 4.4 for different time parameters.

Table 4.4 RMS and reduction ratios for Case-1.

Motion	F_{1d} (Hz) Experiment	F_{1d} (Hz) ANSYS	$t_i=[*,0,t_{1h},t_m]$	RMS Experiment	Reduction (%)	RMS ANSYS	Reduction (%)
M1_a			$[*,0,t_{1h},t_m]$	6.2764	-	6.4215	-
M1_b			$[*,0,2t_{1h},t_m]$	0.69	79.18	0.8215	87.21
M1_c	9.03	9.20	$[*,0,3t_{1h},t_m]$	1.1806	75.75	1.35	79.78
M1_d			$[*,0,4t_{1h},t_m]$	0.7239	88	0.8503	86.76
M1_e			$[*,0,5t_{1h},t_m]$	1.3699	83.2	1.5412	76
M1_f			$[*,0,6t_{1h},t_m]$	0.4928	87.16	0.6137	90.44

Example signals obtained by the simulation in ANSYS and experiment presented in the paper are shown in Figure 4.9 and Figure 4.10. Since vibration signals are given in ANSYS with respect to the global coordinates, transformation matrices are used to obtain the desired vibration signal with respect to the measured point of the robot.

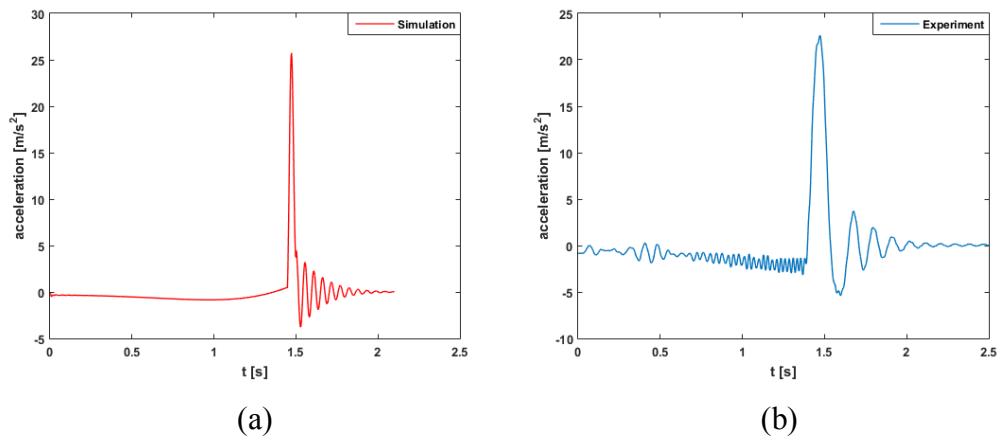


Figure 4.9 Example signals for $[t_{acc}, t_{con}, t_{dec}, t_m]=[*,0,T_{1h},1]$ (a) Simulation, (b) Experiment

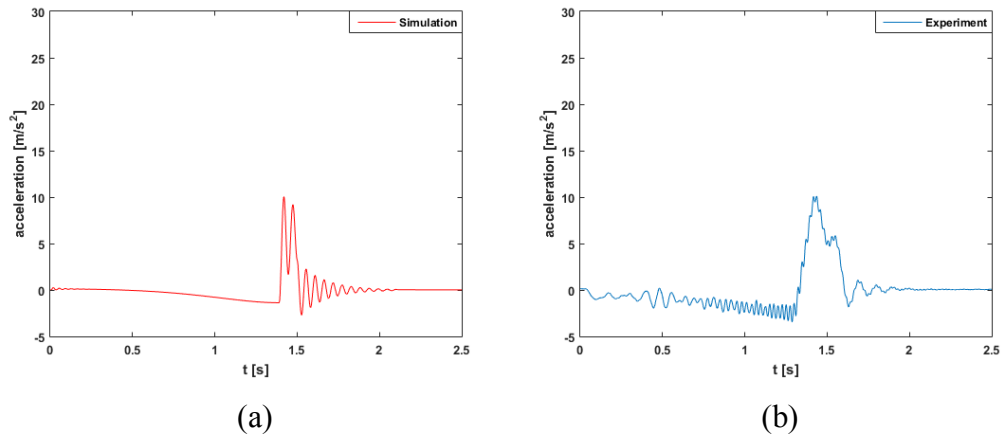


Figure 4.10 Example signals for $[t_{acc}, t_{con}, t_{dec}, t_m]=[*,0,2T_{1h},1]$ (a) Simulation, (b) Experiment

Increasing multiples of half the period of the first natural frequency of the system, vibration levels decreases. As seen in the table even multiples of t_{1h} has more effective reduction compared to odd multiples of t_{1h} . The comparison is given in Figure 4.11. The theory is achieved for the six axis rigid robot.

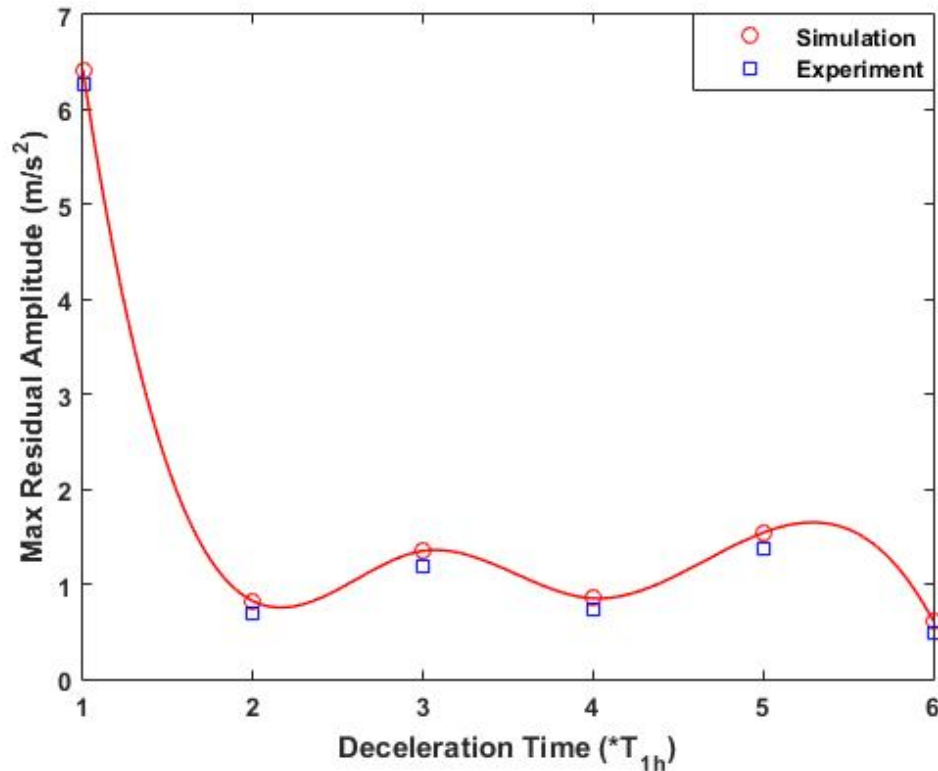


Figure 4.11 Change of rms values of residual vibration signals versus the deceleration time for M1.

It is observed from the figures and tables given above that the simulation results obtained by the transient analysis in ANSYS are in good agreement with experimental results. The RMS value is the highest when the deceleration time equals to T_{1h} .

It is observed from Table 4.4 and Figure 4.10-4.11 that vibration suppressions can be achieved at all stopping positions of the robot for $2T_{1h}$, $4T_{1h}$ and $6T_{1h}$. For $2T_{1h}$, the reduction is 94.16 % in the simulation obtained in ANSYS while the reduction is 90.33 % in the experiment. For $4T_{1h}$, the reduction is 86.32 % in the simulation obtained in ANSYS while the reduction is 83.33 % in the experiment. The similar reductions can be provided for $4T_{1h}$. The deceleration time of $2T_{1h}$ is better than $4T_{1h}$ for shorter motion times of the robot manipulator such as high speed applications in case of trapezoidal motion profiles. The experimental results encouraged that the approach can be successful for robot manipulators in practical engineering applications.

4.4 Conclusion

The residual vibration of flexible systems can be suppressed by command input pre-shaping technique. Pulse sequences considering the system frequency and damping estimation are used. This method has been studied extensively for various structures. Another approach is to select the deceleration time in the velocity profile considering the natural frequency of the system. This approach was developed for one-link flexible manipulator. The vibration control of single-link flexible manipulators was explored in the literature. It was observed that the deceleration time of the cycloidal velocity profile is important to suppress the residual vibration of the single-link. The natural frequencies do not change as it moves in single-link manipulators.

In this study, the vibration control of a six-axis serial robot is presented. The six-axis robot is modeled in ANSYS and simulation results are given by using ANSYS APDL code. An experimental system is used to verify the simulation results. Arbitrary starting and stopping position for the end point is considered with

triangular motion profiles. The idea of selecting an appropriate deceleration time based on the natural frequency is extended to the six-axis serial robot. The natural frequency of the six-axis robot changes as it moves. It is observed that the deceleration time of the triangular velocity profile based on the natural frequency of the six-axis robot at the stopping point is important to suppress the residual vibration. Comparison of the simulation obtained by ANSYS and experimental results shows that they are in good agreement.

The modeling procedure for the simulation and vibration control approach given in this study can be used for the dynamic analysis of multi-body flexible systems such as multi-link serial robots or Cartesian robots. The results of this study can be used in pick and place applications to control residual vibrations.

CHAPTER FIVE

CONCLUSION

In this study, the modeling and dynamic analysis of the multi-degree-of-freedom system are performed as first and the dynamic responses are obtained with Runge-Kutta and Newmark method. Passive vibration control using motion profiles is applied to the system and the results are compared with both numerical methods. It is observed that both numerical methods are in good agreement.

For the active vibration control, a procedure is developed to integrate proportional-integral-derivative (PID) control action into the Newmark solution. The numerical control action is applied to the error signal value at a time step to find the actuator signal value and the Newmark algorithm is applied to find the output values at the subsequent time step. A step function is considered as the reference input signal for the closed loop system. An approximate model for the samples of the step function is used to obtain bounded derivatives. The numerical results are compared with analytical solutions obtained by the Laplace transform method. Various results are given for undamped or damped system by setting PID parameters. It is observed that the numerical and analytical results are in good agreement. The results of this study can be used to simulate the active vibration control of flexible mechanical systems which are more complex and have their finite element models.

PID controllers are widely used in control systems. Classical theory of PID control of closed loop control systems were developed before the developments in digital electronics and computers. The controllers were analog. Graphical methods were used for simple systems. The effect of P, I, and D control actions were explored well. The P, I, and D parameters were determined by the trial and error method for complex systems considering the effects of the control actions. This approach is called as the PID tuning. The PID tuning method is still used today, if the mathematical model of the system is not available. The developments in the computers and computer aided engineering (CAE) software enable engineers to generate the virtual models of systems. The users of CAE programs define the

system by using graphical user interfaces (GUI), and the programs generate the mathematical model, solve them and give simulation results.

It is proposed that PID control actions can be integrated to the numerical solutions of the mathematical models where the solutions are found step by step. The output value of the control system is subtracted from the reference value to calculate the error value at one step, and the input value of the control action is calculated by applying the control action to the error value numerically at the subsequent step, as given in this study. A numerical model for the step input is also introduced. The proposed integration of PID control action into the numerical solution have been tested on a four degree of freedom system, and the results have been compared with the well-known analytical solutions obtained by the Laplace transform method. The results are in good agreement.

The results of this study show that PID control actions can be integrated to CAE programs. Then, the users can generate virtual experimental approach to evaluate the closed loop control of complex systems. The users can decide about the feedback and PID parameters and design the control system by PID tuning. The passive or active vibration control of rigid-flexible or flexible multi-link manipulators whose finite element models are generated by CAE programs can be studied with the proposed approach. Simulation results may be verified by the experiments for future works. Decreasing the residual vibrations of multi-link flexible manipulators is important in practice especially in pick and place applications.

Passive control of flexible systems has been studied in the literature extensively. Command input pre-shaping has been used to control the residual vibrations. The use of pulse sequence superimposed on the motion input by considering the system frequency and damping reduces the end point vibrations. Another approach is to select the deceleration time in the velocity profile considering the natural frequency of the system. This approach was developed for a single-link flexible manipulators. The vibration control of single-link flexible manipulators was explored in the

literature. It was observed that the deceleration time of the cycloidal velocity profile was important to suppress the residual vibration of the single-link manipulators.

For passive vibration control, different manipulators has been studied with different methods. Single-link flexible composite manipulators with different lay-ups and six-axis serial robot are considered in this thesis. Motion profiles are used to reduce the residual vibrations of the manipulators. The trapezoidal and triangular velocity profiles are considered for the motion commands. The time intervals of the trapezoidal motion input such as the acceleration time, the constant time, and the deceleration time are expressed in relation to the fundamental frequency of the manipulators. The constant time is taken as zero for the triangular motion input since the triangular motion can be assumed as a special case of the trapezoidal motion. The vibration analyses are performed and the experiments are realized to verify simulation results. The residual vibration results are given as the acceleration signals. The RMS values of these signals are calculated to evaluate the effectiveness of the vibration control. It is observed that simulation and experimental results for the manipulators are in good agreement.

A single-link flexible composite manipulator is considered to analyze in ANSYS and reduce end-point vibrations. The finite element vibration analysis is performed and an experimental system is introduced to verify simulation results. [0/90] and [45/-45] lay-ups, trapezoidal and triangular velocity profiles are studied by creating cases for different stopping positions and motion times. The time intervals of the motion profiles are determined from the natural frequency of the composite manipulator. Residual vibrations which are occurred after stopping the movement of the manipulator are obtained and the root mean square (RMS) values of these signals are calculated. It is observed from the results that the first vibration mode dominates to reduce the residual amplitudes.

Finally, the vibration control of a six-axis serial robot is presented. For the six-axis robot, simulation results are given by using ANSYS APDL code. An experimental system is used to verify the simulation results. Arbitrary starting and

stopping position for the end point is considered with triangular motion profiles. The idea of the selecting an appropriate deceleration time based on the natural frequency is extended to the six-axis serial robot. The natural frequency of the six-axis robot changes as it moves. It is observed that the deceleration time of the velocity profile based on the natural frequency of the six-axis robot at the stopping point is important to suppress the residual vibration. Comparison of the simulation obtained by ANSYS and experimental results shows that they are in good agreement. It is observed that the passive control approach is applicable to multi-degree of freedom systems.

The trapezoidal motion inputs are widely used to drive servo motors of industrial and manufactured robots. The results obtained in this study encourage that the proposed method can be used in practice, especially in pick and place applications to control residual vibrations. It is expected that the proposed method can be successful in the vibration control of complex and realistic manipulators.

The future works in order to extend this study can be summarized as follows,

- The active vibration control integrated into the Newmark solution can be realized to verify with the experimental system.
- The active vibration control integrated into the Newmark solution can be realized for the flexible manipulators whose finite element models exist.
- The passive vibration control can be applied to realistic composite box manipulators.
- The active control can be integrated into ANSYS APDL and so complex systems such as six-axis robot can be controlled with hybrid control.

REFERENCES

- Abe, A. (2009). Trajectory planning for residual vibration suppression of a two-link rigid-flexible manipulator considering large deformation. *Mechanism and Machine Theory*, 44, 1627–1639.
- Abramovich, H. (1992). Shear deformation and rotary inertia effects of vibrating composite beams, *Composite Structures*, 20, 165–173.
- Abramovich, H., & Livshits, A. (1994). Free vibrations of non-symmetric cross-ply laminated composite beams. *Journal of Sound and Vibration*, 176, 807–828.
- Adlink Technology Inc.* (2015). Retrieved November 2, 2015, from <http://www.adlinktech.com>.
- Aksencer, T., & Aydogdu, M. (2015). Flapwise vibration of rotating composite beams. *Composite Structures*, 134, 672-679.
- Alberts, T.E., Hastings, G.G., Book, W.J., & Dickerson S.L. (1973). Experiments in optimal control of a flexible arm with passive damping. *Fifth VPISSU/AIAA Symposium on Dynamics and Control of Large Structures*, Blacksburg, VA, Boca Raton, FL: CRC Press.
- Ankarali, A., & Diken, H. (1997). Vibration control of an elastic manipulator link. *Journal of Sound and Vibration*, 204 (1), 162-170.
- Ankarali, A., Mecitoglu, Z., & Diken, H. (2012). Response spectrum of a coupled flexible shaft-flexible beam system for cycloidal input motion. *Mechanism and Machine Theory*, 47, 89–102.

- Arvin, H., & Lacarbonara, W. (2014). A fully nonlinear dynamic formulation for rotating composite beams: nonlinear normal modes in flapping. *Composite Structures*, *109*, 93–105.
- Arvin, H., & Nejad, F.B. (2013). Nonlinear free vibration analysis of rotating composite Timoshenko beams. *Composite Structures*, *96*, 29-43.
- Atkinson, K. (1989). *An introduction to numerical analysis* (2nd Ed.), New York: John Wiley & Sons, ISBN 978-0-471-50023-0.
- Badour, F.A., Sunar, M., & Cheeded, L. (2011). Vibration analysis of rotating machinery using time-frequency analysis and wavelet techniques. *Journal of Mechanical Systems and Signal Processing*, *25*, 2083-2101.
- Bandopadhyaya, D., Bhattacharya, B., & Dutta, A. (2008). Active vibration control strategy for a single-link flexible manipulator using ionic polymer metal composite. *Journal of Intelligent Material Systems and Structures*, *19*, 487-496.
- Bathe, K.J. (2014). *Finite element procedures* (2nd Ed.), New Jersey: Prentice-Hall.
- Benosman, M., & LeVey, G. (2004). Control of flexible manipulators: A survey. *Robotica*, *22*, 533-545.
- Book, W.J., & Cetinkunt, S. (1985). Near optimal control of flexible robot arms on fixed paths. *IEEE International Conference on Robotics and Automation*, St. Louis, MO.
- Brigham, E.O. (1988). *The fast Fourier transform and its applications* (1st Ed.), Prentice-Hall.
- Cannon, R.H., & Schmitz, E. (1984). Initial experiments on the end-point control of a flexible one link robot. *The International Journal of Robotics Research*, *3*(3).

- Chandiramani, N.K., Librescu, L., & Shete C.D. (2002). On the free-vibration of rotating composite beams using a higher-order shear formulation. *Aerospace Science and Technology*, 6(8), 545–561.
- Chitode, J.S. (2005). *Digital signal processing*, Technical Publications Pune.
- Das, S.K., Ray, P.C., & Pohit, G. (2007). Free vibration analysis of a rotating beam with nonlinear spring and mass system, *Journal of Sound and Vibration*, 301, 165–188.
- DeValve, C., & Pitchumani, R. (2014). Analysis of vibration damping in a rotating composite beam with embedded carbon nanotubes. *Composite Structures*, 110, 289–296.
- Diken, H., & Alghamdi, A. A. A. (2003). Residual vibration response spectra for a servomotor-driven flexible beam, *Journal of Mechanical Engineering Science*, 217 (5), 577-583.
- Dwivedy, S.K., & Eberhard, P. (2006). Dynamic analysis of flexible manipulators, a literature review. *Mechanism and Machine Theory*, 41, 749–777.
- Fung, T.C. (1997). Unconditionally stable higher-order Newmark methods by substepping procedure. *Computer Methods in Applied Mechanics and Engineering*, 147, 61-84.
- Gao, Y., Wang, F.Y., & Xiao, Z.Q (2012), Flexible manipulators, modeling, analysis and optimum design, *Intelligent system series*, Elsevier: Oxford, UK.
- Green, A., & Sasiadek, J.Z. (2004). Dynamics and trajectory tracking control of a two-link robot manipulator. *Journal of Vibration and Control*, 10, 1415–1440.

- Gurses, K., Bradley, J.B., & Edward, J.P. (2009). Vibration control of a single-link flexible manipulator using an array of fiber optic curvature sensors and PZT actuators. *Mechatronics*, 19, 167–177.
- Haosheng, L., Su, W., & Kratz, H. (2007). FFT and wavelet-based analysis of the influence of machine vibrations on hard turned surface topographies. *Tsinghua Science and Technology*, 12(4), 441-446.
- Hollars, M.G., & Cannon, R.H. (1986). Experiments on the end-point control of a two-link robot with elastic drives. *Proceedings of the AIAA Guidance, Navigation and Control Conference*, Williamsburg, VA, 19-27.
- Hoshichima, K., & Ikada, M. (2007). Vibration suppression control for mechanical transfer systems by jerk reduction. *International Journal of Control, Automation, and Systems*, 5(6), 614-620.
- Jansen, J.F. (1992). Control and analysis of a single-link flexible beam with experimental verification. *ORNL/TM-12198*, Oak Ridge National Laboratory.
- Ji, H., Qiu J., Badel, A., & Zhu, K. (2009). Semi-active vibration control of a composite beam using an adaptive SSDV approach. *Journal of Intelligent Material Systems and Structures*, 20, 401-412.
- Jiang, B.K., Xu, J., & Li, YH. (2014). Flapwise vibration analysis of a rotating composite beam under hygrothermal environment. *Composite Structures*, 117, 201–211.
- Kang, Y.K., Park, H.C., Kim, J., & Choi, S.B. (2002). Interaction of active and passive vibration control of laminated composite beams with piezoceramic sensors/actuators. *Journal of Materials and Design*, 23, 277-286.

- Kabel, M., Merkert, D., & Schneider, M. (2015). Use of composite voxels in FFT-based homogenization. *Computer Methods in Applied Mechanics and Engineering*, 294, 168–188.
- Kapania, R., & Raciti, S. (1989). Nonlinear vibration of unsymmetrically laminated beams. *AIAA Journal*, 27, 201–210.
- Karagülle, H., & Malgaca, L. (2003). Mekanik sistemlerin kapalı kontrolünün Runge-Kutta yöntemiyle incelenmesi. *11. Ulusak Makine Teorisi Sempozyumu*
- Karagülle, H., & Malgaca, L. (2004). Analysis of end point vibrations of a two-link manipulator by integrated CAD/CAE procedures. *Finite Elements in Analysis and Design*, 40, 2049-2061.
- Karagülle, H., Malgaca, L., & Öktem, H.F. (2004). Analysis by active vibration control in smart structures by ANSYS, *Smart Materials and Structures*, 13, 661–667.
- Khot, S.M., & Yelve, N.P. (2011). Modeling and response analysis of dynamic systems by using ANSYS[®] and MATLAB[®]. *Journal of Vibration and Control*, 17(6), 953 - 958.
- Lu, W., Ge, F., Wu, X., & Hong, Y. (2013). Nonlinear dynamics of a submerged floating moored structure by incremental harmonic balance method with FFT. *Marine Structures*, 31, 63–81.
- Magee, D.P., & Book, W.J. (1994). Filtering schilling manipulator commands to prevent flexible structure vibration. *American Control Conference*, Baltimore, MD.

- Mariot, S., Leroy, V., Pierre, J., Elias, F., Bouthemy, E., Langevin, D., et al. (2015). An FFT approach to the analysis of dynamic properties of gas/liquid interfaces. *Colloids and Surfaces A: Physicochemical and Engineering Aspects*, 473, 11-17.
- MicroStrain Inc. (2015). Retrieved November 2, 2015, from <http://www.microstrain.com/wireless/sensors>.
- Mimmi, G., & Pennacchi, P. (2001). Pre-shaping motion input for a rotating flexible link. *International Journal of Solids and Structures*, 38, 2009-2023.
- Mirzaee, E., Eghtesad, M., & Fazelzadeh, S.A. (2010). Maneuver control and active vibration suppression of a two-link flexible arm using a hybrid variable structure/Lyapunov control design. *Acta Astronautica*, 67, 1218–1232.
- Monciet, V. (2015). Combining FFT methods and standard variational principles to compute bounds and estimates for the properties of elastic composites. *Computer Methods in Applied Mechanics and Engineering*, 283, 454-473.
- Newmark, N.M. (1959). A method of computation for structural dynamics. *Journal of Engineering Mechanics, ASCE* 85, 67-94.
- Owren, B., & Simonsen, H.H. (1995). Alternative integration methods for problems in structural dynamics. *Computer Methods in Applied Mechanics and Engineering*, 122, 1-10.
- Ozer, A., & Semercigil, S.E. (2008). An event-based vibration control for a two-link flexible robotic arm: Numerical and experimental observations. *Journal of Sound and Vibration*, 313, 375–394.
- Ozgumus, O.O., & Kaya, M.O. (2006). Flapwise bending vibration analysis of double tapered rotating Euler–Bernoulli beam by using the differential transform method. *Meccanica*, 41(6), 661–670.

- Park, K.J. (2004). Flexible robot manipulator path design to reduce the endpoint residual vibration under torque constraints. *Journal of Sound and Vibration*, 275, 1051–1068.
- Pennachi, P. (2004). Robustness of command input preshaping technique applied to residual vibration reduction. *Shock and Vibration*, 11, 377-382.
- Pereira, E., Trapero, J.R., Diaz, I. M., & Feliu, V. (2012). Adaptive input shaping for single-link flexible manipulators using an algebraic identification, *Control Engineering Practice*, 20, 138–147.
- Preumont, A. (2002.) *Vibration control of active structures an introduction* (2nd Ed.): Kluwer Academic Publishers, Netherlands.
- Rand, O. (1995). Experimental study of the natural frequencies of rotating thin-walled composite blades. *Thin-Walled Structures*, 21(2), 191–207.
- Rao, S. (2011). *Mechanical vibrations* (5th Ed.), Upper Saddle River: Prentice-Hall.
- Reis, J.C.P., & da Costa, J.S. (2012). Motion planning and actuator specialization in the control of active-flexible link robots. *Journal of Sound and Vibration*, 331, 3255–3270.
- Shan, J., Liu, H.T., & Sun, S. (2005). Modified input shaping for a rotating single-link flexible manipulator. *Journal of Sound and Vibration*, 285, 187–207.
- Shin, H.C., & Choi, S.B. (2001). Position control of a two link flexible manipulator featuring piezoelectric actuators and sensors. *Mechatronics*, 11, 707-729.
- Shin, K., & Brennan, M.J. (2008). Two simple methods to suppress the residual vibrations of a translating or rotating flexible cantilever beam. *Journal of Sound and Vibration*, 312, 140–150.

- Singer, N.C. (1989). Residual vibration reduction in computer controlled machines. *MIT Artificial Intelligence Lab Technical Report No. AITR-1030*.
- Singer, N.C., & Seering, W.P. (1990). Preshaping command inputs to reduce system vibration. *Journal of Dynamic Systems, Measurement and Control*, 112, 76-82.
- Singh, M., & Abdelnaser, A. (1992). Random response of symmetric cross-ply composite beams with arbitrary boundary conditions. *AIAA Journal*, 30, 201–210.
- Singhose, W. (2009). Command shaping for flexible systems: a review of the first 50 years. *International Journal of Precision Engineering and Manufacturing*, 10(4), 153-168.
- Singhose, W., Singer, N., & Seering, W. (1994). Design and implementation of time-optimal negative input shapers. *ASME Winter Annual Meeting*, Chicago, IL.
- Teo, C.L., Ong, C.J., & Xu, M. (1998). Pulse input sequences for residual vibration reduction. *Journal of Sound and Vibration*, 211(2), 157-177.
- Thomson, W.T., & Dahleh, M.D. (1988). *Theory of vibration with applications* (3rd Ed.). Englewood Cliffs: Prentice-Hall.
- Tuttle, T.D., & Seering, W.P. (1995). Vibration reduction in 0-g using input shaping on the MIT Middeck active control experiment. *American Control Conference*, Seattle, WA.
- Xu, S.X., & Koko, T.S. (2004). Finite element analysis and design of actively controlled piezoelectric smart structures. *Finite Element Analysis Designs*, 40, 241–262.

- Yang, H., Ang, M.H., & Krishnan, H. (1998). Control of a tip-loaded flexible-link robot using shaped input command. *Proceedings of the American Control Conference Philadelphia, Pennsylvania*.
- Yoo, H.H., Lee, S.H., & Shin, S.H. (2005). Flapwise bending vibration analysis of rotating multi-layered composite beams. *Journal of Sound and Vibration*, 286, 745-761.
- Wiederrich, J.L., & Roth, B. (1974). Design of low vibration cam profiles. *Conference on Cams and Cam Mechanisms, Liverpool, England*.
- Zhang, L., Zhu, J.W., & Zheng, Z. (1999). The stochastic Newmark algorithm for random analysis of multi-degree-of-freedom nonlinear systems. *Computers and Structures*, 70, 557-568.